UNIVERSITÉ DE STRASBOURG

Caractérisation métabolique multi échelle des Tumeurs Neuroendocrines gastro-éntero-pancréatiques et surrénaliennes

Mémoire de synthèse
présenté à Strasbourg le 16 Septembre 2016
pour l'obtention de l'

Habilitation à Diriger des Recherches
de l'Université de Strasbourg

par

Alessio IMPERIALE

préparé au sein du

Service de Biophysique et Médecine Nucléaire, Hôpitaux Universitaires de Strasbourg
Laboratoire ICube, UMR 7357/CNRS, Université de Strasbourg

Garant :	Pr I.J. NAMER	PU-PH	Université de Strasbourg
Rapporteurs :	Pr P. VERA	PU-PH	Université de Rouen
	Pr F. MESNARD	PU	Université de Picardie
	Pr B. GENY	PU-PH	Université de Strasbourg
Examinateurs :	Pr H. LEFEBVRE	PU-PH	Université de Rouen
	Pr E. HINDIE	PU-PH	Université de Bordeaux
	Pr B. GOICHOT	PU-PH	Université de Strasbourg

Table de matières

1. Imperiale A, et al. ^{18}F-fluorodihydroxyphenylalanine PET/CT in patients with neuroendocrine tumors of unknown origin: relation to tumor origin and differentiation. J Nucl Med. 2014;55:367-72.
2. Imperiale A, et al. ^{18}F-FDOPA PET/CT imaging of insulinoma revisited. Eur J Nucl Med Mol Imaging. 2015;42:409-18.
3. Imperiale A, et al. Metabolomic profile of the adrenal gland: from physiology to pathological conditions. Endocr Relat Cancer 2013;20:705-16.

4. Imperiale A, et al. Metabolome profiling by HRMAS NMR spectroscopy of pheochromocytomas and paragangliomas detects SDH deficiency: clinical and pathophysiological implications. Neoplasia. 2015;17:55-65.
5. Imperiale A, et al. *In vivo* Detection of Catecholamines by Magnetic Resonance Spectroscopy: A potential specific biomarker for pheochromocytoma diagnosis. Surgery. 2016;159:1231-3.

CURRICULUM VITAE *37*

Contexte général et racines du projet

En tant que médecin, spécialiste en Médecine Nucléaire, une discipline diagnostique en constante évolution technologique et intrinsèquement liée à l'étude de la compréhension des mécanismes physiopathologiques, la recherche a fait partie intégrante de mon parcours universitaire, dès mes quatre années d'internat.

En tant que praticien hospitalier au sein de l'équipe médicale du Service de Biophysique et Médecine Nucléaire du **CHU de Strasbourg**, mon importante activité clinique, centrée principalement sur l'oncologie, m'a permis de développer d'étroites collaborations interdisciplinaires à la fois cliniques et fondamentales. En raison de mon intérêt pour la pathologie tumorale neuroendocrine, en **recherche clinique** j'ai œuvré à l'optimisation de l'approche diagnostique et à la caractérisation du phénotype métabolique tumorale à l'aide de plusieurs techniques d'imagerie isotopique, notamment la tomographie par émission de positons à la ^{18}F-fluorodihydrohyphénylalanine, ayant conduit à la publication d'études de recherche clinique ciblant principalement les tumeurs neuroendocrines (TNE) gastro-entéro-pancréatiques (GEP). Ma participation au réseau diagnostique et thérapeutique local (réunion de concertation pluridisciplinaire) ainsi que mon intégration au réseau RENATEN (Réseau national de prise en charge des tumeurs neuroendocrines malignes rares sporadiques et héréditaires) et au groupe « Endocrinologie » de la Société Française de Médecine Nucléaire (SFMN) a joué un rôle important dans le développement de cette thématique.

Afin de répondre à plusieurs questions soulevées lors de la pratique clinique et d'expliquer les mécanismes physiopathologiques subjacents la maladie, j'ai entrepris une activité de **recherche préclinique** focalisée sur des modèles murins de TNEs pancréatiques (insulinome, TNE pancréatique non sécrétant) développées à partir d'injections sous cutanée de cellules tumorales, en intégrant l'équipe « Imagerie Moléculaire » du Département de Radiobiologie Hadronthérapie et Imagerie Moléculaire (DRHIM) de l'**Institut Pluridisciplinaire Hubert Curien (IPHC)** – CNRS/Université de Strasbourg. L'IPHC, est un exemple de réussite de la pluridisciplinarité où trois départements de cultures scientifiques différentes (écologie, physiologie et éthologie, chimie et physique subatomique) développent des programmes pluridisciplinaires de très haut niveau avec pour socle l'instrumentation scientifique et comme résultat de nombreuses publications d'un haut niveau international dans leurs domaines scientifiques respectifs. Cette expérience s'intègre dans mon projet de mobilité de douze mois (Novembre 2015 – Octobre 2016) dédié à mettre en place un axe de recherche d'imagerie moléculaire préclinique autour des TNE. L'âme de ce projet est ouvertement translationnelle puisque les résultats pourront influencer directement les pratiques cliniques actuelles.

Depuis 2009, mon activité de recherche fondamentale se fait au sein des équipes de recherche de l'Université de STRASBOURG, en particulier le Laboratoire LINC, puis le Laboratoire ICube (UMR 7357, Université de Strasbourg/CNRS) en tant que doctorant et personnel permanent dans le Groupe Métabolomique Médicale de l'équipe Imagerie Médicale Intégrative en Santé (IMIS) depuis 2014.

Le laboratoire **ICube** regroupe des moyens de recherche dans les domaines des sciences de l'information et des sciences de l'ingénieur. Le thème de l'imagerie est décliné dans plusieurs des 14 équipes qui constituent le laboratoire, notamment l'équipe IMIS. Cette dernière a des compétences en imagerie et en sciences de la santé. Elle associe sur le campus « Médecine » de Strasbourg, des chercheurs, des ingénieurs et des médecins qui développent des thèmes et des projets pluridisciplinaires de recherche fondamentale et translationnelle, afin de répondre à des questions médicales en utilisant l'imagerie multimodale. Cette intégration des activités lui confère une efficacité dans les transferts vers les applications cliniques des résultats obtenus en recherche fondamentale et préclinique. A ce propos, la caractérisation métabolique tumorale effectuée dans la plateforme de métabolomique médicale des Hôpitaux Universitaires de Strasbourg/ICube-UNISTRA, utilisant la Spectroscopie RMN à Haute résolution ou HR-MAS (il s'agit du premier spectromètre implanté en site clinique au niveau international, et un des rares au monde encore), représente une autre technique maîtrisée par notre équipe, afin d'apporter des réponses à des questions encore non résolues en pratique clinique. On retrouve alors le lien étroit existant entre l'analyse exploratoire RMN *ex vivo* et la spectroscopie RMN *in vivo* en vue du développement de biomarqueurs cliniques pour des applications en imagerie fonctionnelle, en IRM ou en médecine nucléaire (TEP). Détecter le cancer à un stade précoce ou prédire son agressivité aurait alors un impact décisif sur le diagnostic et le choix du traitement.

Concernant la **recherche fondamentale**, je me suis impliqué dès son lancement dans le Projet CARMeN (coordinateur : Pr I.J. Namer) qui a été labellisé en 2006 par le Pôle de Compétitivité «Innovations Thérapeutiques» de la Région Alsace. Ce projet a offert d'importantes pistes de recherche dans le domaine de l'oncologie, en permettant une caractérisation métabolique (métabolomique) tumorale par spectroscopie par résonance magnétique (RMN) à partir de biopsies tissulaires (*ex vivo*). C'est dans ce contexte que s'intègre mon doctorat d'université, ciblé sur la pathologie tumorale surrénalienne avec focus sur les tumeurs d'origines neuroendocrines (i.e. : phéochromocytome/paragangliome). Néanmoins, forts des résultats métabolomiques *ex vivo*, nous avons pu développer la spectroscopie RMN *in vivo* afin de caractériser des masses surrénaliennes et cervicales avant la chirurgie d'exérèse, avec des conséquences potentielles sur la prise en charge thérapeutique du patient.

Actuellement, notre objectif primaire est de développer un axe de recherche multi échelle autour des TNE intégrant la dimension cellulaire, l'expérimentation animale, l'imagerie préclinique, l'imagerie clinique et la caractérisation métabolomique tumorale en vue d'explorer les caractéristiques métaboliques propres à ces tumeurs, d'en améliorer la connaissance fondamentale et d'optimiser la prise en charge clinique du patient (**Figure 1**).

Ce projet a une claire vocation fédératrice en réunissant de nombreuses figures professionnelles impliquées dans la prise en charge des patients avec des TNE. Remporter ce défi au niveau régional permettra à terme d'amener Strasbourg au sein des centres d'excellence dans le domaine de l'imagerie appliquée à la santé à l'échelle nationale.

Nous allons détailler le chemin parcouru ayant permis d'aboutir aux résultats actuels. Nous aborderons les travaux en cours et les perspectives attendues, en explorant les résultats obtenus ainsi que les collaborations menées avec les différentes spécialités et horizons scientifiques.

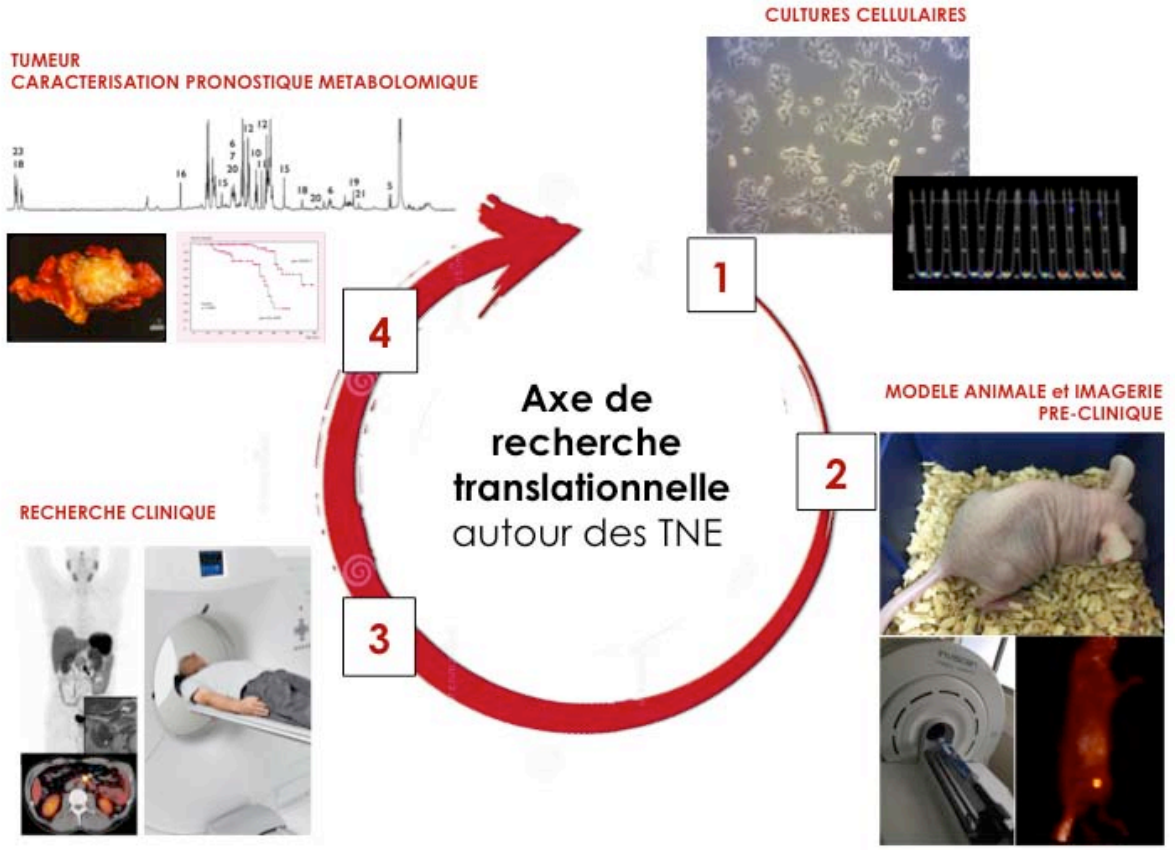

Figure 1. Axe de recherche multi échelle autour des TNE intégrant la culture cellulaire (**1**), l'expérimentation animale (**2**), l'imagerie clinique (**3**) et la caractérisation métabolomique tumorale (**4**).

1. RECHERCHE CLINIQUE

Caractérisation du phénotype métabolique des Tumeurs Neuroendocrines par techniques d'imagerie isotopique

Mon activité de recherche clinique repose sur l'imagerie des pathologies tumorales neuroendocriniennes de différente origine dérivant à la fois du neuro-ectoderme (cancer médullaire de la thyroïde, phéochromocytome, paragangliome) et de l'endoderme neural (tube digestif, pancréas et poumons). Dans le domain des TNE gastro-éntero-pancréatiques (GEP) mes travaux s'inscrivent dans une démarche expérimentale où l'exploration approfondie de chaque patient a permis de soulever des problématiques qui ont ensuite été étudiées et validées sur des cohortes de patients pour mieux comprendre la pathologie et apporter des arguments diagnostiques et/ou pronostiques indispensables pour le patient.

TNE GEP : comprendre pour mieux diagnostiquer

Les TNE GEP constituent un groupe de tumeurs épithéliales rares et hétérogènes avec différenciation neuroendocrine. Seule une faible proportion est fonctionnelle et dans ce cas, les symptômes sont induits par la sécrétion tumorale de peptides et d'amines biologiques. L'extension tumorale locale et l'évolution métastatique représentent les causes majeures de décès. Cependant, une longue survie, liée à la croissance lente de ces tumeurs, n'est pas inhabituelle (*1*). La différentiation histologique et l'index de prolifération tumorale (à partir desquels a été définie l'actuelle classification OMS en trois grades G1, 2 et 3) sont des facteurs pronostiques déterminants pour la survie du patient (*2*). L'imagerie permet la définition de la stratégie thérapeutique. Une approche multidisciplinaire est consensuelle, associant explorations radiologiques aux examens de médecine nucléaire (*3*).

Au cours des dernières années, la connaissance approfondie des caractéristiques singulières des TNEs a mené à la conception de nouvelles méthodes diagnostiques isotopiques prenant en compte les caractéristiques cellulaires du phénotype neuroendocrine. En outre, l'étude du métabolisme glucidique, ce qui n'est pas spécifique des TNE, a été également proposé pour l'imagerie isotopique dans la pratique clinique. A partir de ces considérations, les radiopharmaceutiques dédiés à l'imagerie isotopique des TNE GEP peuvent être divisés en trois principales catégories, selon qu'ils explorent :

a. L'expression des récepteurs de la somatostatine. Les analogues de la somatostatine (AS) radiomarqués se fixent sur les récepteurs de la somatostatine (SSTR), qui sont surexprimés dans les TNE, notamment le sous type 2 (SSTR2). Le couple peptide radiomarqué-récepteur est internalisé par endocytose dans les cellules tumorales et le niveau de fixation est corrélé

à la densité des récepteurs membranaires. L'octréotide conjugué avec l'acide diéthylène-triamine-penta-acétique (DTPA) et marqué avec l'^{111}In (Octreoscan®) est largement utilisé pour l'imagerie scintigraphique monophotonique (*4*). Dans la dernière décennie, une nouvelle classe d'AS radiomarqués pour l'imagerie positonique (TEP) a émergé et représente le gold standard actuel (*5*).

b. La voie de biosynthèse des amines biogènes. La captation d'acides aminés comme la dihydroxyphénylalanine (DOPA) a été utilisée pour le développement de radiotraceurs (*6*). Pour l'imagerie fonctionnelle, la DOPA est marquée au ^{18}F (^{18}F-FDOPA), aboutissant à l'accumulation intracellulaire de ^{18}F-dopamine. Dans le cas des TNE, le recours à la ^{18}F-FDOPA est basé sur une augmentation de la captation des acides aminés intervenants dans la synthèse des amines biogènes via une augmentation des transporteurs transmembranaires des acides aminés (LAT) et de la décarboxylation.

c. Le métabolisme glucidique. Le ^{18}F-fluorodéoxyglucose (^{18}F-FDG) étant un analogue du glucose marqué au fluor-18, il est transporté à l'intérieur de la cellule par les transporteurs du glucose, puis est phosphorylé par l'hexokinase en ^{18}F-FDG-6-phosphate. Ce dernier n'étant pas un substrat pour l'enzyme d'aval, il s'accumule au sein de la cellule, proportionnellement à la consommation de glucose (*7*).

Au final, à partir de l'analyse de l'intensité et de la cinétique de captation d'un ou plusieurs radiotraceurs, on parvient à caractériser l'état fonctionnel tumoral. Il semble alors évident que la médecine nucléaire ne représente pas seulement une puissante technique diagnostique mais aussi un moyen pour intimement décrypter *in* vivo la pathologie.

Caractérisation tumorale multi-traceur : rôle de l'imagerie des récepteurs de la somatostatine et de la TEP au ^{18}F-FDG

Depuis la preuve de concept des pionniers hollandais en 1989 (*8*), l'imagerie des récepteurs de la somatostatine par Octreoscan® obtient l'AMM française en 1993 et devient l'examen de premier choix pour la visualisation de TNE faisant preuve de bonnes performances diagnostiques surtout pour les tumeurs carcinoïdes et les TNE pancréatiques. Mon expérience Strasbourgeoise avec ce radiotraceur commence en 2005. A ce moment la TEP au ^{18}F-FDG commençait à s'imposer de manière prépondérante dans le domaine de l'oncologie mais les résultats observés dans les TNE étaient globalement décevants (*9*) ou limités aux cas avec scintigraphie à l'Octreoscan® négative. On commençait alors à s'apercevoir que dans ces cas, les localisations tumorales montraient souvent une fixation très importante du ^{18}F-FDG et les patients avaient un pronostic moins favorable. De plus, un métabolisme glucidique accru était associé de plus en plus à des tumeurs avec un index de prolifération élevé et/ou une faible différentiation (*10*). En effet, plus la tumeur est dédifférenciée, plus l'utilisation du glucose tumoral augmente et moins les SSTR sont exprimés sur la membrane

cellulaire avec pour conséquence une faible fixation de l'Octreoscan® (*11*). Sur la base de ces observations, à ce jour on peu définir deux patterns typiques d'imagerie moléculaire : (a) fixation intense des analogues de la somatostatine marqués vs. fixation faible du ^{18}F-FDG, situation représentative des tumeurs de bas grade et peu agressives, et (b) fixation faible des analogues de la somatostatine marqués vs. fixation intense du ^{18}F-FDG, situation représentative des tumeurs de haut grade et très agressives (**Figure 1**).

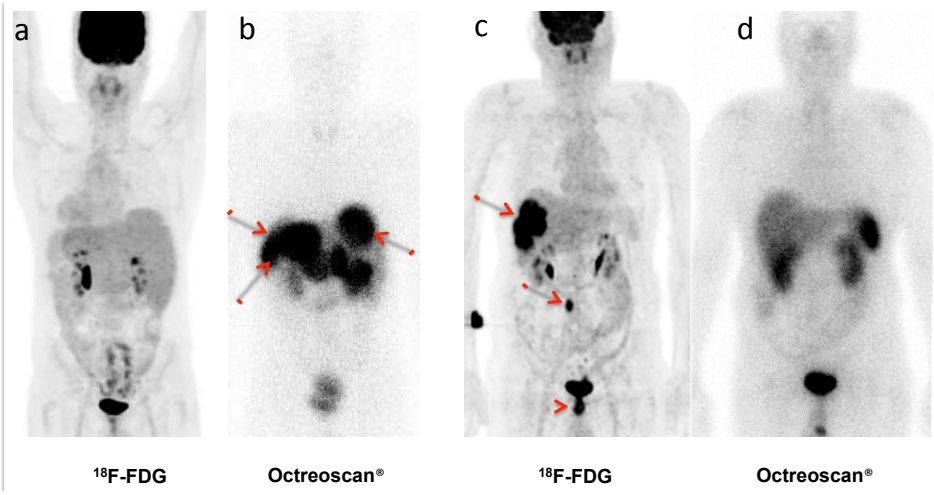

Figure 1. Patterns typiques d'imagerie moléculaire (^{18}F-FDG vs. Octreoscan®) en fonction de la différentiation et du grade tumorale (Flip-flop effect). **a, b** : TNE G1 iléale avec multiples et volumineuses métastases hépatiques. **c, d** : TNE G3 rectale avec métastases hépatiques et ganglionnaires (**Imperiale A. Functional Imaging of Gastro-Entero-Pancreatic Neuro-Endocrine Tumors. Shining New Lights: Cutting Edge Imaging in Endocrinology. ENDOCRINE, San Diego, California, 2015**).

Ces deux situations peuvent être considérées comme les extrêmes de tous les résultats possibles. Malheureusement, cette classification binaire n'est pas applicable dans toutes les situations. En effet, un continuum de résultats combinant un degré d'uptake variable des analogues radiomarqués de la somatostatine et du ^{18}F-FDG est habituellement rencontré dans la pratique quotidienne. De plus, l'intensité de la fixation peut varier dans différentes lésions du même patient, en raison principalement de l'hétérogénéité de la tumeur, sans pouvoir exclure une différenciation tumorale variable. La succession temporelle des études qui ont amené à ces conclusions a été analysée et détaillée par notre équipe (*12*).

TEP à la ^{18}F-fluorodihydrohyphénylalanine (^{18}F-FDOPA)

La ^{18}F-FDOPA est un traceur positonique ayant eu l'AMM française en 2006. Notre expérience avec la TEP à la ^{18}F-FDOPA dans les TNE a débuté en décembre 2007. La comparaison directe avec la scintigraphie à l'Octreoscan® montrait depuis les premiers cas des performances diagnostiques surprenantes, justifiant l'augmentation progressive au cours du temps du nombre de patients examinés. On s'est rapidement rendu compte que la sensibilité de la TEP à la ^{18}F-FDOPA, principalement influencée par l'origine embryologique

tumorale, était excellente pour les TNE fonctionnelles de bas grade du moyen intestin (carcinoïdes). La surexpression des LAT et une activité importante de décarboxylation intracellulaire (impliquée dans la biosynthèse tumorale de la sérotonine) sont vraisemblablement à la base de ces résultats. En analogie à la scintigraphie à l'Octreoscan®, on a pu observer que le niveau de fixation de la ^{18}F-FDOPA se réduit drastiquement dans les formes tumorales plus agressives (G2 avec index de prolifération élevé et G3) (**Figure 2**) sans pourtant afficher un phénotype on/off comme souvent observé à la comparaison Octreoscan® vs. ^{18}F-FDG.

A notre avis, la TEP à la ^{18}F-FDOPA ne représente pas seulement un excellent outil diagnostique mais semble aussi intéressante pour la caractérisation phénotypique des TNE digestifs, avec des implications thérapeutiques potentielles. En effet, compte tenu de la relation entre les transporteurs d'acides aminés (LAT) et la signalisation de la voie mTOR, on pourrait envisager l'évaluation de la réponse thérapeutique à un inhibiteur de mTOR par TEP à la ^{18}F-FDOPA, un outil thérapeutique émergent dans cette indication (*13*).

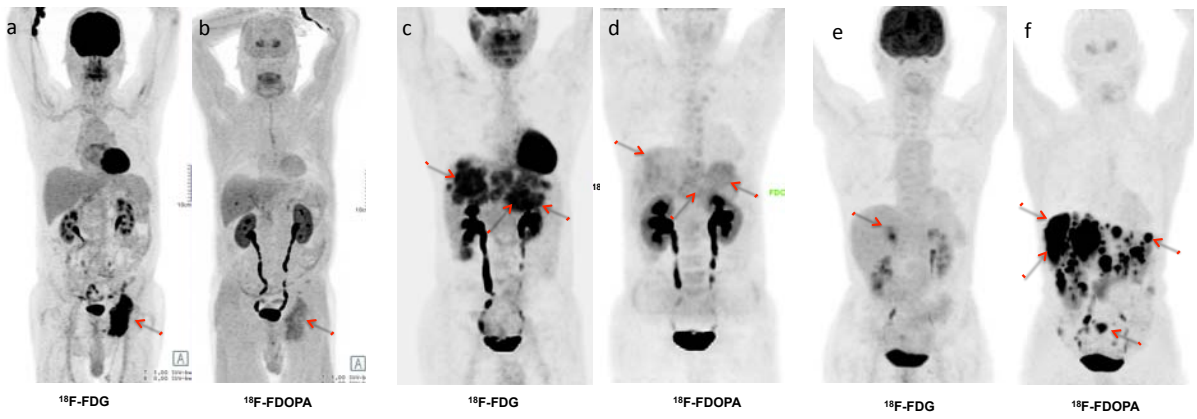

Figure 2. Patterns d'imagerie moléculaire (^{18}F-FDOPA vs. ^{18}F-FDG) en fonction du grade tumorale. **a, b** : Métastase osseuse d'une TNE G3 d'origine indéterminée. **c, d** : Métastase hépatiques multiples d'une TNE G3 d'origine indéterminée. **e, f** : TNE G1 iléale avec multiples métastases hépatiques et ganglionnaires (**Imperiale A. Functional Imaging of Gastro-Entero-Pancreatic Neuro-Endocrine Tumors. Shining New Lights: Cutting Edge Imaging in Endocrinology. ENDOCRINE, San Diego, CA, 2015**).

a. Les TNE intestinales d'origine inconnue

La détection fortuite de métastases hépatiques est la circonstance de diagnostic de TNE la plus fréquente. Cependant, la lésion tumorale primitive reste fréquemment inconnue à l'issue des explorations radiologiques et fonctionnelles. L'identification de la tumeur primitive est cruciale dans la planification du traitement, car la résection chirurgicale est associée à une meilleure survie sans symptôme, survie globale et qualité de vie, même chez les patients présentant des métastases à distance. Ce sujet a fait l'objet d'un travail collaboratif avec le CHU La Timone à Marseille, publié dans le JNM (*14*). Dans cette étude, on a évalué les performances diagnostiques de la TEP à la ^{18}F-FDOPA dans la détection de la

tumeur primitive non retrouvée à la scintigraphie à l'Octreoscan® ni lors de l'imagerie conventionnelle, chez 27 patients avec maladie tumorale neuroendocrine métastatique histologiquement prouvée. Selon les résultats obtenus, la TEP à la ^{18}F-FDOPA est un outil d'imagerie fonctionnelle sensible pour la détection de la tumeur primitive occulte en particulier chez les patients avec des tumeurs de bas grade du moyen intestin. Fait intéressant, les patients avec une TEP à la ^{18}F-FDOPA positive ont montré des niveaux plus élevés de chromogranine A et de sérotonine sérique ainsi que d'acide 5-hydroxyindoleacetic urinaire (5-HIAA). Ces conclusions ont des implications potentielles chez les patients avec TNE occulte afin de définir la modalité d'imagerie la plus appropriée en fonction du phénotype sécrétoire.

Partant de ces résultats, une étude bi centrique en partenariat avec le CHU de Brabois à Nancy est en cours, afin d'évaluer la sensibilité de la TEP à la ^{18}F-FDOPA dans la détection des formes tumorales intestinales multifocales en comparaison avec les méthodes radiologiques standard et la scintigraphie à l'Octreoscan (**Figure 3**). En effet, les tumeurs carcinoïdes sont multiples chez environ 30% des cas et la sensibilité des explorations diagnostiques pré-chirurgicales est encore loin d'être exhaustive. Sur la base de notre expérience, nous pensons que la TEP à la ^{18}F-FDOPA pourrait améliorer la détection des carcinoïdes multifocales (*15*). Une comparaison directe avec la TEP aux AS serait un axe de recherche clinique intéressant.

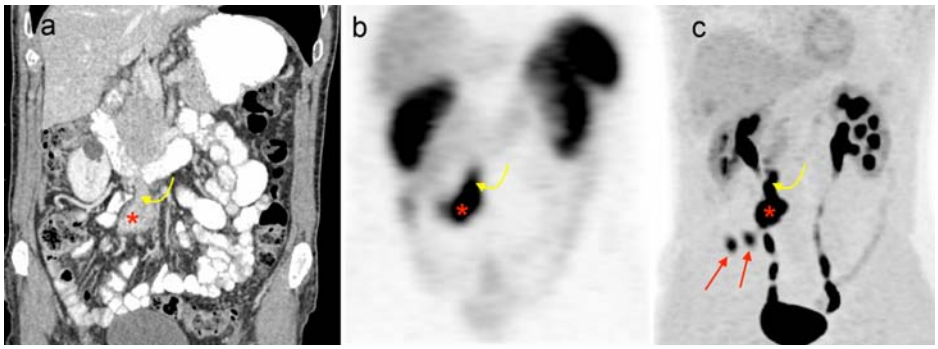

Figure 3. Recherche de la tumeur primitive chez un patient présentant une atteinte ganglionnaire mésentérique (*) secondaire à un TNE G1 non retrouvée lors de l'éntero-TDM (**a**) et de la scintigraphie à l'Octreoscan (**b**). La TEP à la ^{18}F-FDOPA (**c**) montrait deux foyer d'hyperfixation pathologique iléale en fosse iliaque droit correspondants à deux TNE G1 à l'examen anatomopathologique après chirurgie (**Imperiale et al. JNM 2015).**

b. Intérêt de la prémédication par carbidopa pour le diagnostic de TNE pancréatiques

Au présent, le rôle de la TEP à la ^{18}F-FDOPA dans l'exploration des patients atteints de TNE pancréatiques (TNEP) reste controversée. Chez l'adulte, la ^{18}F-FDOPA a été proposée pour l'imagerie TEP de l'insulinome avec des résultats discordants en fonction des études. La principale limitation de l'utilisation de cette technique chez les patients adultes est liée à

l'absorption intense et prolongée de la ^{18}F-FDOPA par le pancréas exocrine mature (en rapport avec les propriétés de décarboxylation de granules de zymogène) et donc un rapport de fixation tumeur/tissu sain non optimal. De plus, dans les tubules proximaux rénaux, la ^{18}F-FDOPA est rapidement convertie en ^{18}F-Dopamine, qui est ensuite éliminée avec pour conséquence une perte rapide du radiotraceur et des artéfacts iconographiques liés à son accumulation urinaire.

Depuis le début de notre activité diagnostique, on s'est intéressé à cette problématique identifiant dans la prémédication du patient avec Carbidopa (CD) un outil potentiellement utile. La CD est un inhibiteur compétitif de la décarboxylase des acides aminés aromatiques (DAAA) périphérique exprimée dans les cellules pancréatiques. L'administration orale de CD (200 mg) peut être effectuée préalablement à un examen TEP à la ^{18}F-FDOPA. Il est bien établi que la CD inhibe la conversion de la ^{18}F-FDOPA en ^{18}F-dopamine avec une nette réduction de l'accumulation pancréatique du radiotraceur. Cependant, un effet inhibiteur de la CD sur la DAAA tumorale avec pour conséquence des résultats faussement négatifs ne peut pas être à priori exclu en particulier devant une suspicion clinico-biologique d'insulinome. A ce propos, on a pu étudier la cinétique de fixation de la ^{18}F-FDOPA sur des insulinomes par des acquisitions TEP dynamiques (*16*). Il semble exister 2 motifs de cinétique tumorale: (1) visualisation rapide et wash-out rapide, (2) visualisation moins précoce et wash-out lent (**Figure 5**). Cet aspect est particulièrement important car la sensibilité de la méthode est influencée directement car dépendante du chronogramme et du protocole d'acquisition des images TEP.

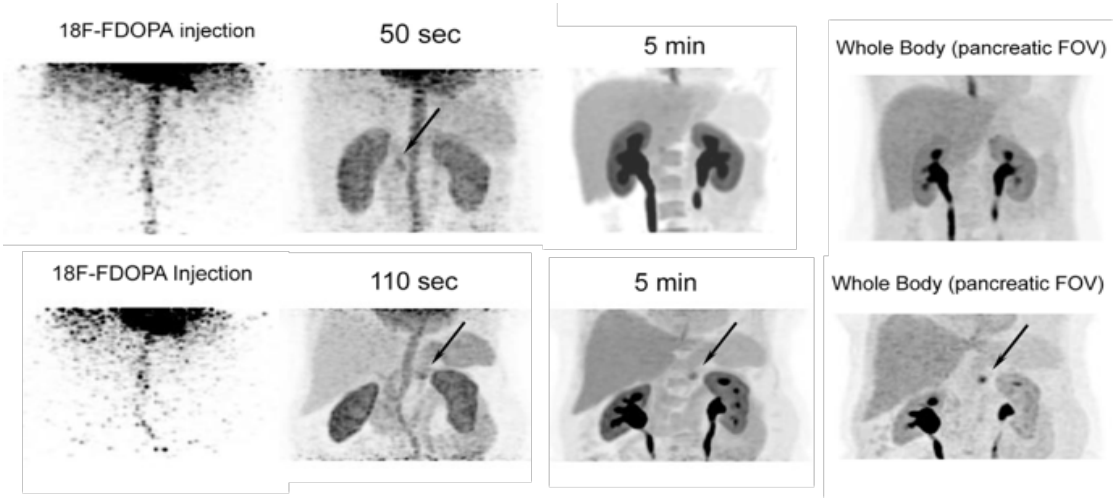

Figure 5. Deux motifs cinétiques de fixation de la ^{18}F-FDOPA observés après prémédication par carbidopa et acquisitions TEP dynamiques chez 2 patients avec insulinome bénin (**Imperiale et al. CNM 2015**).

A partir de ces observations, nous avons mené un travail collaboratif avec le CHU La Timone à Marseille, publié dans le EJNM (*17*) et incluant 16 patients avec hypoglycémie hyper insulinémique (HH) et suspicion d'insulinome. Le protocole d'acquisition TEP comprenait une acquisition précoce abdominale supérieure (5 min après injection de ^{18}F-FDOPA) et une

acquisition corps entier 20 à 30 min plus tard. Selon notre expérience, l'administration de CD avant l'injection de ^{18}F-FDOPA réduit la fixation pancréatique physiologique en préservant la captation tumorale du traceur, permettant la détection d'un insulinome chez plus de la moitié des patients et dans plus de 70% des cas avec un diagnostic final d'insulinome. De plus, la TEP à la ^{18}F-FDOPA avec prémédication par CD permettait d'identifier la tumeur lors des acquisitions précoces chez 8 des 11 patients (73%) avec insulinome prouvé histologiquement, et seulement chez 5 d'entre eux (45%) lors des images corps entier (**Figure 6**). Par conséquence, nous supposons que les insulinomes sont probablement moins sensibles à l'effet inhibiteur de la CD par rapport aux cellules acineuses, avec en conséquence un ratio élevé lésion/tissu sain.

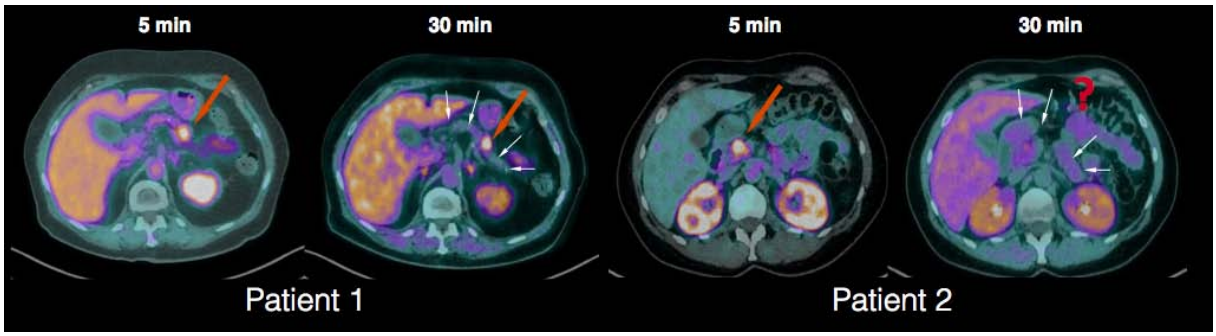

Figure 6. Résultats de la TEP à la ^{18}F-FDOPA après prémédication avec CD chez 2 patients avec insulinome bénin. Si les images à 5 min montrent la tumeur dans les 2 cas, les images effectuées à 30 min sont faussement négatives pour 1 patient (**Imperiale et al. EJNM 2015**).

Comme observé chez les patients atteints d'un carcinome médullaire de la thyroïde, il semblerait que le protocole d'acquisition TEP joue un rôle dans le diagnostic de l'insulinome permettant un meilleur taux de détection à partir de 5 minutes après l'injection du radiotraceur. Dès lors, nous recommandons de combiner une prémédication par CD à une acquisition précoce centrée sur le pancréas chez les patients explorés pour HH. Finalement, l'effet de la carbidopa sur l'absorption de la ^{18}F-FDOPA dans les insulinomes reste encore à explorer.

De façon analogue, nous avons évalué les performances diagnostiques de la TEP à la ^{18}F-FDOPA avec prémédication par CD chez 20 patients avec suspicion de TNEP non fonctionnelle (*18*). L'histologie des tumeurs pancréatiques ou d'une métastase hépatique a été considérée comme gold standard dans respectivement 13 et 3 cas. Dans les cas restants, le diagnostic de TNEP a été fait par confrontation des différentes modalités d'imagerie disponibles (au moins deux examens positifs entre : scintigraphie à l'Octreoscan, TDM, IRM). La TEP été positive dans 18/20 cas (90%) alors que la scintigraphie à l'Octreoscan l'était dans 13/19 cas (68%) (**Figure 7**). La TEP était faussement négative dans deux tumeurs kystiques. Tous les patients métastatiques ont été correctement identifiés par la TEP. Cette étude semble élargir donc l'intérêt de la TEP à la ^{18}F-FDOPA avec prémédication par CD pour la détection et le bilan d'extension de TNEP.

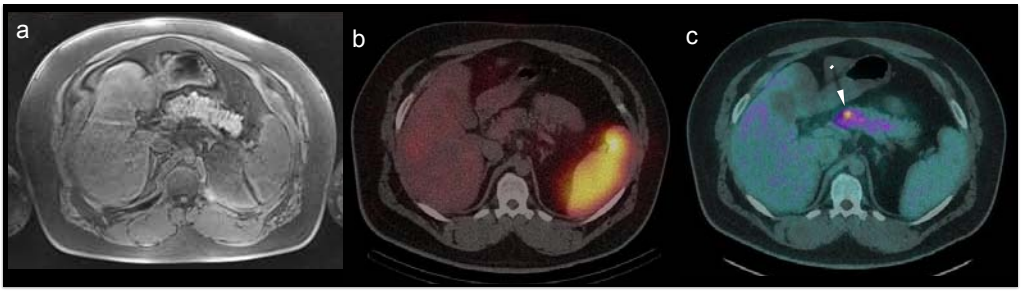

Figure 7. Résultats de la scintigraphie à l'Octreoscan (**b**) et de la TEP à la ^{18}F-FDOPA après prémédication avec CD (**c**) chez un patient avec TNEP non secrétant de 12 mm (**a** : IRM abdominale).

c. Biopsie guidée par l'imagerie métabolique

La prise en charge des patients atteints de TNE dépend du résultat de l'examen anatomo pathologique qui est souvent obtenu à partir d'un échantillon tissulaire suite à une biopsie et qui pourrait ne pas être vraiment représentatif de l'agressivité tumorale. Au contraire, la médecine nucléaire fournit une exploration non invasive corps entier, permettant une caractérisation tumorale extensive potentiellement utile pour guider la biopsie, en particulier vers les lésions avides en ^{18}F-FDG même pour les patients avec des TNE de bas grade. La biopsie TEP-guidée (utilisant à la fois le ^{18}F-FDG ou la ^{18}F-FDOPA) constitue un projet en cours de notre équipe (*19, 20*) en stricte collaboration avec l'équipe de radiologie interventionnelle dirigée par le Pr Gangi des Hôpitaux Universitaires de Strasbourg (**Figure 4**).

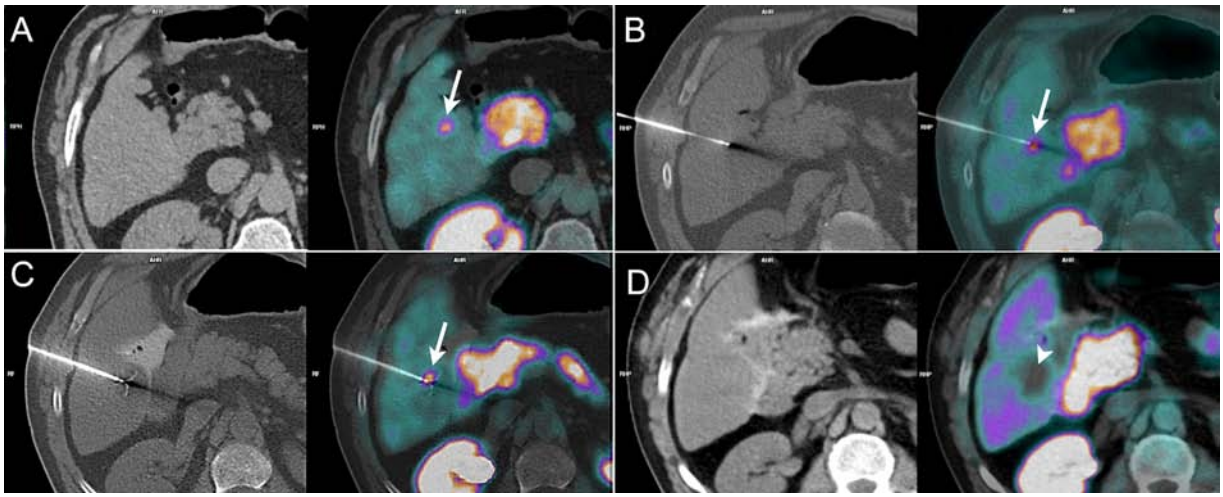

Figure 4. Biopsie (**b**) et radiofréquence (**c**) simultané d'une métastase hépatique (**a**) chez un patient avec une TNE iléale G1 opéré. L'ensemble de la procédure diagnostique et thérapeutique a été guidé par la TEP à la ^{18}F-FDOPA. Le contrôle TEP effectué immédiatement après le traitement confirme l'efficacité du geste thérapeutique montrant une plage photophénique correspondant à la lésion hépatique traitée (**d**) (**Imperiale et al. CNM 2015).**

Perspectives en recherche clinique

Deux axes de recherche clinique seront développés à moyen terme, à l'aide des techniques d'imagerie isotopique pour une meilleure caractérisation diagnostique et pronostique des TNE notamment GEP :

1. Imagerie TEP des récepteurs de la somatostatine. Ces dernières années, l'arrivée de nouveaux analogues de la somatostatine (DOTATOC, DOTATATE, DOTANOC), marqués avec un émetteur de positons, le Gallium-68 (^{68}Ga), permettant l'utilisation de la TEP a bouleversé l'approche diagnostique des TNE, en particulier digestives. Un des avantages majeurs du ^{68}Ga est sa disponibilité par simple élution d'un générateur de ^{68}Ge/^{68}Ga. Les caractéristiques physiques du ^{68}Ga (demi-vie : 270,8j) permettent de réaliser 1 à 3 élutions (donc radiomarquages) par jour. Le générateur peut être hébergé au sein du service de médecine nucléaire et est utilisable plusieurs mois en fonction de sa date de calibration. Si l'utilisation de ces molécules est actuellement restreinte aux seuls protocoles cliniques, elles seront très prochainement disponibles pour une utilisation clinique. L'acquisition d'un équipement de radiopharmacie nécessaire à leur synthèse est en cours de finalisation. Disposer de cette technique permettrait d'élargir encore l'arsenal diagnostique isotopique disponible et de s'afficher comme un des centres nationaux de référence pour l'imagerie clinique des TNE, déjà clairement défendue par le substrat médico-chirurgical local. Parmi les analogues disponibles, le DOTATOC, DOTATATE et DOTANOC possèdent une excellente affinité pour les récepteurs SST2. Le DOTATATE possède la meilleure affinité pour le SST2 et le DOTANOC est le seul ayant une affinité significative pour les SST3 et SST5. Le choix du DOTATATE peut être justifié par son utilisation dans le cadre de la radiothérapie interne vectorisée, marqué au ^{177}Lu. Ainsi, le développement d'un agent d'imagerie diagnostique utilisant le même peptide permettrait d'évaluer les patients éligibles au traitement ainsi que la réponse thérapeutique. A ce jour, les performances entre la TEP à la ^{18}F-FDOPA et la TEP au ^{68}Ga-DOTATATE n'ont été comparées que dans peu d'études à faible effectif de patients. Nous avons décidé d'étudier cela de façon prospective en y intégrant l'évaluation de l'impact médical de l'utilisation d'un tel outil diagnostique. La décision médicale sera donc recueillie avant et après la TEP au ^{68}Ga-DOTATATE et les patients seront suivis pendant une durée de 6 mois après la TEP. Parmi les patients opérés une attention particulaire sera dédiée à la détection de tumeurs multiples et une comparaison directe entre la TEP à la ^{18}F-FDOPA et la TEP au ^{68}Ga-DOTATATE sera effectué. Ce projet multicentrique est en train d'être constitué sous forme d'un PHRC national. Néanmoins, le calendrier reste encore difficile à définir car strictement dépendant de l'acquisition des équipements de radiopharmacie.

2. Évaluation précoce de la réponse thérapeutique aux thérapies ciblées par TEP au ^{18}F-FDG dans les TNE bien différenciées avancées du pancréas. A ce jour, la streptozotocine seule ou en combinaison avec la doxorubicine reste la seule chimiothérapie approuvée pour le traitement des TNE pancréatiques bien différenciées avancées. Cependant, son efficacité

inconstante invite à la recherche d'autres voies thérapeutiques. A ce jour, deux thérapies ciblées ont été testées dans le traitement des TNE bien différenciés avancées et évolutives du pancréas dans deux essais internationaux de phase III contrôlés en double aveugle contre placebo. L'administration quotidienne continue d'évérolimus (Afinitor, Novartis Pharma), un anti-mTOR, ou de sunitinib (Sutent, Pfizer), un inhibiteur des tyrosines kinases, prolonge significativement la survie sans progression et se montre efficace dans la stabilisation tumorale. La toxicité et la tolérance semblent acceptables mais les effets secondaires représentent la principale cause d'arrêt du traitement. Plusieurs questions demeurent encore ouvertes concernant leur utilisation intégrée dans l'arsenal thérapeutique existant. Il est donc essentiel de développer des techniques permettant d'identifier rapidement les patients non répondeurs, afin d'éviter un traitement lourd et peu efficace, et de proposer des alternatives thérapeutiques. De plus, le coût de ces traitements est non négligeable. La TEP au ^{18}F-Fluorodésoxyglucose (FDG) représente un potentiel intéressant dans la prédiction du pronostic à long terme chez les patients atteints de TNE en permettant d'identifier les formes agressives et rapidement évolutives. Dès lors, nous envisageons d'évaluer l'utilité de la TEP au FDG pour identifier précocement après le début du traitement par thérapies ciblées, les patients non répondeurs (i.e. absence de stabilisation radiologique) avec maladie évolutive présentant une TNE du pancréas bien différenciée, avancée, progressive et inopérable (localement avancée ou métastatique) avec une indication de traitement par thérapie ciblée selon les recommandations du Thésaurus National de Cancérologie Digestive dans le cadre d'une étude prospective multicentrique. L'absence d'études publiées ou enregistrées sur le sujet, à objectif et méthodologie équivalents, conforte l'originalité et le caractère innovant de la démarche. Les données relatives à l'évaluation des performances pronostiques de la TEP au FDG pourraient être à` l'origine d'un changement important dans la stratégie thérapeutique. L'approche diagnostique proposée ici pourrait potentiellement conduire à` optimiser la prise en charge des patients avec TNE pancréatiques évolutives avec des bénéfices médicaux et économiques directs.

Références

1. Yao JC, Hassan M, Phan A, Dagohoy C, Leary C, Mares JE, et al. One hundred years after "carcinoid": epidemiology of and prognostic factors for neuroendocrine tumors in 35,825 cases in the United States. J Clin Oncol. 2008;26:3063-72.
2. Klöppel G, Rindi G, Perren A, Komminoth P, Klimstra DS. The ENETS and AJCC/UICC TNM classifications of the neuroendocrine tumors of the gastrointestinal tract and the pancreas: a statement. Virchows Arch. 2010;456:595-7.
3. Bodei L, Sundin A, Kidd M, Prasad V, Modlin IM. The status of neuroendocrine tumor imaging: from darkness to light? Neuroendocrinology. 2015;101:1-17.
4. Krenning EP, Kwekkeboom DJ, Bakker WH, Breeman WA, Kooij PP, Oei HY, et al. Somatostatin receptor scintigraphy with [111In-DTPA-D-Phe1]- and [123I-Tyr3]octreotide: The Rotterdam experience with more than 1000 patients. Eur J Nucl Med. 1993; 20: 716-31.
5. Sadowsky SM, Neychev V, Millo C, Shih J, Nilubol N, Herscovitch P, et al. Prospective Study of 68Ga-DOTATATE Positron Emission Tomography/Computed Tomography for Detecting Gastro-Entero-Pancreatic Neuroendocrine Tumors and Unknown Primary Sites. J Clin Oncol. 2016 Feb 20; 34(6):588-96.
6. Jager PL, Chirakal R, Marriott CJ, Brouwers AH, Koopmans KP, Gulenchyn KY. 6-L-18F-fluorodihydroxyphenylalanine PET in neuroendocrine tumors: basic aspects and emerging clinical applications. J Nucl Med 2008;49:573-86.
7. Townsend DW, Carney JP, Yap JT, Hall NC. PET/CT today and tomorrow. J Nucl Med. 2004; 45: 4S-14S.
8. Krenning EP, Bakker WH, Breeman WAP, Koper JW, Kooij PP, Ausema L, et al. Localisation of endocrine-related tumours with radioiodinated analogue of somatostatin. Lancet. 1989;1:242-4.
9. Adams S, Baum R, Rink T, Schumm-Drager PM, Usadel KH, Hor G. Limited value of fluorine-18 fluorodeoxyglucose positron emission tomography for the imaging of neuroendocrine tumours. Eur J Nucl Med 1998; 25:79-83.
10. Binderup T, Knigge U, Loft A, Mortensen J, Pfeifer A, Federspiel B, et al. Functional imaging of neuroendocrine tumors: a head-to-head comparison of somatostatin receptor scintigraphy, 123I-MIBG scintigraphy, and 18F-FDG PET. J Nucl Med 2010; 51: 704-712.
11. Garin E, Le Jeune F, Devillers A, Cuggia M, de Lajarte-Thirouard AS, Bouriel C, et al. Predictive value of 18FFDG PET and somatostatin receptor scintigraphy in patients with metastatic endocrine tumors. J Nucl Med 2009; 50: 858-64.
12. Rust E, Hubele F, Marzano E, Goichot B, Pessaux P, Kurtz JE, Imperiale A. Nuclear medicine imaging of gastro-entero-pancreatic neuroendocrine tumors. The key role of cellular differentiation and tumor grade: from theory to clinical practice. Cancer Imaging. 2012; 12: 173-84.

13. Taieb D, Imperiale A, Pacak K. 18F-DOPA: the versatile radiopharmaceutical. Eur J Nucl Med Mol Imaging. 2016 [Epub ahead of print].
14. Imperiale A, Rust, Gabriel S, Detour J, Goichot B, Duclos B, et al. ^{18}F-fluorodihydroxyphenylalanine PET/CT in patients with neuroendocrine tumors of unknown origin: relation to tumor origin and differentiation. J Nucl Med. 2014; 55: 367-72.
15. Imperiale A, Averous G, Chilinseva-Natorov N, Hubelé F, Triki E, Bellocq JP, et al. Unknown Multifocal Ileal Carcinoid Revealed by (18)F-FDOPA PET/CT. J Clin Endocrinol Metab. 2014; 99:1510-1.
16. Imperiale A, Bahougne T, Goichot B, Bachellier P, Taïeb D, Namer IJ. Dynamic 18F-FDOPA PET Findings After Carbidopa Premedication in 2 Adult Patients With Insulinoma-Related Hyperinsulinemic Hypoglycemia. Clin Nucl Med. 2014;29 [Epub ahead of print].
17. Imperiale A, Sebag F, Vix M, Castinetti F, Kessler L, Moreau F, et al. $_{18}$F-FDOPA PET/CT imaging of insulinoma revisited. Eur J Nucl Med Mol Imaging. 2015;42:409-18.
18. Helali M, Addeo P, Detour J, Heimburger C, Goichot B, Bachellier P, et al. Carbidopa-assisted ^{18}F-fluorodihydroxyphenylalanine PET/CT for the localization and staging of low-grade non-functioning neuroendocrine pancreatic tumors (Soumis).
19. Imperiale A, Garnon J, Bachellier P, Gangi A, Namer IJ. Simultaneous 18F-FDOPA PET/CT-Guided Biopsy and Radiofrequency Ablation of Recurrent Neuroendocrine Hepatic Metastasis: Further Step Toward a Theranostic Approach. Clin Nucl Med. 2015; 40: e334-5.
20. Cazzato RL, Garnon J, Ramamurthy N, Tsoumakidou G, Imperiale A, Namer IJ, et al. 18F-FDOPA PET/CT-guided radiofrequency ablation of liver metastases from neuroendocrine tumors: technical note on a preliminary experience Cardiovasc Intervent Radiol. 2016; 5 [Epub ahead of print].

2. RECHERCHE PRECLINIQUE

De la culture cellulaire au modèle animal

L'axe de recherche préclinique qu'actuellement je développe est directement lié à mon activité de recherche clinique. Les observations cliniques concernant le profil de fixation de la ^{18}F-FDOPA dans l'insulinome (*1*) ainsi que les données contrastants sur le rôle de la TEP à la ^{18}F-FDOPA dans le diagnostic de cette pathologie (*2, 3*), constituent le point de départ et le fil conducteur de mon projet incluant la manipulation de lignées cellulaires (études *in vitro*) et le développement d'un modèle murin d'insulinome (études *in vivo*). Explorer l'effet de la carbidopa (CD) sur la fixation tumorale de la ^{18}F-FDOPA représente un des nos objectifs principaux. Ce projet a une claire identité translationnelle permettant d'alimenter le débat concernant l'apport de la prémédication à base de CD dans l'exploration fonctionnelle des insulinomes (*4*). En parallèle, d'autres pistes diagnostiques d'imagerie moléculaire pour les TNEP sécrétants et non sécrétants, sont en train d'être explorées à partir de modèles animaux.

Les études expérimentales *in vitro* sont d'un intérêt capital : elles requièrent des connaissances théoriques importantes, une expertise dans la manipulation des lignées cellulaires ainsi qu'une logistique spécialisée. Dans ce contexte, nous avons débuté une collaboration pour les manipulations des lignées cellulaires des TNE pancréatiques avec : (1) l'EA 7293 Stress Vasculaire et Tissulaire en Transplantation, Faculté de Pharmacie, Université de Strasbourg (Responsable : Pr Laurence Kessler), et (2) l'équipe « Trafic membranaire dans les cellules du système nerveux » (Responsables : Stéphane Gasman & Nicolas Vitale) de l'Institut des Neurosciences Cellulaires et Intégratives, CNRS UPR 3212, Université de Strasbourg.

Parallèlement, les techniques d'imagerie *in vivo* permettent d'obtenir des images anatomiques, biochimiques, fonctionnelles et métaboliques, tout en respectant l'intégrité cellulaire. De plus, l'imagerie *in vivo* du petit animal fournit des informations quantitatives qui complètent et dépassent les données de l'approche *in vitro*. Compte tenu des enjeux, du coût des équipements et de la nécessité d'utiliser des savoir-faire, ces travaux seront effectués au sein d'une plate-forme qui assurera également l'hébergement dédié aux animaux, puisqu'il s'agit souvent de rongeurs athymiques et donc très fragiles. C'est dans ce cadre que se développe mon année de mobilité (1 Novembre 2015 – 31 Octobre 2016) intégrant la plateforme d'imagerie du petit animal de l'équipe « Imagerie Moléculaire » (Responsable Dr David Brasse) du Département de Radiobiologie Hadronthérapie et Imagerie Moléculaire (DRHIM) de l'Institut Pluridisciplinaire Hubert Curien (IPHC) – CNRS/Université de Strasbourg.

La littérature disponible concernant le sujet de ce projet de recherche est extrêmement limitée (*5*-*7*); en conséquence, nos résultats se situent parmi les premières explorations expérimentales concernant l'insulinome avec des possibles retombées en pratique clinique.

Insulinome et TEP à la ^{18}F-FDOPA : effet de la Carbidopa

a. Etude *in vitro* à partir de cultures cellulaires d'insulinome

L'objectif de ce travail a été d'évaluer l'effet de la CD sur la fixation de la ^{18}F-FDOPA à partir de cultures cellulaires d'insulinome de la lignée RIN-m5F (*8*) compte tenu de leur différentiation neuroendocrine et une activité élevée de la DAAA. Ce projet représente le sujet de la thèse d'exercice en pharmacie de Mme Alice Pierre, que j'ai récemment dirigée en codirection avec le Dr Julien Detour (Radiopharmacie, Hôpitaux Universitaires de Strasbourg).

Les cellules RIN-m5F ont été cultivées dans un milieu RPMI 1640 à 37°C dans une atmosphère à 5% de CO_2 enrichie par du sérum de veau fœtal (FBS) à 10%. Les cellules ont été repiquées régulièrement tous les 3 jours pendant 3 semaines avant le début des expériences. Les éventuelles croissances bactériennes ont été inhibées par l'ajout de gentamicine dans le milieu de culture.

Une étude comparative entre les cellules ayant incubées au préalable avec de la CD et des cellules témoin non traitées a été menée. Après ajout de la ^{18}F-FDOPA aux cultures cellulaires, un prélèvement a été effectué à 5, 30 et 60 min. Une fois le culot cellulaire séparé du surnageant, les deux composantes ont été analysées par compteur gamma Wallac Wizard et TEP/TDM Siemens Biograph mCT TOF afin d'estimer l'uptake cellulaire de la ^{18}F-FDOPA en fonction du traitement par CD. De plus, en vue d'étudier l'effet de la déplétion en acides aminés sur la captation cellulaire de la ^{18}F-FDOPA, la même procédure a été effectuée incubant les cellules dans un milieu contenant uniquement du NaCl et du glucose. Enfin, on a évalué l'effet de l'inhibition pharmacologique par 2-aminobicyclo[2.2.1]heptane-2-carboxylic acid (BCH) et de la tétrabénazine. Le BCH est un inhibiteur de type compétitif des transporteurs d'acides aminés de type L (LAT) et la tétrabénazine est un inhibiteur des transporteurs VMAT entrainant respectivement une diminution de l'uptake cellulaire de la ^{18}F-FDOPA et de l'accumulation intra vésiculaire de la ^{18}F-FDopamine après décarboxylation de la ^{18}F-FDOPA.

Le pourcentage et la cinétique de captation de la ^{18}F-FDOPA n'étaient pas statistiquement différents au sein de chaque condition (i.e. : témoin et CD). On n'a pas observé de différence significative entre les taux de captation des cellules ayant incubé avec de la CD et les cellules témoins (**Figure 1**). En mettant en évidence l'absence d'effet de la CD sur les cellules

d'insulinome, cette étude renforce l'hypothèse selon laquelle la CD permettrait d'améliorer le contraste tumeur/tissu sain et ainsi d'optimiser la détection des insulinomes.

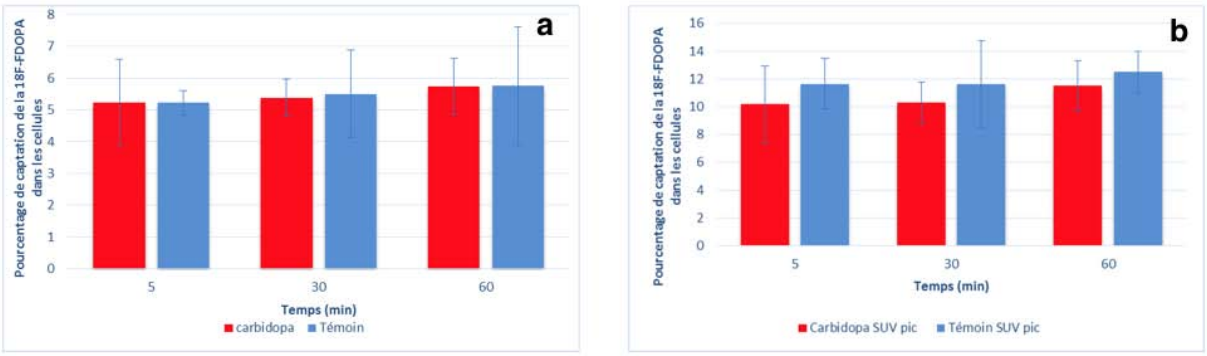

Figure 1. Pourcentage de captation de la ^{18}F-FDOPA pour 1 600 000 cellules en présence ou non de CD à 80µM (n=8 pour chaque temps). **a.** Résultats du compteur gamma **b.** Résultats du TEP-TDM

En revanche, en condition de déplétion, l'importante captation observée à 5min dans les deux conditions (i.e. : CD et témoin), se réduisait de façon importante à 30min restant stable à 60min. Le taux de captation de la ^{18}F-FDOPA apparaît moins important (mais statistiquement non significatif) dans le groupe carbidopa (**Figure 2a**). Au final, la cinétique de captation de la ^{18}F-FDOPA diffère en fonction du milieu de culture. En effet, lorsque les cellules sont incubées dans du NaCl additionné de glucose (condition de déplétion en acides aminés) le pourcentage de captation diminue fortement au cours du temps, une tendance inverse est observée lorsque les cellules sont incubées dans du RPMI (**Figure 2b**).

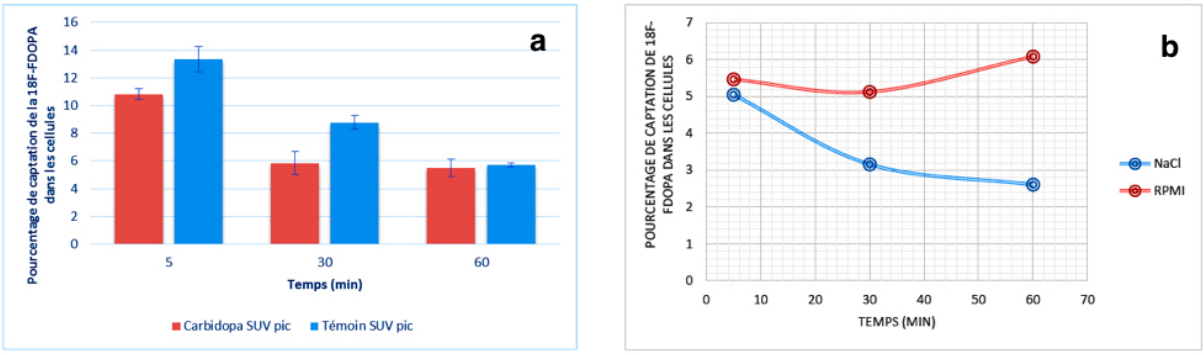

Figure 2. a. Pourcentage de captation de la ^{18}F-FDOPA pour 1 600 000 cellules en condition de déplétion en acides aminés avec et sans CD (n=2 pour chaque temps ; résultats du TEP-TDM) **b.** Cinétique de captation de la 18F-FDOPA pour 1 600 000 cellules avec et sans déplétion en acides aminés (et sans CD dans les deux cas) obtenue utilisant le compteur gamma.

Une réduction du taux de captation après incubation en présence de BCH a pu être observée dans les insulinomes, ce qui laisse supposer le passage quasi unique de la ^{18}F-FDOPA par les transporteurs LAT (**Figure 3a**). Enfin, le taux d'accumulation de la ^{18}F-FDOPA obtenus après incubation cellulaire avec tetrabenazine était très faible (**Figure 3b**). L'inhibition du VMAT par la tétrabénazine, pourrait diminuer la séquestration de ^{18}F-FDopamine issue de la décarboxylation de la ^{18}F-FDOPA. Il semblerait que la dopamine restant dans le cytosol

ressortirait des cellules, ce qui expliquerait les valeurs des taux de captation obtenus.

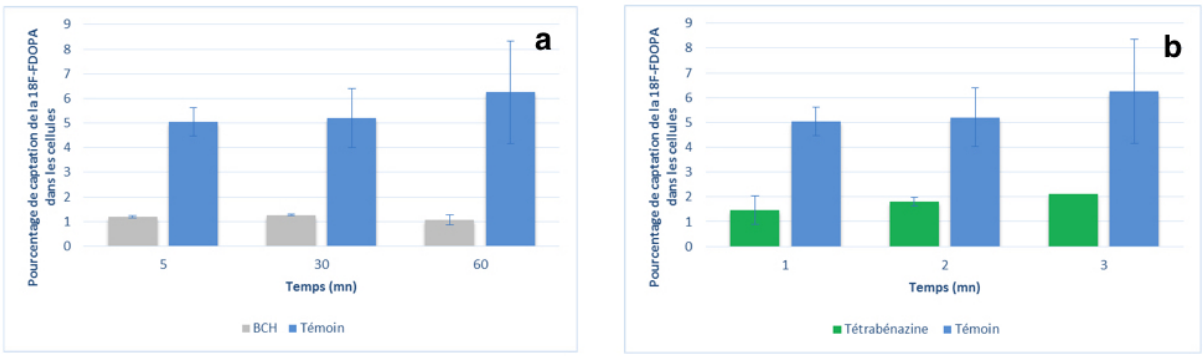

Figure 3. Pourcentage de captation de la ^{18}F-FDOPA pour 1 600 000 cellules en présence ou non de (**a**) 10mM de BCH et (**b**) 10µM de tetrabenazine**.** Résultats du compteur gamma ; n=2 pour chaque temps.

b. Etude *in vivo* à partir d'un modèle murin d'insulinome

L'étude in vivo à partir d'un modèle murin d'insulinome et analysé par tomographe TEP dédié au petit animal (microTEP) représente l'étape successive du travail qui a été finalisé à partir des cultures cellulaires. Nous avons visé l'effet de la prémédication par CD sur la fixation tumorale de la ^{18}F-FDOPA en termes d'intensité et de cinétique de fixation, à partir d'un modèle animal que j'ai pu développer suite à la xénogreffe sous cutanée de cellules RIN-m5F (6-7x10^6 cellules) dans des souris femelles athymiques (Swiss nude, Charles River) (**Figure 4**). Cette étude est actuellement en cours de déroulement. Récemment, la fixation de la ^{18}F-FDOPA a été explorée utilisant un modèle animal d'insulinome développé sur des souris nudes athymiques après injection sous cutanée de cellules RIN-m5F mais sans prémédication par CD (*7*).

Selon le protocole défini, l'analyse par microTEP est réalisée lorsque le volume de la tumeur aura atteint les 50-100 mm^3 après environ 5 semaines de l'inoculation cellulaire sous cutanée. La glycémie capillaire de chaque animal pendant la poussée tumorale est établie par méthode standard utilisant un dispositif commercial. Une supplémentation glucidique par eau glucosée (G20%) est utilisée afin de prévenir ou réduire le plus possible les effets létaux de l'hypoglycémie liée à la sécrétion tumorale d'insuline. Dans notre étude, 10 souris athymiques seront étudiées. Chaque animal bénéficiera de 2 explorations TEP à la ^{18}F-FDOPA, respectivement avec et sans prémédication par CD. Un partenariat scientifique a été obtenu avec les sociétés IBA et IASON concernant l'approvisionnement des doses de ^{18}F-FDOPA nécessaires pour un correct déroulement du protocole expérimental. Pendant chaque examen TEP, la souris est anesthésiée avec 2% d'isoflurane/air et la température du corps maintenue constante. Des acquisitions TEP dynamiques de la durée d'environ 1h sont effectuées après injection de 10 MBq de ^{18}F-FDOPA par la veine de la queue. La prémédication par CD (1 mg/kg intra péritonéale) est effectuée environ 1h avant l'injection

de la ^{18}F-FDOPA. L'analyse de l'intensité de la fixation tumorale et des courbes de cinétique de fixation est effectuée à l'aide de régions d'intérêt (ROI). La comparaison entre le groupe de souris prétraitées et non prétraitées par CD se fera par test non paramétrique. Selon le calendrier prévisionnel, ce projet se terminera en Juillet 2016 et les résultats obtenus *in vivo* seront couplés à ceux obtenus *in vitro* afin de finaliser une publication scientifique.

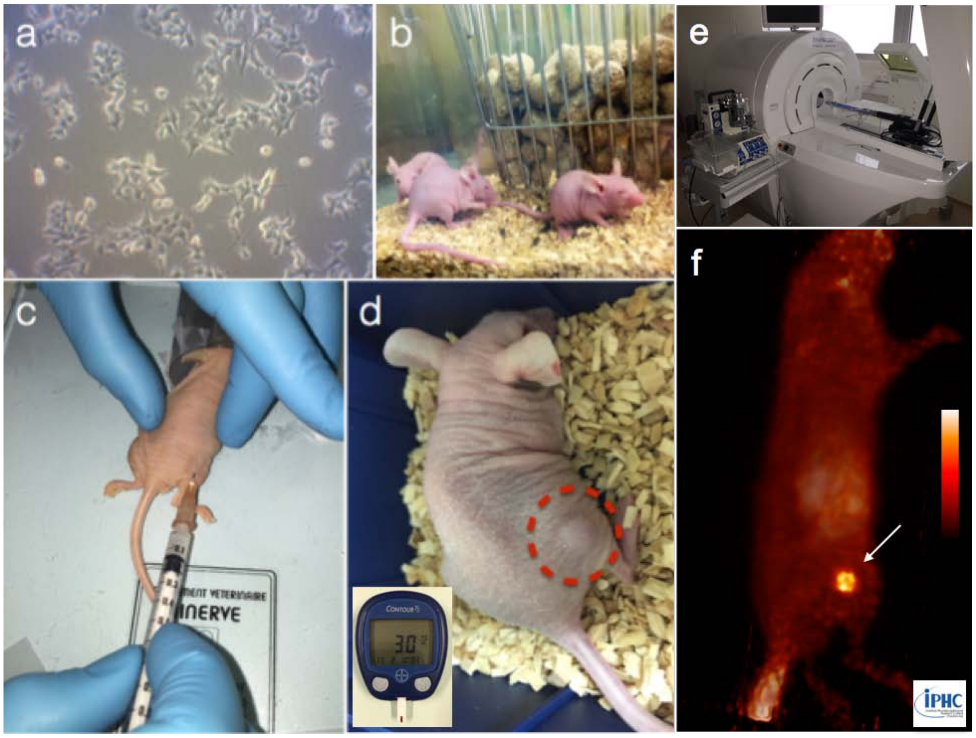

Figure 4. Résultats préliminaires obtenus après 4 mois du démarrage du projet : **a**. Cellules RIN-m5F (microscopie optique, x10), **b.** Souris athymiques avant injection cellulaire, **c**. Injection sous cutané de 7x10^{6} cellules RIN-m5F, **d**. Croissance tumorale et glycémie capillaire 4 semaines après l'inoculation cellulaire sous cutané, **e.** Tomographe MicroTEP (Inviscan Imaging System), **f.** Résultat de la TEP à la ^{18}F-FDOPA (3D rendu volumique).

La ^{18}F-fluoroéthyltyrosine pour le diagnostic de TNEP

La ^{18}F-fluoroéthyltyrosine (^{18}F-FET) est un radiotraceur positonique prometteur qui a montré des résultats probants en particulier dans le diagnostic des tumeurs cérébrales (*9, 10*). Contrairement aux autres acides aminés radiomarqués, il est produit par un cyclotron avec un rendement élevé et distribué facilement pour une utilisation clinique. Bien que la ^{18}F-FET n'est pas incorporé dans les protéines, elle montre une fixation importante dans les gliomes cérébraux et dans les carcinomes épidermoïdes extra crâniens en raison du transport intracellulaire élevé via les transporteurs transmembranaires des acides aminés neutres LAT. On rappelle que le même système de transport est utilisé pour l'incorporation cellulaire de la ^{18}F-FDOPA. En revanche, la DAAA ne semble pas jouer un rôle prépondérant dans le processus de fixation tumorale de la ^{18}F-FET, au contraire de ce qu'on observe pour la ^{18}F-FDOPA. A partir de ces considérations, l'utilisation de la CD n'apparaît pas comme

indispensable lors d'une étude TEP à la ^{18}F-FET. La stabilité in vivo, la fixation tumorale élevée et une faible fixation de la ^{18}F-FET dans le tissu inflammatoire sont des atouts intéressants pour une utilisation optimale en imagerie clinique. De plus, aucune fixation physiologique significative au niveau pancréatique n'a été décrite chez l'homme, rendant ce radiopharmaceutique potentiellement intéressant pour le diagnostic par imagerie moléculaire des TNEP.

Selon notre hypothèse, la ^{18}F-FET est potentiellement captée par l'insulinome en analogie à la ^{18}F-FDOPA compte tenu du système de transport transmembranaire LAT commun aux deux radiopharmaceutiques. A l'état actuel, aucune étude préclinique ou clinique n'a été menée vérifiant l'utilité diagnostique potentielle de la TEP à la ^{18}F-FET dans les tumeurs pancréatiques de type neuroendocrine. Partons de cette considération, nous avons voulu tester la ^{18}F-FET dans un modèle animal d'insulinome (issue de xénogreffe de cellules RIN-m5f) et de TNEP non secrétant (issue de xénogreffe de cellules BON1). Une comparaison directe sera effectuée avec les résultats de la TEP à la ^{18}F-FDOPA.

Les expériences préliminaires effectuées à ce jour nous ont permis d'obtenir la preuve de concept sur les deux modèles tumoraux développés (**Figure 5**). Ce projet se terminera en Août 2016 et les résultats obtenus permettront de finaliser une publication scientifique.

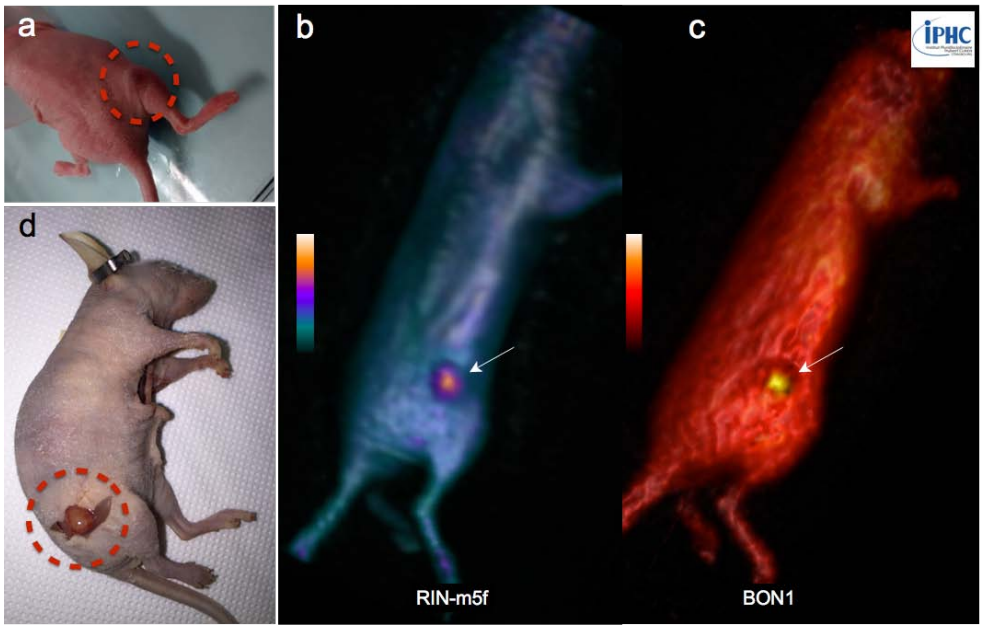

Figure 5. TNEP et TEP à la ^{18}F-FET : preuve de concept. Xénogreffe tumorale d'environ 8mm de grand axe transversal à 4 semaines après l'inoculation cellulaire de sous cutané de 7x10^{6} cellules RIN-m5F (**a**)**.** TEP à la ^{18}F-FET TEP (3D rendu volumique) : modèle tumoral RIN-m5f (**b**) et BON1 (**c**). Aspect macroscopique post mortem de l'insulinome développé après xénogreffe (**d**) et responsable du décès de la souris suite à un état d'hypoglycémie sévère (18 mg/dl).

Références

1. Imperiale A, Bahougne T, Goichot B, Bachellier P, Taïeb D, Namer IJ. Dynamic 18F-FDOPA PET Findings After Carbidopa Premedication in 2 Adult Patients With Insulinoma-Related Hyperinsulinemic Hypoglycemia. Clin Nucl Med. 2014;29. [Epub ahead of print]
2. Imperiale A, Sebag F, Vix M, Castinetti F, Kessler L, Moreau F, Bachellier P, Guillet B, Namer IJ, Mundler O, Taïeb D. $_{18}$F-FDOPA PET/CT imaging of insulinoma revisited. Eur J Nucl Med Mol Imaging. 2015;42:409-18.
3. Tessonnier L, et al. Limited value of 18F-F-DOPA PET to localize pancreatic insulin-secreting tumors in adults with hyperinsulinemic hypoglycemia. J Clin Endocrinol Metab. 2010;95:303–7.
4. Kauhanen S, et al. Fluorine-18-L-dihydroxyphenylalanine (18F-DOPA) positron emission tomography as a tool to localize an insulinoma or betacell hyperplasia in adult patients. J Clin Endocrinol Metab. 2007;92:1237–44.
5. Neels OC, Koopmans KP, Jager PL, Vercauteren L, van Waarde A, Doorduin J, et al. Manipulation of [11C]-5-hydroxytryptophan and 6-[18F]fluoro-3,4-dihydroxy-L-phenylalanine accumulation in neuroendocrine tumor cells. Cancer Res. 2008; 68: 7183-90.
6. Kuik WJ, Kema IP, Brouwers AH, Zijlma R, Neumann KD, Dierckx RA, et al. In vivo biodistribution of no-carrier-added 6-18F-fluoro-3,4-dihy- droxy-L-phenylalanine (18F-DOPA), produced by a new nucleophilic substitution approach, compared with carrier-added 18F-DOPA, prepared by conventional electrophilic substitution. J Nucl Med 2015; 56: 106–12.
7. Collantes et al. Lessons from ^{11}C-Dihydrotetrabenazine Imaging in a Xenograft Mouse Model of Rat Insulinoma: is PET Imaging of Pancreatic Beta Cell Mass Feasible? Q J Nucl Med Mol Imaging. 2015; 17 [Epub ahead of print].
8. Gazdar AF, et al. Continuous clonal insulin- and somatostatin-secreting cell lines established from a transplantable rat islett cell tumor. Proc Natl Acad Sci USA. 1980;77: 3519-23.
9. Langen KJ, Hamacher K, Weckesser M, Floeth F, Stoffels G, Bauer D, et al. O-(2-[18F]fluoroethyl)-l-tyrosine: uptake mechanisms and clinical applications. Nucl Med Biol. 2006; 33: 287-94.
10. Habermeier A, Graf J, Sandhöfer BF, Boissel JP, Roesch F, Closs EI. System L amino acid transporter LAT1 accumulates O-(2-fluoroethyl)-L-tyrosine (FET). Amino Acids. 2015; 47:335-44.

3. RECHERCHE FONDAMENTALE

Métabolomique des TNE surrénaliennes : de l'ex vivo à l'in vivo

Depuis mon Doctorat d'Université, ma recherche fondamentale est centrée sur l'étude du métabolome de la glande surrénale par spectroscopie en résonance magnétique (RMN) utilisant la technologie « HRMAS » (High Resolution Magic Angle Spinning ou haute résolution en rotation à l'angle magique) à partir de biopsies tissulaires (*ex vivo*) (*1-6*). Chez l'adulte, je me suis particulièrement intéressé à l'étude du phéochromocytome (PHEO) et du paragangliome (PGL), deux tumeurs d'origine neuroendocrine. Il s'agit de formes tumorales avec un comportement biologique variable, potentiellement très agressives avec une évolution rapide et une survie limitée. La caractérisation anatomo-pathologique est indispensable mais demeure non exhaustive, particulièrement sur un plan pronostique. Pour cette raison, différentes approches de la maladie ont été proposées, impliquant notamment les investigations génétiques qui ont contribué de façon importante à la compréhension de la pathologie tumorale. Dans ce domain, une collaboration avec les équipes de Marseille, Nancy et du NIH (Bethesda, USA) a permis d'établir la signature métabolique des PGL/ PHEO, de différencier des tumeurs selon leur profil sécrétoire biologique et leur substrat génétique. Au final, un modèle métabolomique statistiquement robuste pour prédire la présence de mutations agressives a été établi. Notre expérience a été ensuite transférée au domaine de la spectroscopie RMN *in vivo* afin de caractériser des masses surrénaliennes et cervicales avec un but diagnostique avant prise en charge thérapeutique du patient.

Métabolomique par spectroscopie RMN

Le terme métabolomique est assez récent et désigne l'analyse d'un ensemble de métabolites (métabolome) présents dans un milieu biologique. Il s'agit de petites molécules de masse molaire inférieure à 1 kDa (acides aminés, sucres, nucléotides, lipides) qui sont produites par les protéines et qui, ensemble, prennent part aux réactions biochimiques vitales de la cellule. Dans l'organisation biologique classique, la métabolomique est l'étape finale, la résultante, de l'effet des gènes (et celui de l'environnement auquel on peut rattacher les médicaments) assurant le fonctionnement cellulaire (métabolisme cellulaire). La métabolomique est un sous-ensemble des «-omiques» génomique, transcriptomique et protéomique. Le but général de la métabolomique est d'identifier, de mesurer et d'interpréter la concentration, l'activité et les flux complexes des métabolites responsables d'un comportement biologique. Ainsi, grâce à la surveillance des variations métaboliques d'un système biologique, on peut imaginer déterminer la fonction de gènes inconnus (*7-9*).

Le développement technologique des dernières années a permis la mise au point et la commercialisation de spectromètres RMN à haute résolution (HR) utilisant la technologie « MAS » (Magic Angle Spinning ou rotation à l'angle magique) permettant la caractérisation métabolique tissulaire à partir d'échantillons de tissu intact. La technique HRMAS offre une alternative valable à l'extraction chimique en donnant une excellente résolution spectrale et un excellent rapport signal sur bruit sans nécessiter des étapes de préparation de l'échantillon à analyser. La technique consiste en une rotation de l'échantillon à grande vitesse sur lui-même à un angle de 54,7° (angle magique) par rapport au champ magnétique principal B_0 (*10*). Cette inclinaison permet de réduire significativement l'élargissement des spectres induit par les effets des interactions dipolaires et l'anisotropie intrinsèque liée à la matière solide (*11*). Les premières études en métabolomique sur le cancer ont visé à comparer la lésion tumorale avec le tissu sain de même origine anatomique et embryologique avec l'objectif de discriminer les deux populations. Dans ce domaine, de nombreux travaux ont été entrepris afin de caractériser et quantifier des biomarqueurs métabolomiques potentiellement utiles pour la détection et/ou l'évaluation de l'efficacité de traitements, à partir de cultures cellulaires, de modèles précliniques animaux et d'échantillons tumoraux humains. Bien que sa sensibilité soit plus faible que celle de la spectroscopie de masse, la spectroscopie RMN HRMAS reste une technique rapide et solide qui permet l'analyse de nombreux échantillons dans un temps relativement court et d'obtenir des spectres aussi bien résolus que la RMN liquide à partir de faibles quantités de matériel biologique. En outre, il s'agit d'une technique non destructrice du tissu biologique; ceci a pour avantage l'utilisation potentielle du même échantillon pour d'autres analyses.

L'implantation du premier Spectromètre HRMAS (Bruker Avance III à 500 MHz) dans un milieu hospitalier au sein du Service d'Anatomie Pathologique des Hôpitaux Universitaires de Strasbourg, sur le site de Hautepierre, a représenté une occasion unique d'exploiter les potentialités de cette technique pour décrypter les mécanismes physiopathologiques tumoraux. Notre équipe a pu démontré la fiabilité de cette technique dans la détection de patterns métaboliques analysant de séries de biopsies tumorales dans nombreux domaines de la cancérologie et notamment dans la pathologie neuroendocrine surrénalienne. Les études métabolomiques dans ce domaine sont très peu nombreuses et donc notre travail se situe parmi les premières approches métabolomiques de la glande surrénale par RMN HRMAS.

Profil métabolomique *ex vivo* du Phéochromocytome et Paragangliome

La place de la métabolomique dans le domaine des pathologies tumorales surrénales a été extrêmement limitée et quasi systématiquement appliquée à des modèles cellulaires expérimentaux utilisant la spectroscopie de masse couplée à la chromatographie en phase liquide. Pour ces raisons, nous avons décidé d'aborder l'étude de la surrénale sous l'angle métabolomique en analysant des échantillons solides tumoraux par spectroscopie RMN

HRMAS, afin de caractériser le métabolome de la surrénale normale et de ses principales formes tumorales primitives. Nous restons persuadés que l'amélioration de la compréhension des voies métaboliques moléculaires permettra d'améliorer le diagnostic de ces tumeurs et d'envisager un ciblage diagnostique ou thérapeutique plus spécifique.

Les PGL sont des TNE développées à partir de cellules originaires de la crête neurale. Les cellules associées au système parasympathique ont la même origine. On distingue les PGL extra-surrénaliens abdominaux et thoraciques (médiastin postérieur) associés au système sympathique, les PGL cervicaux et thoraciques (médiastin moyen) associés au système parasympathique et les PHEO ou paragangliomes surrénaliens qui dérivent des cellules chromaffines de la médullo-surrénale. Les PHEO et PGL sont associés à des mutations germinales dans plus de 30% des cas, avec à ce jour plus de 10 gènes de susceptibilité identifiés dans les formes héréditaires : *NEM2, VHL, NF1, SDHA/B/C/D, SDHAF2 (ou SDH5), TMEM127, SDHA et MAX, HIF2A, FH*. Ces gènes mutés codent pour des oncoprotéines. Soulignons que les protéines *SDHA-D* constituent les sous-unités du complexe II mitochondrial (CII) et que la *SDHAF2* régule ce complexe. Le CII participe à la fois au cycle de Krebs et au transfert d'électrons au sein de la chaîne respiratoire mitochondriale. La mutation d'un gène du CII entraîne une accumulation de succinate qui induit d'une part l'activation de la voie HIF et d'autre part des modifications epigénétiques par hyperméthylation des histones.

Rao et al. (*12*) ont montré que le succinate peut être considéré comme un biomarqueur et mesuré par spectroscopie RMN en phase liquide sur des échantillons de PGL et PHEO. Cette équipe a établi les relations entre le contenu tumoral en catécholamines et l'activité mitochondriale en fonction des différents génotypes. Ces auteurs ont également montré la possibilité de détecter des catécholamines par spectroscopie RMN, confirmant les résultats de notre première étude obtenus à partir de l'analyse des échantillons de médullosurrénale normale (*1*). Notre équipe a démontré initialement l'apport de la métabolomique par RMN HRMAS dans la distinction du tissu surrénalien normal versus tumoral et des tumeurs bénignes versus malignes (*2*). Contrairement à l'étude de Rao, qui nécessite des procédures préanalytiques laborieuses, nous avons étudié des échantillons tissulaires par RMN HRMAS sans aucune préparation préalable. Bien que la sensibilité de notre technique soit moindre, nous avons obtenu une bonne qualité spectrale avec une quantification métabolique fiable permettant d'afficher le RMN HRMAS comme une alternative méthodologique efficace pour l'étude du métabolome surrénalien normal et pathologique (*2*).

En collaboration avec les Hôpitaux Universitaires de Marseille et Nancy ainsi qu'avec le NIH (USA) nous avons étendu la signature métabolique des PHEO/PGL (3). On a pu différencier les tumeurs de différents génotypes par RMN HRMAS à l'aide de 4 métabolites ayant un rôle clef potentiel dans la physiopathologie tumorale: le succinate, l'ATP/ADP/AMP, le glutamate et le glutathion. Dans ce travail, nous nous sommes intéressés aux PHEO/PGL associés à des

mutations germinales au niveau des gènes impliqués dans le métabolisme énergétique et en particulier les gènes codant pour l'enzyme succinate déshydrogénase (SDH). Une fois quantifiés, ces métabolites ont été utilisés afin de caractériser les PHEO/PGL héréditaires et les différencier des formes *a priori* sporadiques avec une sensibilité de 92%, une spécificité de 90%, des valeur prédictive positive et négative de 92% et 90% respectivement, et une précision globale de 91%. Les tumeurs *SDHx* présentaient une augmentation significative du taux de succinate par rapport aux autres sous-types tumoraux. Ce résultat reflète directement le blocage métabolique lié à l'absence de fonctionnalité de l'enzyme SDH, cruciale dans l'oxydation du succinate en fumarate dans le cycle de Krebs. En outre, les tumeurs *SDHx* étaient caractérisées par des valeurs significativement plus faibles de glutamate par rapport aux formes sporadiques, suggérant ainsi une altération possible du métabolisme du glutamate intracellulaire principalement produit par la désamination oxydative de la glutamine. Nos résultats suggèrent l'existence d'une empreinte spécifique succinate-glutamate pour les PHEO/PGL *SDHx* (**Figure 1**), potentiellement utile dans l'amélioration du diagnostic, le suivi de ces patients et la conception de nouvelles options de traitement.

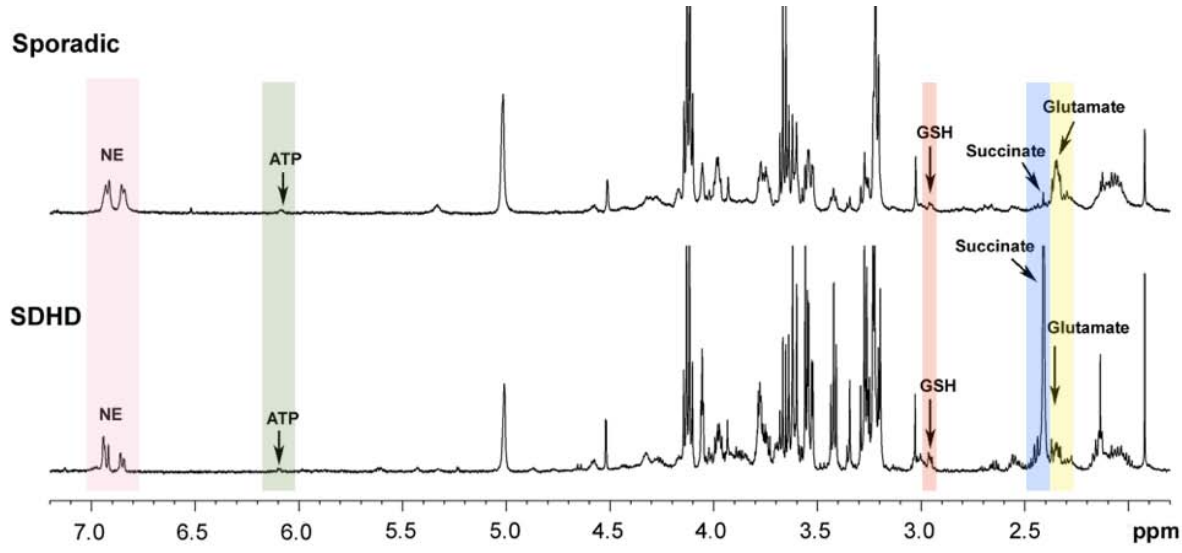

Figure 1. Spectre 1D ^{1}H CPMG HRMAS représentatif des phéochromocytomes/paragangliomes sporadiques et *SDHx*. Le succinate, le glutamate, le glutathion (GSH), l'ATP/ADP/AMP et la norépinephrine (NE) sont indiqués (**Imperiale et al. PLoS One 2013**).

A partir de ces considérations, nous avons poursuivi nos recherches consolidant la collaboration avec Marseille, Nancy et le NIH (*4*). Nous avons pu confirmer les résultats précédents dans une population de malades plus importante (87 échantillons tumoraux) et notamment le phénotype spécifique succinate-glutamate. De plus, les PHEO/PGL *SDHx* présentaient aussi des valeurs plus élevées de méthionine, ce qui concorde avec le pattern d'hyperméthylation de ces tumeurs. A partir de cette cohorte de patients, nous avons déterminé le seuil de succinate qui identifie les tumeurs *SDHx* avec une excellente précision

diagnostique (sensibilité/spécificité: 100/100%) indiquant une potentielle utilisation clinique (**Figure 2**).

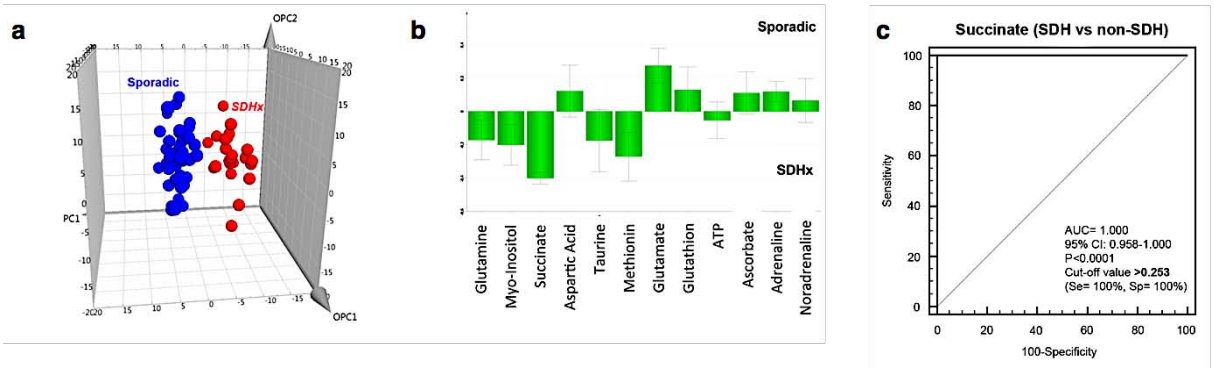

Figure 2. Résultats du modèle OPLS-DA à partir d'une population de 71 PHEO/PGL *SDHx* (n=23) et sporadiques (n=48) (**a**). Loading plot représentant les 12 principaux métabolites discriminants entre les PHEO/PGL *SDHx* et sporadiques (**b**). Courbe ROC obtenue à partir de la quantité de succinate estimée par RMN HRMAS sur une cohorte de 87 PHEO/PGL dont 23 *SDHx* et 64 non-SDHx (AUC=1) (**Imperiale et al. Neoplasia 2015**).

RMN HRMAS pour l'évaluation des mutations SDHx de pathogénicité inconnue ou fonctionnellement incertaine

L'immunohistochimie analyse la présence des protéines codées par des gènes cibles. Si le marquage est anormal, il est possible que la protéine ait une structure altérée suite aux mutations du gène qui l'encode. Par exemple, un examen normal montre clairement le marquage correspondant au complexe SDHB-SDHC-SDHD. Si le marquage est absent, la mutation d'un de ces trois gènes est probable. Le résultat va orienter en conséquence les recherches génétiques sanguines. Bien que l'immunohistochimie soit très performante dans l'identification des tumeurs liées aux mutations *SDHx*, elle nécessite parfois une certaine prudence dans l'interprétation des résultats (*13*). Pour pouvoir considérer une tumeur comme SDH-déficiente, l'ensemble du matériel analysé doit être négatif à la coloration pour SDH. Cependant, le marquage pour le complexe SDHB peut être hétérogène (« patchy »), montrant de larges zones de perte de marquage au sein desquelles on retrouve une positivité seulement focale. On pourrait alors imaginer la RMN HRMAS comme un outil diagnostique intégrant les techniques d'immunohistochimie dans le dépistage des mutations SDH (**Figure 3**). La spectroscopie RMN HRMAS pourrait avoir un rôle dans les situations qualifiées d'équivoques à l'immunohistochimie (*4*). De plus, lorsque l'analyse génétique révèle une nouvelle mutation la question se pose de savoir si la mutation est pathogène ou s'il s'agit d'un polymorphisme rare (*14*).

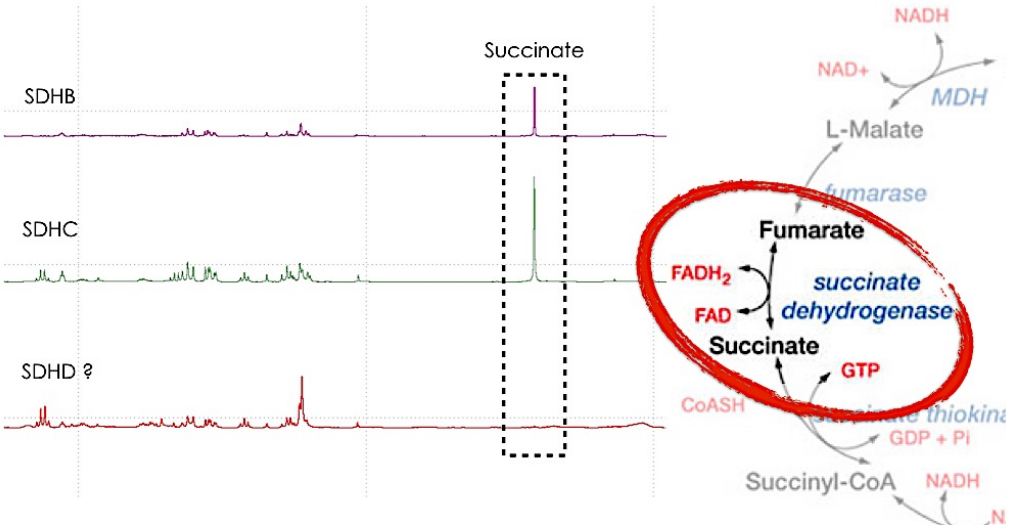

Figure 3. Spectre 1D ^{1}H CPMG HRMAS de trois PGL *SDHx* dont un, le dernier, correspond à un variant *SDHD* (c40C/T) n'entraînant pas de changement apparent d'acide aminé au niveau de la protéine. L'absence d'accumulation du succinate à l'analyse HRMAS confirme l'absence d'anomalie fonctionnelle de l'enzyme SDH.

De l'*ex vivo* à l'*in vivo*

L'analyse des échantillons de PHEO/PGL a permis de mettre en évidence des métabolites spécifiques à ces types tumoraux (i.e. : catécholamines) et, en particulier, de certains profils génétiques (i.e. : succinate).

Dès les premières expériences RMN, nous nous sommes aperçus de la nécessité d'ajouter à la région spectrale typique, comprise entre 0,5 et 4,7 ppm, la région située entre 6,7 et 8 ppm qui n'est pas habituellement prise en considération. C'est dans cette région que l'on retrouve les signaux du groupe 3,4-dihydroxybenzène, commun aux catécholamines comme l'épinéphrine et la norépinéphrine. Les informations métaboliques contenues dans cette région spectrale sont donc spécifiques aux tissus dérivés de la crête neurale. De plus, les signaux du groupe 3,4-dihydroxybenzène se situent dans une région relativement pauvre en signal, et donc facile à identifier et à quantifier. Au vu de ces considérations, les signaux du groupe 3,4-dihydroxybenzène prennent une signification diagnostique et peuvent avoir un impact sur la pratique clinique.

A ce titre, l'évolution de la spectroscopie RMN *in vivo* intégrant l'analyse des régions spectrales spécifiques aux catécholamines a constitué un nouvel axe de recherche visant à explorer des masses surrénaliennes atypiques, difficiles à caractériser par les examens paracliniques usuels. A ce propos, des résultats préliminaires intéressants ont été récemment rapportés par notre équipe (**Figure 4**) mettant en oeuvre des acquisitions RMN *in vivo* synchronisées au cycle respiratoire afin d'éliminer les artefacts liés aux mouvements abdominaux (*15*). En parallèle, une étude en collaboration avec l'équipe Marseillaise a

permis avec succès de détecter *in* vivo le succinate, le biomarqueur clef des PHEO/PGL liés aux mutations SDH (*16*) (**Figure 5**). L'ensemble des nos résultats ont été récemment confirmés par d'autres équipes (17). Ce sujet représente la conséquence directe des résultats des nos études *ex vivo* à partir d'échantillons tumoraux. On retrouve alors le lien étroit existant entre l'analyse exploratoire RMN *ex vivo* et la spectroscopie RMN *in vivo* en vue du développement de biomarqueurs cliniques pour des applications en imagerie fonctionnelle par IRM ou en médecine nucléaire (TEP). En effet, un objectif important de la métabolomique est l'identification de biomarqueurs spécifiques pour un diagnostic efficace en routine clinique. Détecter le cancer à un stade précoce ou prédire son agressivité aurait alors un impact décisif sur le diagnostic et le choix du traitement. Cependant, il reste à déterminer si les premiers changements métaboliques indicateurs de la maladie seront suffisamment importants pour être détectés par l'analyse ciblée.

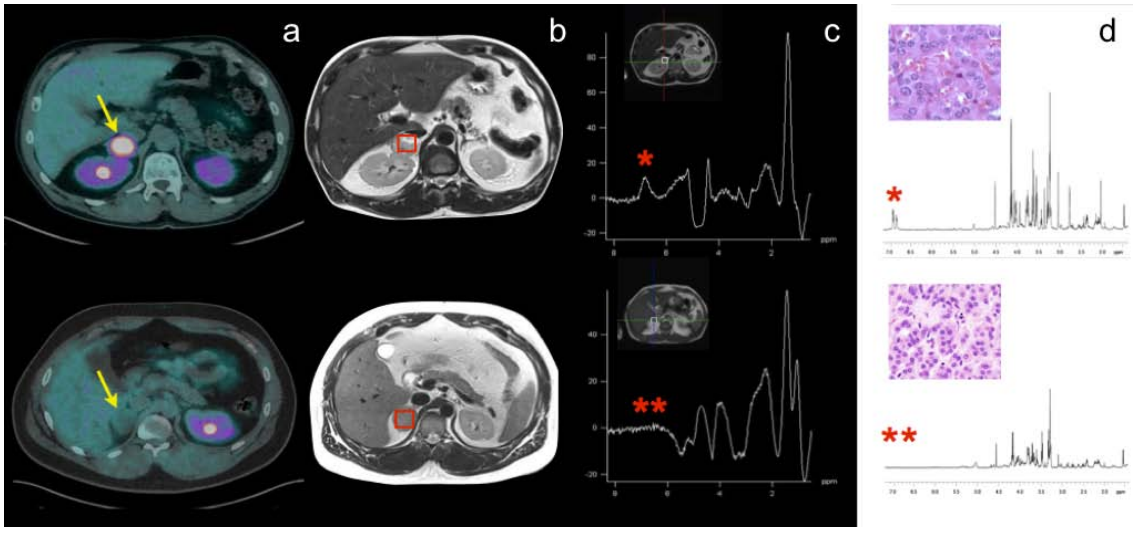

Figure 4. Détection des catecholamines par spectroscopie RMN *in vivo* avec synchronisation au cycle respiratoire: preuve de concept chez deux patients avec un phéochromocytome sporadique et un adénome surrénalien, respectivement. **a.** TEP à la ^{18}F-FDOPA. **b.** IRM abdominale. **c.** RMN *in* vivo. **d.** RMN HRMAS *ex* vivo et anatomopathologie post opératoire. *** :** pic spectral avec significat diagnostic correspondant au groupe 3,4-dihydroxybenzène des catecholamines. **** :** absence de catecholamines (**Imperiale et al. Surgery 2015**).

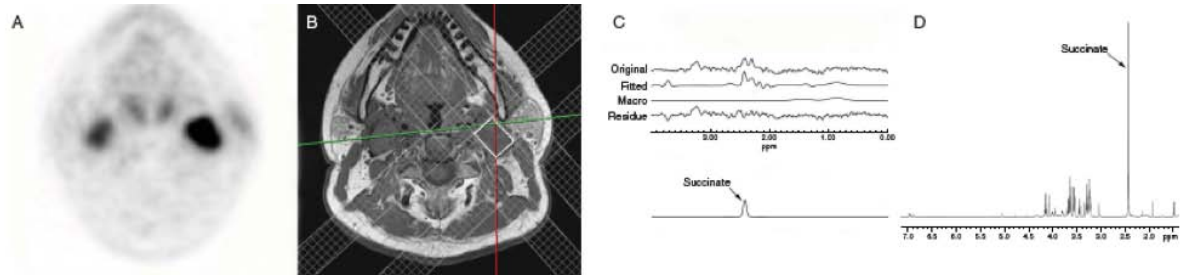

Figure 5. Détection du succinate par spectroscopie RMN *in vivo* mono-voxel : preuve de concept chez un patient avec paraganglioma cervical bilatéral SDHD. **a.** TEP au ^{68}Ga-DOTATATE. **b.** IRM cervicale. **c.** RMN *in* vivo. (**Varoquaux et al. Endocr Relat Canc. 2015**).

En conclusion, la spectroscopie RMN HRMAS est une technique robuste permettant une analyse rapide d'échantillons minimaux de tissu sans sursoir à la qualité des spectres obtenus. De plus, il s'agit d'une technique non destructive qui a pour avantage d'utiliser le même échantillon pour d'autres analyses. Nous considérons donc que la métabolomique par RMN HRMAS peut être efficacement appliquée à l'étude de la pathologie tumorale et pourrait être potentiellement intégrée dans un environnement médical avec un coût d'investissement non prohibitif. L'optimisation et le développement de techniques de spectroscopie RMN in vivo permettraient un transfert en routine clinique des informations acquises sur la pièce tumorale (RMN HRMAS). Toutefois, des essais cliniques à plus grande échelle, multicentriques, doivent être menés afin de valider des résultats souvent obtenus sur des cohortes à faible effectif de patients.

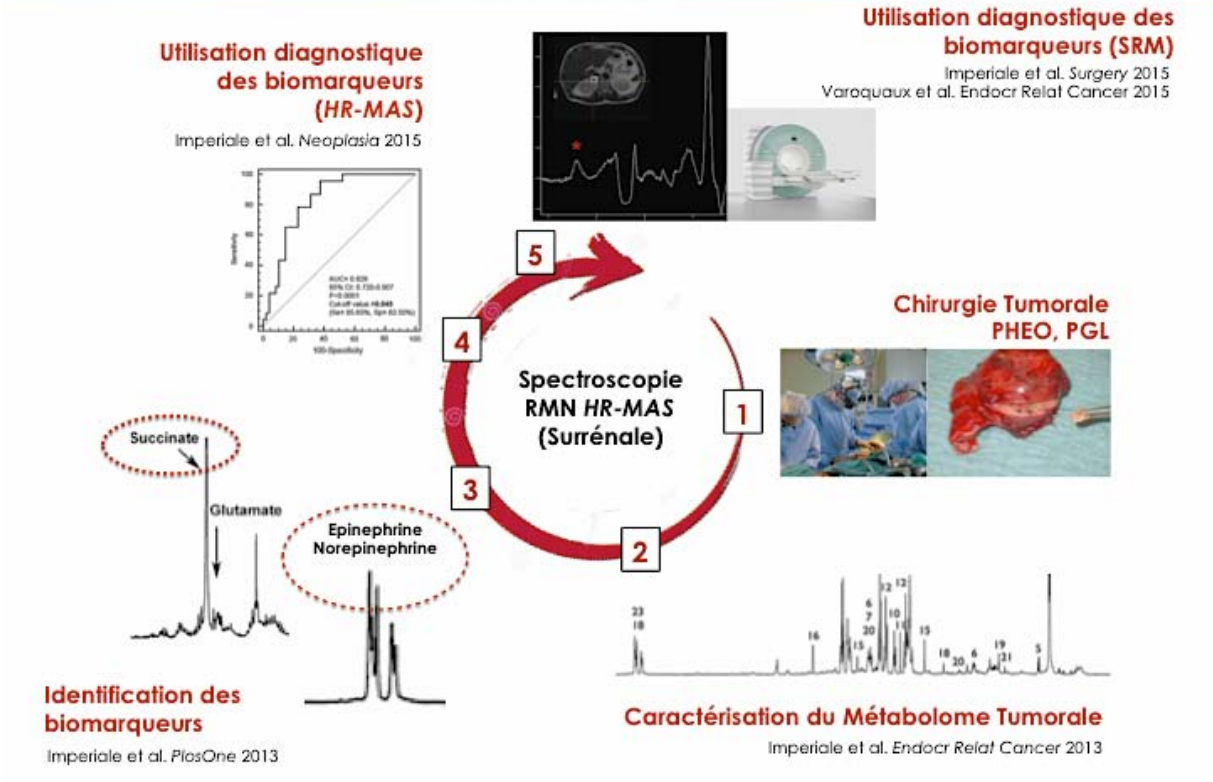

Figure 1. Schéma récapitulatif des différentes étapes parcourues en métabolomique des PHEO/PGL.

Perspectives en métabolomique

Caractérisation pronostique par analyse métabolomique de TNE pancréatiques

La classification OMS distingue trois groupes principaux de TNE selon : le degré de différenciation, l'index de prolifération et l'index mitotique. Quel que soit le siège de la

tumeur primitive, les tumeurs peu différenciées ont un mauvais pronostic, avec une survie inférieure à 1 an en l'absence de traitement et un taux de survie à 5 ans inférieur à 20%, lorsque les patients sont traités par chimiothérapie systémique. Le pronostic des formes bien différenciées se caractérise par une grande variabilité, au stade non métastatique comme au stade métastatique. Plusieurs études ont tenté de mettre en évidence des biomarqueurs pronostiques, mais avec des résultats contradictoires et parfois sans corrélation avec l'évolution de la maladie.

Dans ce contexte, cet axe de recherche aura pour perspective l'étude de nouveaux marqueurs pronostiques des TNE pancréatiques à l'aide d'une analyse métabolomique par spectroscopie RMN pour : (1) déterminer l'évolutivité des formes à comportement incertain, (2) adapter la prise en charge thérapeutique et (3) rechercher de nouvelles voies thérapeutiques. Une analyse rétrospective d'une population sélectionnée à partir du registre local de malades sera effectuée parallèlement au recrutement prospectif des patients. Le modèle obtenu sera alors utilisé afin de prédire l'évolution des nouveaux malades. La littérature disponible concernant ce projet est extrêmement limitée, en conséquence il s'inscrit parmi les premières explorations métabolomiques des TNE avec des retombées potentielles en pratique clinique. Finalement, l'expérience acquise par notre équipe ces dernières années constitue un atout pour développer de nouvelles connaissances concernant les TNE. Ce projet, qui s'annonce multicentrique, renforcera le réseau multidisciplinaire local, alimentera les collaborations existantes et permettra d'en créer de nouvelles par le biais du réseau national RENATEN, GTE et du groupe « Endocrinologie » de la SFMN.

Références

1. Imperiale A, Elbayed K, Moussallieh FM, Neuville A, Piotto M, Bellocq JP, Lutz P, Namer IJ. Metabolomic pattern of childhood neuroblastoma obtained by 1H-High-resolution magic angle spinning (HRMAS) NMR spectroscopy. Pediatr Blood Cancer 2011; 56: 24-34.
2. Imperiale A, Elbayed K, Moussallieh FM, Reix N, Piotto M, Bellocq JP, Goichot B, Bachellier P, Namer IJ. Metabolomic profile of the adrenal gland: from physiology to pathological conditions. Endocr Relat Cancer 2013; 20: 705-16.
3. Imperiale A, Moussallieh FM, Sebag F, Brunaud L, Barlier A, Elbayed K, Bachellier P, Goichot B, Pacak K, Namer IJ, Taïeb D. A new specific succinate-glutamate metabolomic hallmark in SDHx-related paragangliomas. PLoS One. 2013;8:e80539.
4. Imperiale A, Moussallieh FM, Roche P, Battini S, Cicek AE, Sebag F, Brunaud L, Barlier A, Elbayed K, Loundou A, Bachellier P, Goichot B, Stratakis CA, Pacak K, Namer IJ, Taïeb D. Metabolome profiling by HRMAS NMR spectroscopy of pheochromocytomas and paragangliomas detects SDH deficiency: clinical and pathophysiological implications. Neoplasia. 2015; 17: 55-65.
5. Szarek E, Ball ER, Imperiale A, Tsokos M, Faucz FR, Giubellino A, Moussallieh FM, Namer IJ, Abu-Asab MS, Pacak K, Taïeb D, Carney JA, Stratakis CA. Carney triad, SDH-deficient tumors, and Sdhb+/- mice share abnormal mitochondria. Endocr Relat Cancer. 2015; 22: 345-52.
6. Abdullah AE, Guerin C, Imperiale A, Barlier A, Battini S, Pertuit M, Roche P, Essamet W, Vaisse B, Pacak K, Sebag F, Taïeb D. Paraganglioma of the organ of Zuckerkandl associated with somatic HIF2A mutation. Oncol Lett. 2016 (sous-presse).
7. Gary J. Patti, Oscar Yanes & Gary Siuzdak. Metabolomics: the apogee of the omics trilogy. *Nature Reviews Molecular Cell Biology* 13, 263-269 (April 2012)
8. Lindon JC, Holmes E, Nicholson JK. So what's the deal with metabonomics? Anal Chem. 2003; 75: 384A-91A.
9. Nicholson JK, Wilson ID. Understanding 'global' systems biology: Metabonomics and the continuum of metabolism. Nature Rev Drug Disc. 2003; 2: 668–76.
10. Andrew ER, Bradbury A, Eades RG. Removal of dipolar broadening of nuclear magnetic resonance spectra of solids by specimen rotation. Nature. 1959;183:1802-3.
11. Cheng LL, Lean CL, Bogdanova A, Wright SC, Jr, Ackerman JL, Brady TJ, et al. Enhanced resolution of proton NMR spectra of malignant lymph nodes using magic-angle spinning. Magn Reson Med. 1996; 36: 653–8.
12. Rao JU, Engelke U, Rodenburg R, Wevers R, Pacak K, Eisenhofer G, et al. Genotype-specific abnormalities in mitochondrial function associate with distinct profiles of energy metabolism and catecholamine content in pheochromocytoma and paraganglioma. Clin Cancer Res. 2013; 30:3787-95.
13. Barletta JA, Hornick JL. Succinate Dehydrogenase-deficient Tumors: Diagnostic

Advances and Clinical Implications. Adv Anat Pathol. 2012; 19: 193-203.

14. Canu L, Rapizzi E, Zampetti B, Fucci R, Nesi G, Richter S, et al. Pitfalls in Genetic Analysis of Pheochromocytomas/Paragangliomas-Case Report. J Clin Endocrinol Metabol. 2014; 99: 2321-6.
15. Imperiale A, Battini S, Averous G, Mutter D, Goichot B, Bachellier P, Pacak K, Taïeb D, Namer IJ. *In vivo* Detection of Catecholamines by Magnetic Resonance Spectroscopy: A potential specific biomarker for pheochromocytoma diagnosis. Surgery. 2016;159: 1231-3.
16. Varoquaux A, Le Fur Y, Imperiale A, Reyre A, Montava M, Fakhry N, Namer IJ, Moulin G, Pacak K, Guye M, Taieb D. Magnetic resonance spectroscopy of paragangliomas: new insights into in vivo metabolomics. Endocr Relat Cancer. 2015; 22:M1-8.
17. Lussey-Lepoutre C, Bellucci A, Morin A, Buffet A, Amar L, Janin M, et al. In Vivo Detection of Succinate by Magnetic Resonance Spectroscopy as a Hallmark of SDHx Mutations in Paraganglioma. Clin Cancer Res. 2016; 22: 1120-9.

Publications Sélectionnées

1. Imperiale A, et al. ^{18}F-fluorodihydroxyphenylalanine PET/CT in patients with neuroendocrine tumors of unknown origin: relation to tumor origin and differentiation. J Nucl Med. 2014; 55: 367-72.

2. Imperiale A, et al. ^{18}F-FDOPA PET/CT imaging of insulinoma revisited. Eur J Nucl Med Mol Imaging. 2015; 42: 409-18.

3. Imperiale A, et al. Metabolomic profile of the adrenal gland: from physiology to pathological conditions. Endocr Relat Cancer 2013; 20:705-16.

4. Imperiale A, et al. Metabolome profiling by HRMAS NMR spectroscopy of pheochromocytomas and paragangliomas detects SDH deficiency: clinical and pathophysiological implications. Neoplasia. 2015; 17: 55-65.

5. Imperiale A, et al. *In vivo* Detection of Catecholamines by Magnetic Resonance Spectroscopy: A potential specific biomarker for pheochromocytoma diagnosis. Surgery. 2016; 159: 1231-3.

^{18}F-Fluorodihydroxyphenylalanine PET/CT in Patients with Neuroendocrine Tumors of Unknown Origin: Relation to Tumor Origin and Differentiation

Alessio Imperiale[1,2], Edmond Rust[1], Sophie Gabriel[3], Julien Detour[4], Bernard Goichot[5], Bernard Duclos[6], Jean-Emmanuel Kurtz[7], Philippe Bachellier[8], Izzie-Jacques Namer[1,2], and David Taïeb[3]

[1]Biophysics and Nuclear Medicine, Hautepierre University Hospital, Strasbourg, France; [2]ICube, University of Strasbourg/CNRS (UMR 7357) and FMTS, Faculty of Medicine, Strasbourg, France; [3]Nuclear Medicine, La Timone University Hospital, European Center for Research in Medical Imaging, Aix-Marseille University, Provence, France; [4]Radiopharmacy, Hautepierre University Hospital, Strasbourg, France; [5]Internal Medicine, Hautepierre University Hospital, Strasbourg, France; [6]Gastroenterology, Hautepierre University Hospital, Strasbourg, France; [7]Oncology, Hautepierre University Hospital, Strasbourg, France; and [8]Visceral Surgery and Transplantation, Hautepierre University Hospital, Strasbourg, France

This work was performed to evaluate the performance of ^{18}F-fluorodihydroxyphenylalanine (^{18}F-FDOPA) PET/CT in detecting primary neuroendocrine tumors (NETs) occult on morphologic and functional imaging, in relation to tumor origin and differentiation. **Methods:** A retrospective study of NET patients who were investigated with ^{18}F-FDOPA PET/CT imaging in 2 academic endocrine tumor centers was conducted. Only patients with negative conventional and somatostatin receptor scintigraphy (SRS) results were studied. **Results:** Twenty-seven patients were evaluated with ^{18}F-FDOPA PET/CT, 23 at their initial staging and 4 during their follow-up. The primary occult NET was localized by ^{18}F-FDOPA PET/CT in 12 patients (overall sensitivity, 44%; 52% in patients evaluated at initial diagnosis), leading to tumor resection in all cases. The primary tumors were distributed and graded as follows: 1 duodenum G2 lesion, 7 ileum G2 lesions, 2 terminal ileum G1 lesions, 1 pancreas G2 lesion, and 1 gallbladder G3 lesion. Patients with positive ^{18}F-FDOPA PET/CT results had higher values of serum chromogranin A (100% vs. 20%, $P = 0.0003$), serotonin, or urinary 5-hydroxyindolacetic acid (83% vs. 20%, $P = 0.003$). Two false-negative results were related to poorly differentiated duodenal and prostatic NETs (G3). ^{18}F-FDOPA PET/CT showed more metastatic anatomic regions than SRS in 17 patients. **Conclusion:** ^{18}F-FDOPA PET appears to be a sensitive functional imaging tool for the detection of primary NETs occult on SRS, especially tumors with a well-differentiated pattern and serotonin secretion.

Key Words: neuroendocrine; unknown primary tumor; somatostatin receptor scintigraphy; ^{18}F-FDOPA; PET/CT

J Nucl Med 2014; 55:367–372
DOI: 10.2967/jnumed.113.126896

Neuroendocrine tumors (NETs) are epithelial neoplasms derived from cells of the diffuse neuroendocrine system. Their incidence is usually reported as 40–50 cases per million individuals, accounting for about 0.5% of all cancers in the adult population (*1*). NETs can be classified as functioning or nonfunctioning according to the presence or absence of tumoral secretion of peptides or hormones. In about 20%–50%, the primary tumor is of unknown origin, accounting for 2%–4% of all carcinomas of unknown primary origin (*2–6*). The identification of the primary tumor is crucial in treatment planning since resection of the primary tumor is associated with improvement of symptom-free survival, overall survival, and quality of life even at later stages of the disease with presence of distant metastases (*7–10*). Furthermore, the detection of a primary tumor of pancreatic origin enables the use of new, highly efficient molecular targeted therapies such as everolimus (an inhibitor of mammalian target of rapamycin) and sunitinib (an antiangiogenic agent) (*11,12*).

A multimodality imaging approach is usually needed to fully evaluate the extent of disease and to localize the primary tumor. Nevertheless, the primary tumor frequently remains occult on the recommended morphologic and functional imaging studies based on the use of multiphasic CT, MR imaging, endoscopic sonography, and somatostatin receptor scintigraphy (SRS) (*2,13,14*).

In recent years, dihydroxyphenylalanine radiolabeled with ^{18}F (^{18}F-FDOPA) has been developed to image NETs originating in different areas (*15,16*). The uptake and retention of ^{18}F-FDOPA is dependent on the expression of the large neutral amino acid transporter system and the activity of amino acid decarboxylase (*17*). It is widely recognized that the sensitivity of ^{18}F-FDOPA is influenced by the embryologic origin of the NETs, with a higher sensitivity for midgut NETs than for others (*18,19*).

Analysis of the relevant literature is hampered by the frequent mixing of different clinical situations. Moreover, patients with NETs of unknown origin are rarely investigated in a specific manner. Reported sensitivities for ^{18}F-FDOPA PET and PET/CT in the detection of primary NETs have ranged from 29%–100% (*19–23*), and sensitivity for SRS-negative lesions has scarcely been investigated. It is therefore important to specifically evaluate the diagnostic performance of ^{18}F-FDOPA PET in the detection of primary NETs.

The aim of the present retrospective study was to evaluate the performance of ^{18}F-FDOPA PET/CT in the detection of neuroendocrine primary tumors in a cohort of patients with negative findings on conventional imaging and SRS.

Received May 29, 2013; revision accepted Sep. 24, 2013.
For correspondence or reprints contact: Alessio Imperiale, Department of Biophysics and Nuclear Medicine, Hautepierre University Hospital, 1, Avenue Molière, 67098 Strasbourg Cedex 09, France.
E-mail: alessio.imperiale@chru-strasbourg.fr
Published online Dec. 16, 2013.

MATERIALS AND METHODS

Patient Population

Among all the patients evaluated by ^{18}F-FDOPA PET/CT between January 2009 and December 2012 in the Nuclear Medicine Department of the university hospitals of Strasbourg and Marseille, only patients with histologically proved metastatic disease of neuroendocrine origin were evaluated. Tumors were classified for differentiation and grade according to the criteria of the World Health Organization and the European Neuroendocrine Tumour Society (*24,25*). Imaging work-up included at least liver sonography, triphasic thoracoabdominal CT, abdominal MR imaging, and SRS performed less than 3 mo before the ^{18}F-FDOPA PET/CT. Follow-up data were obtained for at least 12 mo after ^{18}F-FDOPA PET/CT in surviving patients.

All selected subjects underwent a standard physical examination investigating the presence of symptoms related to tumoral secretion, particularly flushing and diarrhea. Serum chromogranin A, serum serotonin, and urinary 5-hydroxyindolacetic acid were measured in all patients. Serum gastrin, insulin, glucagon, and ACTH were measured only in selected patients. In addition to the conventional imaging work-up, endoscopic sonography combined with fine-needle aspiration cytology or large-bowel colonoscopy, video capsule endoscopy, or ^{18}F-FDG PET/CT were available in a limited number of patients. ^{18}F-FDG PET/CT was added to the work-up for selected patients with occult primary NETs on ^{18}F-FDOPA PET/CT, poorly differentiated NETs, or a Ki-67 of at least 15%.

^{18}F-FDOPA was used in the setting of marketing authorization. The Institutional Review Board approved this retrospective study, and the requirement to obtain written informed consent was waived.

Technical Features and Interpretation Criteria for SRS and PET/CT

SRS included anterior and posterior whole-body planar images (matrix, 256 × 1,024; speed, 8–10 cm/min), and abdominopelvic SPECT/CT (21 patients) or abdominopelvic SPECT (6 patients) was performed 4 and 24 h after intravenous injection of 148–259 MBq (4–7 mCi) of ^{111}In-pentetreotide using a 2-head γ camera (ECAM or Symbia T6; Siemens) equipped with medium-energy parallel-hole collimators. Twenty percent energy windows were centered at 172 and 245 keV. Using a 360° arch and step-and-shoot acquisition, 64 projections lasting 45 s each were acquired with a 64 × 64 matrix. Images were reconstructed from projection data using a common iterative algorithm. For SPECT/CT, a CT scan (110 kV, 80 mAs, 2.5-mm slice thickness) was obtained for attenuation correction and localization of scintigraphic abnormalities.

A combined PET/CT scanner was used for all patients (Discovery ST; GE Healthcare). Patients fasted 4 h before tracer injection. They were administered a 4 MBq/kg dose of ^{18}F-FDOPA without carbidopa premedication. ^{18}F-FDOPA PET/CT images were acquired in the early phase (centered over the abdomen) and the delayed phase (whole-body acquisition) at 10 and 30–45 min after injection, respectively. PET/CT images were acquired from head to mid thigh. Unenhanced CT was performed using 140 kV, 80 mAs, and 0.8 s/rotation. Three-dimensional PET was performed using 7 fields of view, 15 cm/field, 3–4 min/field, and a 3.27-mm slice thickness. PET data were reconstructed with and without CT-based attenuation correction using ordered subsets expectation maximization (2 iterations, 21 subsets, 128 × 128 matrix). CT data were reconstructed using an approximately 1-mm section thickness, a 15-cm field of view, and a high-resolution kernel. The same PET/CT scanner was used for ^{18}F-FDG imaging, with CT at the same setting being acquired first, followed by PET (4 min per bed position) 45–60 min after ^{18}F-FDG injection. For ^{18}F-FDG PET/CT, the patients fasted 6 h before the intravenous injection of a 4.5 MBq/kg dose of ^{18}F-FDG. CT, PET (after attenuation correction), and PET/CT fusion images were displayed on a Xeleris workstation (GE Healthcare) for analysis.

Two experienced nuclear medicine physicians who were aware of the clinical and pathologic background of each patient interpreted the SRS and ^{18}F-FDOPA PET/CT images as positive or negative for primary NET localization. A focal extraphysiologic increase of tracer uptake was considered to be tumoral. In cases of conflicting results between the 2 reviewers, a third physician was required for reaching a consensus. Pathologic analysis was used as the gold standard for the diagnosis of primary NETs.

For comparison with SRS, all affected regions were detailed as follows: liver, bone, lung, lymph nodes, brain, and other. Multiple foci of pathologic tracer uptake in the same region were considered to be a single localization. ^{18}F-DOPA PET/CT and SRS results were considered concordant when both tracers detected the same involved organ and discordant when pathologic uptake was present in a single functional imaging modality. In this situation, the final diagnosis was based on the conventional imaging, histology, or follow-up data.

Statistical Analysis

Results are expressed as mean, range, and percentage. ^{18}F-FDOPA PET/CT sensitivity for the localization of the primary tumor was calculated. Between-group comparisons were performed using the χ^2 test for qualitative variables. P values of less than 0.05 were considered statistically significant. All statistical analyses were performed using SPSS software, version 17.0 (IBM).

RESULTS

Patients and Tumors

Twenty-seven patients were eligible for final analysis. There were 16 men (59%) and 11 women, with a mean age of 60 y (range, 25–76 y). Twenty-three patients underwent ^{18}F-FDOPA PET/CT for initial staging and the remaining 4 patients for follow-up during therapy, which consisted of chemotherapy in 3 patients and peptide-receptor radiotherapy in 1 patient. NET was diagnosed from pathologic analysis of liver metastases in 19 patients (70%), retroperitoneal or mesenteric lymph node metastases in 6 patients (22%), upper-clavicular lymph node metastases in 2 patients (7%), peritoneal carcinomatosis in 2 patients (7%), adrenal metastasis in 1 patient (4%), and lung metastasis in 1 patient (4%). NETs were classified as well differentiated and poorly differentiated in, respectively, 23 patients (85%) and 4 patients (15%), and tumor stages were G1, G2, and G3 in 5 patients (18%), 18 patients (67%), and 4 patients (15%), respectively (*24,25*). Most patients (20/27 [74%]) had clinical symptoms consisting of a variable association of diarrhea (55%), flushing (40%), abdominal pain (15%), anorexia (15%), and weight loss (40%). Serum chromogranin A was elevated in 17 patients (63%). Moreover, both serum serotonin and urinary 5-hydroxyindolacetic acid values were elevated in 13 patients (48%).

^{18}F-FDOPA PET/CT Findings for Localization of Primary Tumor

Among the 27 selected patients with negative SRS results, ^{18}F-FDOPA PET/CT successfully detected the primary tumor with subsequent histologic confirmation in 12 patients (overall sensitivity, 44%; 52% in patients evaluated at initial diagnosis). According to tumor differentiation, the sensitivity of ^{18}F-FDOPA PET/CT for detection of the primary tumor was 48% (11/23 patients) and 25% (1/4 patients) in patients with well differentiated and poorly differentiated NET metastases, respectively.

More patients with positive ^{18}F-FDOPA PET/CT results than patients with negative results were symptomatic (100% vs. 53%,

$P = 0.01$) and had higher values of serum chromogranin A (100% vs. 20%, $P = 0.0003$), serotonin, or urinary 5-hydroxyindolacetic acid (83% vs. 20%, $P = 0.003$).

The primary tumors detected by ^{18}F-FDOPA PET/CT were distributed and graded as follows: 1 duodenum G2 lesion, 7 ileum G2 lesions, 2 terminal ileum G1 lesions, 1 pancreas G2 lesion, and 1 gallbladder G3 lesion. The Ki-67 index ranged from 1% to 60% and was always equal to or higher than its metastatic counterpart.

All primary tumors were detected on whole-body images (Fig. 1). The single primary pancreatic NET (patient 6) was visible despite a faint and homogeneous ^{18}F-FDOPA uptake in the whole pancreas. In 2 patients, ^{18}F-FDOPA PET/CT showed prostatic uptake, which was considered unrelated to the NET disease. Histologic analysis was available for 1 patient and showed nonspecific inflammation. Two false-negative results were related to duodenal and prostatic poorly differentiated NETs (G3) (patients 8 and 3). In 13 patients, the primary tumor was not detected within a mean follow-up of 21 mo (range, 12–32 mo) after PET imaging. In the latter case, the patient died 2 mo after PET imaging from his poorly differentiated NET without identification of the primary NET.

^{18}F-FDG PET/CT was performed on 10 patients and was positive in only 1 patient with a poorly differentiated biliary NET (patient 12).

Patient and tumor characteristics and PET/CT findings are detailed in Table 1

^{18}F-FDOPA PET/CT Metastatic Disease Assessment and Clinical Impact

The comparison between ^{18}F-FDOPA PET/CT and SRS showed a concordant pattern in 8 patients (30%) and discordant results in the remaining 19 (70%). ^{18}F-FDOPA PET/CT showed more localizations than did SRS in 17 patients. Additional lesions were localized as follows: upper diaphragmatic lymph nodes in 12 patients (71%), lower diaphragmatic lymph nodes in 12 patients (71%), liver in 5 patients (29%), bone in 3 patients (18%), and peritoneal carcinomatosis in 1 patient (6%). In the additional discordant situations, SRS showed liver metastases that were occult on ^{18}F-FDOPA PET/CT in 2 patients. Serotonin immunoexpression analysis performed on liver tissue samples was negative in these 2 patients. The primary NET remained occult on both functional imaging modalities in the subsequent follow-up.

If resection of the primary tumor based on ^{18}F-FDOPA PET/CT findings is considered to be a major clinical impact, ^{18}F-FDOPA PET/CT induced a major modification in the therapeutic strategy in 12 (44%) of the 27 patients included. None of the patients who underwent surgery for their primary NET had a false-positive lesion.

DISCUSSION

The present study determined the sensitivity of ^{18}F-FDOPA PET/CT in the detection of primary NETs in a large cohort of patients with negative morphologic and functional imaging results. In our series, the sensitivity of ^{18}F-FDOPA PET/CT was 44% overall and increased to 52% in patients evaluated at initial diagnosis. Furthermore, ^{18}F-FDOPA PET/CT detected more of the involved anatomic regions than did SRS in 17 patients.

Localization of the primary NET remains a diagnostic challenge in different clinical situations such as gastroenteropancreatic tumors, hyperinsulinism, and paraneoplastic Cushing syndrome (*2,13,14*). To date, only a few studies have evaluated the clinical value of ^{18}F-FDOPA PET/CT in NETs (*20–23*), probably because ^{18}F-FDOPA is not routinely available at most imaging centers worldwide. The overall reported sensitivity of ^{18}F-FDOPA PET/CT ranged from 29% to 100% (*19–23*), but results on the detection of the primary tumor have only rarely been specifically addressed (*26,27*). Hoegerle et al. (*20*) were the first to uniquely demonstrate the utility of ^{18}F-FDOPA PET to localize gastroenteropancreatic tumors. They found 88% sensitivity for ^{18}F-FDOPA PET in a series of 8 patients with NETs of unknown origin, with a higher detection rate than SRS (50%) and ^{18}F-FDG (25%). In 2006, Montravers et al. compared SRS and ^{18}F-FDOPA PET/CT in 30 patients with metastatic NETs (*21*). ^{18}F-FDOPA PET/CT detected the unknown primary lesion in only 2 of 7 patients (29%). In another study by the same group, the primary NET was detected by ^{18}F-FDOPA PET/CT in 6 of 16 patients (*22*). In these 2 studies, ^{18}F-FDOPA PET/CT was more sensitive than SRS in patients with secreting carcinoid tumors. In contrast, SRS was superior to ^{18}F-FDOPA PET/CT in noncarcinoid tumors. In our series, as in others, the sensitivity of ^{18}F-FDOPA was clearly influenced by the embryologic origin of the NETs and their tumor differentiation. The detection rate of the primary tumor by ^{18}F-FDOPA PET/CT was higher in well-differentiated NETs of the mid gut. This higher value of ^{18}F-FDOPA PET/CT over SRS is probably related to an increased sensitivity of PET/CT cameras over SPECT/CT cameras and to specific features such as overexpression or increased activity of the amino acid decarboxylase involved in the biosynthesis of serotonin. Fiebrich et al. showed that the whole-body metabolic tumor burden correlates with the amount of serotonin secretion (*28*).

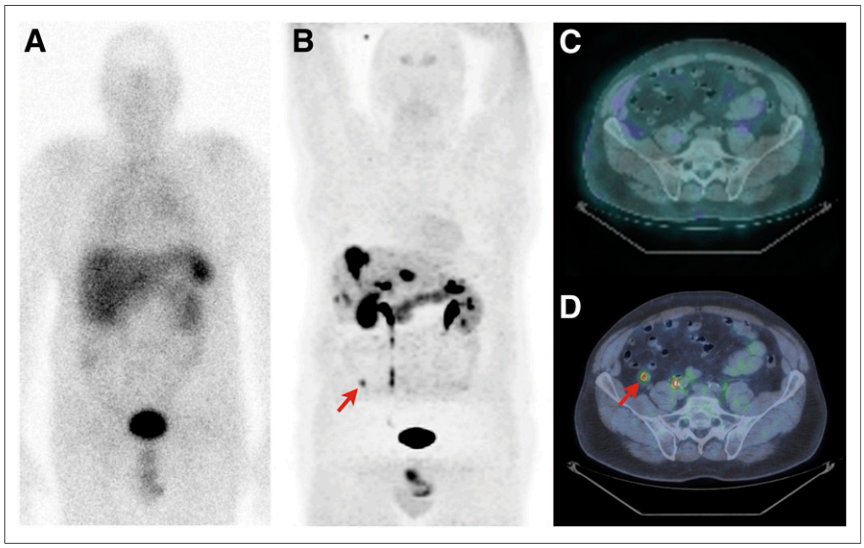

FIGURE 1. SRS anterior whole-body planar imaging (A), ^{18}F-FDOPA PET/CT (anterior maximum-intensity projection) (B), axial SRS SPECT/CT (C), and axial ^{18}F-FDOPA PET/CT (D) performed on a 56-y-old patient (patient 17) with metastatic NET of unknown origin. ^{18}F-FDOPA PET/CT confirmed presence of liver metastases and identified primary tumor in ileum (arrow), occult on both conventional imaging and SRS.

TABLE 1
Patient and Tumor Characteristics and PET/CT Findings

Patient no.	Sex	Age (y)	Clinical symptoms and signs	Tumor markers			Diagnosis of NET (histology)	Treatment before PET/CT	Differentiation and grade (metastasis)			PET/CT findings			Differentiation and grade (primary)		
				Ser	5-HIAA	CgA			Diff (W/P)	Ki67 (%)	G	^{18}F-FDOPA	^{18}F-FDG	Origin	Diff (W/P)	Ki67 (%)	G
1	F	56	None	–	–	–	Liver metastases	None	W	2	1	N	N	Unknown			
2	F	76	Weight loss, diarrhea	+	+	+	Liver metastases	Chemo	W	3	2	N		Unknown			
3	F	62	None	–	–	–	Upper clavicular LN metastasis	None	W	2	1	N		Unknown			
4	F	69	None	–	–	–	Adrenal metastasis	None	W	20	2	N		Unknown			
5	F	69	Weight loss, flushing	+	+	+	Liver metastases	None	W	3	2	Y	N	Ileum	W	5	2
6	F	58	Weight loss	–	–	+	Liver metastases	None	W	5	2	Y		Pancreas	W	7	2
7	M	68	None	–	–	–	Liver metastases	None	W	3	2	N		Unknown			
8	M	55	Weight loss, anorexia	–	–	+	Liver metastases	None	W	10	2	N		Unknown			
9	M	56	Weight loss, anorexia	–	–	–	Liver metastases, peritoneal carcinomatosis	Chemo + MRT	W	15	2	N	N	Unknown			
10	M	66	None	–	–	–	Upper clavicular LN metastasis	None	P	40	3	N	N	Unknown			
11	M	65	Weight loss, flushing	–	–	–	Lung and liver metastases	Chemo	P	35	3	N	N	Unknown			
12	F	50	Abdominal pain	–	–	+	Liver metastases	None	P	60	3	Y	Y	Gallbladder	P	60	3
13	M	48	None	–	–	–	Liver metastases	Chemo	W	3	2	N		Unknown			
14	F	69	None	–	–	–	Retroperitoneal LN metastasis	None	W	3	2	N		Unknown			
15	M	58	Anorexia	–	–	–	Liver metastases	None	P	20	3	N	N	Unknown			
16	M	40	Weight loss, diarrhea	+	+	+	Liver metastases	None	W	2	1	N	N	Unknown			
17	M	55	Flushing, diarrhea	+	+	+	Liver metastases	None	W	5	2	Y		Ileum	W	15	2
18	M	49	Flushing, diarrhea	+	+	+	Mesenteric LN metastases	None	W	3	2	Y		Ileum	W	5	2
19	M	64	Flushing, diarrhea	+	+	+	Retroperitoneal and mesenteric LN metastasis	None	W	5	2	N		Unknown			
20	M	64	Abdominal pain	–	–	–	Intestinal occlusion secondary to peritoneal carcinomatosis	None	W	15	2	N		Unknown			
21	M	66	Weight loss, diarrhea	+	+	+	Liver metastases	None	W	3	2	Y		Ileum	W	5	2
22	M	66	Diarrhea	+	+	+	Liver metastases	None	W	5	2	Y		Ileum	W	7	2
23	F	69	Flushing, diarrhea	+	+	+	Retroperitoneal LN and liver metastasis	None	W	3	2	Y	N	Duodenum	W	5	2
24	M	75	Flushing, diarrhea	+	+	+	Liver metastases	None	W	1	1	Y		Terminal ileum	W	2	1

TABLE 1 (Continued)

Patient no.	Sex	Age (y)	Clinical symptoms and signs	Tumor markers			Diagnosis of NET (histology)	Treatment before PET/CT	Differentiation and grade (metastasis)			PET/CT findings			Differentiation and grade (primary)		
				Ser	5-HIAA	CgA			Diff (W/P)	Ki67 (%)	G	^{18}F-FDOPA	^{18}F-FDG	Origin	Diff (W/P)	Ki67 (%)	G
25	F	25	Diarrhea	+	+	+	Liver metastases	None	W	5	2	Y	N	Ileum	W	5	2
26	M	73	Flushing, diarrhea	+	+	+	Mesenteric LN metastases	None	W	3	2	Y		Ileum	W	5	2
27	F	62	Abdominal pain	+	+	+	Retroperitoneal LN and liver metastasis	None	W	1	1	Y		Terminal ileum	W	1	1

Ser = serum serotonin; 5-HIAA = urinary 5-hydroxyindolacetic acid; CgA = chromogranin A; Diff = differentiation; W = well differentiated; P = poorly differentiated; G = tumor grade; LN = lymph nodes; chemo = chemotherapy; MRT = metabolic radiotherapy.

Accurately localizing NETs plays a critical role in the management of patients with these tumors, especially in determining surgery of the primary tumors (*20–23*). In our series, 12 patients underwent surgery based on ^{18}F-FDOPA PET/CT findings.

Several hypotheses may explain the decrease of ^{18}F-FDOPA PET/CT in noncarcinoid tumors. One hypothesis is that there is a specific imaging phenotype related to the absence of activation of the large neutral amino acid transporter and CD98 transporter systems. It is well established that these tumors exhibit specific responses to targeted therapies, and this molecular singularity may also extend to functional imaging. However, this possibility remains speculative and requires evaluation in further basic science research.

Another explanation may be related to the imaging protocol itself, which may be inappropriate for optimal detection of these tumors. It has been reported that the high physiologic ^{18}F-FDOPA uptake by the whole pancreas potentially reduces the detection rate of pancreatic tumors (*29*). The use of carbidopa before ^{18}F-FDOPA injection for inhibiting amino acid decarboxylase increases the signal-to-background ratio (*30,31*), but negativization of ^{18}F-FDOPA focal pancreatic hot spots has been reported after carbidopa in patients with hyperinsulinemic hypoglycemia.

At present, no recommendation exists concerning the use of carbidopa premedication, but this approach should be further evaluated in this clinical setting as well as the optimal timing for image acquisition.

We acknowledge several limitations to our study: its retrospective design, the limited number of patients, and the short duration of follow-up. However, to our knowledge it is the largest study showing extensive data related to primary tumors.

On the basis of the currently available imaging techniques for diagnosis and staging of NETs, we propose that ^{18}F-FDOPA PET/CT be performed as the first-line functional imaging technique for NETs of unknown origin, especially those with a well-differentiated tumor and serotonin secretion. SRS should be reserved for other situations or when ^{18}F-FDOPA PET/CT findings are negative for a primary tumor or targeted radiotherapy is planned.

The current leading role of ^{18}F-FDOPA PET/CT in the evaluation of NETs will need to be further compared with newly introduced and promising agents for PET imaging such as somatostatin analogs labeled with ^{68}Ga (*32*). High sensitivity has been reported for PET/CT with ^{68}Ga-labeled peptides in patients with clinically, biochemically, or radiologically suspected NET (*33–35*). Recently, some authors prospectively compared ^{68}Ga-DOTANOC and ^{68}Ga-DOTATATE PET/CT in the same patients with gastroenteropancreatic tumor NETs and highlighted the high diagnostic sensitivity of ^{68}Ga-DOTANOC to assess the extent of metastatic disease (*36*). Moreover, ^{68}Ga-DOTANOC PET/CT seems to be a promising diagnostic modality for detecting primary tumor in patients with neuroendocrine carcinoma of unknown origin (*37*). At present, only few clinical investigations involving a limited number of patients with NET have compared the diagnostic role of PET/CT with ^{18}F-FDOPA or ^{68}Ga-labeled somatostatin analogs (*38,39*). ^{68}Ga-DOTANOC PET/CT was found to be more accurate than ^{18}F-FDOPA PET/CT in the detection of primary tumor and metastatic disease. Unfortunately, the heterogeneity of the studied population still represents a major bias for a reliable head-to head comparison of the imaging approaches.

CONCLUSION

^{18}F-FDOPA PET appears to be a sensitive functional imaging tool for the detection of primary NETs occult on SRS. Some

unanswered questions arise from lesions missed by ^{18}F-FDOPA PET, including specific genetic or molecular features and the possibility of inappropriate acquisition protocols.

DISCLOSURE

The costs of publication of this article were defrayed in part by the payment of page charges. Therefore, and solely to indicate this fact, this article is hereby marked "advertisement" in accordance with 18 USC section 1734. No potential conflict of interest relevant to this article was reported.

REFERENCES

1. Plöckinger U, Rindi G, Arnold R, et al. Guidelines for the diagnosis and treatment of neuroendocrine gastrointestinal tumours: a consensus statement on behalf of the European Neuroendocrine Tumour Society (ENETS). *Neuroendocrinology.* 2004; 80:394–424.
2. Modlin IM, Gustafsson BI, Kidd M. Gastrointestinal carcinoid tumors. In Howden CW, Baillie J, Buchman AL, Metz DC, Modlin IM, eds. *Advances in Digestive Disease*. Bethesda, MD: AGA Institute Press; 2007:203–218.
3. Hainsworth JD, Spigel DR, Litchy S, Greco FA. Phase II trial of paclitaxel, carboplatin, and etoposide in advanced poorly differentiated neuroendocrine carcinoma: a Minnie Pearl Cancer Research Network Study. *J Clin Oncol.* 2006;24:3548–3554.
4. Karsell PR, Sheedy PF II, O'Connel MJ. Computed tomography in search of cancer of unknown origin. *JAMA.* 1982;248:340–343.
5. Kwekkeboom DJ, Krenning EP, Lebtahi R, et al. ENETS consensus guidelines for the standards of care in neuroendocrine tumors: peptide receptor radionuclide therapy with radiolabeled somatostatin analogs. *Neuroendocrinology.* 2009;90: 220–226.
6. Öberg K, Castellano D. Current knowledge on diagnosis and staging of neuroendocrine tumors. *Cancer Metastasis Rev.* 2011;30(suppl):3–7.
7. Rothenstein J, Clearly SP, Pond GR, et al. Neuroendocrine tumors of the gastrointestinal tract: a decade of experience at the Princess Margaret Hospital. *Am J Clin Oncol.* 2008;31:64–70.
8. Kirshbom PM, Kherani AR, Onaitis MW, Feldman JM, Tyler DS. Carcinoids of unknown origin: comparative analysis with foregut, midgut, and hindgut carcinoids. *Surgery.* 1998;124:1063–1070.
9. Abbruzzese JL, Abbruzzese MC, Lenzi R, Hess KR, Raber MN. Analysis of a diagnostic strategy for patients with suspected tumors of unknown origin. *J Clin Oncol.* 1995;13:2094–2103.
10. Crocetti E, Paci E. Malignant carcinoids in the USA, SEER 1992-1999: an epidemiological study with 6830 cases. *Eur J Cancer Prev.* 2003;12:191–194.
11. Yao JC, Shah MH, Ito T, et al. Everolimus for advanced pancreatic neuroendocrine tumors. *N Engl J Med.* 2011;364:514–523.
12. Raymond E, Dahan L, Raoul JL, et al. Sunitinib malate for the treatment of pancreatic neuroendocrine tumors. *N Engl J Med.* 2011;364:501–513.
13. Anderson MA, Carpenter S, Thompson NW, Nostrant TT, Elta GH, Scheiman JM. Endoscopic ultrasound is highly accurate and directs management in patients with neuroendocrine tumors of the pancreas. *Am J Gastroenterol.* 2000;95:2271–2277.
14. Landry CS, Scoggins CR, McMasters KM, Martin RC II. Management of hepatic metastasis of gastrointestinal carcinoid tumors. *J Surg Oncol.* 2008;97:253–258.
15. Minn H, Kauhanen S, Seppänen M, Nuutila P. ^{18}F-FDOPA: a multiple-target molecule. *J Nucl Med.* 2009;50:1915–1918.
16. Rust E, Hubele F, Marzano E, et al. Nuclear medicine imaging of gastro-entero-pancreatic neuroendocrine tumors: the key role of cellular differentiation and tumor grade: from theory to clinical practice. *Cancer Imaging.* 2012;12:173–184.
17. Krämer SD, Mu L, Müller A, et al. 5-(2-^{18}F-fluoroethoxy)-L-tryptophan as a substrate of system L transport for tumor imaging by PET. *J Nucl Med.* 2012;53:434–442.
18. Jager PL, Chirakal R, Marriott CJ, Brouwers AH, Koopmans KP, Gulenchyn KY. 6-L-^{18}F-fluorodihydroxyphenylalanine PET in neuroendocrine tumors: basic aspects and emerging clinical applications. *J Nucl Med.* 2008;49:573–586.
19. Balogova S, Talbot JN, Nataf V, et al. ^{18}F-fluorodihydroxyphenylalanine vs other radiopharmaceuticals for imaging neuroendocrine tumours according to their type. *Eur J Nucl Med Mol Imaging.* 2013;40:943–966.
20. Hoegerle S, Altehoefer C, Ghanem N, et al. Whole-body ^{18}F dopa PET for detection of gastrointestinal carcinoid tumors. *Radiology.* 2001;220:373–380.
21. Montravers F, Grahek D, Kerrou K, et al. Can fluorodihydroxyphenylalanine PET replace somatostatin receptor scintigraphy in patients with digestive endocrine tumors? *J Nucl Med.* 2006;47:1455–1462.
22. Montravers F, Kerrou K, Nataf V, et al. Impact of fluorodihydroxyphenylalanine-^{18}F positron emission tomography on management of adult patients with documented or occult digestive endocrine tumors. *J Clin Endocrinol Metab.* 2009;94:1295–1301.
23. Ambrosini V, Tomassetti P, Rubello D, et al. Role of ^{18}F-dopa PET/CT imaging in the management of patients with ^{111}In-pentetreotide negative GEP tumours. *Nucl Med Commun.* 2007;28:473–477.
24. Klimstra DS, Modlin IR, Coppola D, Lloyd RV, Suster S. The pathologic classification of neuroendocrine tumors: a review of nomenclature, grading, and staging systems. *Pancreas.* 2010;39:707–712.
25. Rindi G, Arnold R, Bosman FT. Nomenclature and classification of neuroendocrine neoplasms of the digestive system. In: Bosman FT, Carneiro F, Hruban PH, Theise ND, et al., eds. *WHO Classification of Tumors of the Digestive System.* Lyon, France: IARC; 2010.
26. Becherer A, Szabo M, Karanikas G, et al. Imaging of advanced neuroendocrine tumors with ^{18}F-FDOPA PET. *J Nucl Med.* 2004;45:1161–1167.
27. Koopmans KP, de Vries EG, Kema IP, et al. Staging of carcinoid tumours with ^{18}F-DOPA PET: a prospective, diagnostic accuracy study. *Lancet Oncol.* 2006;7:728–734.
28. Fiebrich HB, de Jong JR, Kema IP, et al. Total ^{18}F-dopa PET tumour uptake reflects metabolic endocrine tumour activity in patients with a carcinoid tumour. *Eur J Nucl Med Mol Imaging.* 2011;38:1854–1861.
29. Tessonnier L, Sebag F, Ghander C, et al. Limited value of ^{18}F-F-DOPA PET to localize pancreatic insulin-secreting tumors in adults with hyperinsulinemic hypoglycemia. *J Clin Endocrinol Metab.* 2010;95:303–307.
30. Neels OC, Koopmans KP, Jager PL, et al. Manipulation of [^{11}C]-5-hydroxytryptophan and 6-[^{18}F]fluoro-3,4-dihydroxy-L-phenylalanine accumulation in neuroendocrine tumor cells. *Cancer Res.* 2008;68:7183–7190.
31. Imperiale A, Addeo F, Averous G, Namer IJ, Bachellier P. Solid-pseudopapillary pancreatic tumor mimicking a neuroendocrine neoplasm on ^{18}F-FDOPA PET/CT. *J Clin Endocrinol Metab.* 2013;98:2643–2644.
32. Ambrosini V, Campana D, Nanni C, et al. Is ^{68}Ga-DOTA-NOC PET/CT indicated in patients with clinical, biochemical or radiological suspicion of neuroendocrine tumour? *Eur J Nucl Med Mol Imaging.* 2012;39:1278–1283.
33. Gabriel M, Decristoforo C, Kendler D, et al. ^{68}Ga-DOTA-Tyr3-octreotide PET in neuroendocrine tumors: comparison with somatostatin receptor scintigraphy and CT. *J Nucl Med.* 2007;48:508–518.
34. Buchmann I, Henze M, Engelbrecht S, et al. Comparison of ^{68}Ga-DOTATOC PET and ^{111}In-DTPAOC (Octreoscan) SPECT in patients with neuroendocrine tumours. *Eur J Nucl Med Mol Imaging.* 2007;34:1617–1626.
35. Srirajaskanthan R, Kayani I, Quigley AM, Soh J, Caplin ME, Bomanji J. The role of ^{68}Ga-DOTATATE PET in patients with neuroendocrine tumors and negative or equivocal findings on ^{111}In-DTPA-octreotide scintigraphy. *J Nucl Med.* 2010;51:875–882.
36. Wild D, Bomanji JB, Benkert P, et al. Comparison of ^{68}Ga-DOTANOC and ^{68}Ga-DOTATATE PET/CT within patients with gastroenteropancreatic neuroendocrine tumors. *J Nucl Med.* 2013;54:364–372.
37. Naswa N, Sharma P, Kumar A, et al. ^{68}Ga-DOTANOC PET/CT in patients with carcinoma of unknown primary of neuroendocrine origin. *Clin Nucl Med.* 2012;37:245–251.
38. Ambrosini V, Tomassetti P, Castellucci P, et al. Comparison between ^{68}Ga-DOTA-NOC and ^{18}F-DOPA PET for the detection of gastro-entero-pancreatic and lung neuro-endocrine tumours. *Eur J Nucl Med Mol Imaging.* 2008;35: 1431–1438.
39. Haug A, Auernhammer CJ, Wangler B, et al. Intraindividual comparison of ^{68}Ga-DOTA-TATE and ^{18}F-DOPA PET in patients with well-differentiated metastatic neuroendocrine tumours. *Eur J Nucl Med Mol Imaging.* 2009;36:765–770.

Eur J Nucl Med Mol Imaging
DOI 10.1007/s00259-014-2943-z

ORIGINAL ARTICLE

^{18}F-FDOPA PET/CT imaging of insulinoma revisited

Alessio Imperiale · Frédéric Sebag · Michel Vix · Frédéric Castinetti · Laurence Kessler · François Moreau · Philippe Bachellier · Benjamin Guillet · Izzie-Jacques Namer · Olivier Mundler · David Taïeb

Received: 15 August 2014 / Accepted: 13 October 2014

Abstract
Purpose ^{18}F-FDOPA PET imaging is increasingly used in the work-up of patients with neuroendocrine tumours. It has been shown to be of limited value in localizing pancreatic insulin-secreting tumours in adults with hyperinsulinaemic hypoglycaemia (HH) mainly due to ^{18}F-FDOPA uptake by the whole pancreatic gland. The objective of this study was to review our experience with ^{18}F-FDOPA PET/CT imaging with carbidopa (CD) premedication in patients with HH in comparison with PET/CT studies performed without CD premedication in an independent population.
Methods A retrospective study including 16 HH patients who were investigated between January 2011 and December 2013 using ^{18}F-FDOPA PET/CT (17 examinations) in two academic endocrine tumour centres was conducted. All PET/CT examinations were performed under CD premedication (200 mg orally, 1 – 2 h prior to tracer injection). The PET/CT acquisition protocol included an early acquisition (5 min after ^{18}F-FDOPA injection) centred over the upper abdomen and a delayed whole-body acquisition starting 20 – 30 min later. An independent series of eight consecutive patients with HH and investigated before 2011 were considered for comparison. All patients had a reference whole-body PET/CT scan performed about 1 h after ^{18}F-FDOPA injection. In all cases, PET/CT was performed without CD premedication.
Results In the study group, ^{18}F-FDOPA PET/CT with CD premedication was positive in 8 out of 11 patients with histologically proven insulinoma (73 %). All ^{18}F-FDOPA PET/CT-avid insulinomas were detected on early images and 5 of 11 (45 %) on delayed ones. The tumour/normal pancreas uptake ratio was not significantly different between early and delayed acquisitions. Considering all patients with HH, including those without imaging evidence of disease, the detection rate of the primary lesions using CD-assisted ^{18}F-FDOPA PET/CT was 53 %, showing 9 insulinomas in 17 studies performed. In the control group (without CD premedication, eight patients), the final diagnosis was benign insulinoma in four, nesidioblastosis in one, and no definitive diagnosis in the

A. Imperiale · I.-J. Namer
Department of Biophysics and Nuclear Medicine, University Hospitals of Strasbourg, Strasbourg, France

A. Imperiale · I.-J. Namer
Faculty of Medicine, ICube - UMR 7357, University of Strasbourg/CNRS and FMTS, Strasbourg, France

F. Sebag
Department of Endocrine Surgery, La Timone University Hospital, Aix-Marseille University, Marseille, France

M. Vix
Department of General, Digestive, and Endocrine Surgery, IRCAD-IHU, University of Strasbourg, Strasbourg, France

F. Castinetti
Department of Endocrinology, Diabetes and Metabolic Disorders, La Timone University Hospital, Aix-Marseille University, Marseille, France

L. Kessler · F. Moreau
Department of Diabetology, University Hospital of Strasbourg, University of Strasbourg, Strasbourg, France

P. Bachellier
Department of Visceral Surgery and Transplantation, University Hospitals of Strasbourg, Strasbourg, France

B. Guillet · O. Mundler · D. Taïeb
Department of Nuclear Medicine, La Timone University Hospital, CERIMED, Aix-Marseille University, Marseille, France

D. Taïeb (✉)
Biophysics and Nuclear Medecine, La Timone University Hospital, European Center for Research in Medical Imaging, Aix-Marseille University, 264, rue Saint-Pierre, 13385 Marseille, France
e-mail: david.taieb@ap-hm.fr

Published online: 01 November 2014

remainder. ^{18}F-FDOPA PET/CT failed to detect any tumour in these patients.

Conclusion According to our experience, CD administration before ^{18}F-FDOPA injection leads to low residual pancreatic ^{18}F-FDOPA activity preserving tumoral uptake with consequent insulinoma detection in more than half of adult patients with HH and more than 70 % of patients with a final diagnosis of insulinoma. If ^{18}F-FDOPA PET/CT is indicated, we strongly recommend combining CD premedication with early acquisition centred over the pancreas.

Keywords ^{18}F-FDOPA · Carbidopa · PET/CT · Hyperinsulinaemic hypoglycaemia · Insulinoma

Introduction

Hyperinsulinaemic hypoglycaemia (HH) is the most common disorder of pancreatic islet cell hyperfunction. The diagnosis of HH is based on the typical positive fast test [1]. In adults, HH is usually caused by insulinoma, which is usually sporadic, unique and benign. Approximately 10 % of insulinomas are malignant, and 10 % are multiple, particularly in patients with multiple endocrine neoplasia type 1 (MEN1) syndrome. Localization of insulinoma remains challenging. The diagnostic approach with functional imaging is not mandatory when the tumour is located using conventional imaging diagnostic techniques such as CT, MRI or endoscopic ultrasonography (EUS) examination. However, when conventional anatomical imaging is negative or inconclusive for a single abnormality, functional imaging may be of particular interest for insulinoma detection or characterization. In clinical practice, imaging work-up of patients with HH often requires a combination of anatomical and functional imaging modalities.

Until recently, a highly sensitive functional imaging tool has not been available for localizing insulinomas. The radiopharmaceutical ^{111}In-pentetreotide (Octreoscan), which mainly targets the subtype 2 of somatostatin receptors (sst2), was introduced in the 1990s with excellent results in some cases, performing so-called in vivo histology. Unfortunately, insulinomas express sst2 with an incidence of 60 %. Moreover, the density of sst2 is often variable and sometimes too low for effective somatostatin receptor targeting [2–4]. Furthermore, one-third of insulinomas are under 1 cm in diameter and can therefore be missed by conventional low-resolution gamma cameras [5, 6]. Consequently, the overall sensitivity of scintigraphic examinations using ^{111}In-radiolabelled somatostatin analogues for insulinoma detection remains unsatisfactory [7]. PET imaging using ^{68}Ga-labelled somatostatin analogues has been introduced for imaging neuroendocrine tumours (NET), but to date its sensitivity in imaging insulinomas is largely unknown, with disappointing preliminary results [8].

Although in recent years, a scientific effort focusing on the development of more specific radiopharmaceuticals has been initiated, to date, the gold-standard functional imaging technique remains to be determined. The radiolabelled glucagon-like peptide-1 (GLP-1) analogues for conventional scintigraphic studies or PET/CT imaging have shown promising results related to the overexpression of the GLP-1 receptor (GLP1R) in most insulinomas [9–11]. However, these radiopharmaceuticals are not available at most imaging centres worldwide and should be used in humans in the setting of clinical trials only. ^{18}F-Fluorodihydroxyphenylalanine (^{18}F-FDOPA) has been previously proposed for PET imaging of insulinoma, showing encouraging results in a single series of ten adult patients [12]. However, our initial experience with ^{18}F-FDOPA PET/CT has been somewhat disappointing, a finding that was mainly attributed to the intense and prolonged ^{18}F-FDOPA uptake by the mature exocrine pancreas [13]. Indeed, the pancreas has been shown to have an efficient mechanism for the uptake and decarboxylation of amino acids and their precursors such as L-DOPA. Evidence exists that carbidopa (CD), an efficient inhibitor of the peripheral aromatic amino acid decarboxylase (AADC), may improve both ^{18}F-FDOPA and ^{11}C-5-hydroxytryptophan PET interpretation by significantly increasing tumour uptake while lowering physiological pancreatic uptake [14, 15].

Nevertheless, patient premedication with CD remains inconsistently performed across oncological studies using ^{18}F-DOPA PET imaging [16]. On the other hand, no final consensus has been reached about the usefulness of AADC inhibition by CD premedication before ^{18}F-FDOPA PET in patients with insulinoma or β-cell hyperplasia [17–19]. Furthermore, the CD dosage and the optimal protocol for ^{18}F-FDOPA PET/CT acquisitions are not definitively standardized in clinical practice (200 mg [20], 100 mg [21], 2 mg/kg [22, 23]). The aim of the present study was to assess the performance of an ^{18}F-FDOPA PET/CT protocol combining CD premedication and early PET acquisitions for detecting insulinomas in a cohort of adult patients with HH. This diagnostic approach was also compared with a standard ^{18}F-FDOPA PET/CT protocol without CD administration in an independent patient series.

Materials and methods

Patient population

Among all patients who underwent ^{18}F-FDOPA PET/CT between January 2011 and December 2013 for clinical and biological suspicion of insulinoma in two academic endocrine tumour centres (La Timone University Hospital, Marseille, and Hautepierre University Hospital, Strasbourg), only those who fulfilled the following criteria were retrospectively included: (1) age 18 years or older (i.e., adult patients), (2) HH

defined by a positive fasting test [1], (3) absence of personal or familial history of MEN-1 or MEN-1-related syndromic manifestations, (4) patient premedication by CD before ^{18}F-FDOPA injection, and (5) early and delayed PET/CT acquisitions.

In all selected patients, the imaging work-up was performed during the 3 months prior to PET/CT, and included both contrast-enhanced three-phase thoracoabdominal CT and pancreatic MRI. Imaging findings were considered concordant and positive when they showed the same pancreatic abnormality that was subsequently proven histologically to be an insulinoma. Most of the patients were also investigated using EUS. Follow-up data were obtained for at least 12 months following ^{18}F-FDOPA PET/CT. An independent series of nine consecutive patients with HH who were investigated before 2011 with ^{18}F-FDOPA PET/CT without CD premedication were considered for comparison. A subgroup of the cohort has been previously reported [13]. ^{18}F-FDOPA was used in the setting of marketing authorization. In keeping with local institutional guidelines, all patients gave informed consent for the use of anonymized personal data extracted from their medical records for scientific or epidemiological purposes.

^{18}F-FDOPA PET/CT: imaging protocols

PET/CT with carbidopa premedication

A combined PET/CT scanner was used for all scans (Discovery ST, GE Medical Systems). Patients did not fast before radiotracer injection. ^{18}F-FDOPA (4 MBq/kg) was injected intravenously 1 – 2 h after CD premedication (200 mg orally). Pharmaceutical grade CD was purchased from Inresa (Bartenheim, France), and 200-mg capsules were delivered as pharmaceutical compounding (according to the European Pharmacopoeia; Ph Eur monograph 0755) by the hospital central pharmacy to the nuclear medicine unit in both institutions. The ^{18}F-FDOPA PET/CT acquisition protocol included an early acquisition (5 min after injection) centred over the upper abdomen (one 10-min step) and a delayed whole-body acquisition (starting between 20 and 30 min after injection) from the top of the skull to the upper thigh (3 – 5 min/step).

PET/CT without carbidopa premedication

Patients did not receive any antihypoglycaemic medication or glucose infusion and had fasted for 6 h before radiotracer injection. ^{18}F-FDOPA was injected at 4 MBq/kg body mass. All patients had a whole-body reference acquisition about 1 h after radiotracer injection from the skull to the upper thigh. In all patients, ^{18}F-FDOPA PET/CT was performed without CD premedication.

^{18}F-FDOPA PET/CT: image interpretation

PET image datasets from both patient groups were reconstructed iteratively (OSEM algorithm) using CT data for attenuation correction. Coregistered images were displayed on a workstation (Xeleris; GE Healthcare) and independently interpreted by two experienced nuclear medicine physicians who were blinded to the results of other imaging investigations. A positive pancreatic abnormality was defined as a focal area of increased ^{18}F-FDOPA uptake compared to surrounding tissue. ^{18}F-FDOPA PET/CT studies were qualitatively interpreted as positive or negative for pancreas primary tumour location (i.e. insulinoma). In the event of results conflicting between the two reviewers, a third physician was required to reach a consensus. Extrapancreatic uptake foci in nonphysiological areas were considered as metastases.

In positive PET/CT studies, both the tumour maximum standardized uptake value (SUV_{max}) and the normal pancreatic mean standardized uptake value (SUV_{mean}) were measured for quantitative assessment of ^{18}F-FDOPA uptake. Tumour SUV_{max} was defined within a spherical volume of interest centred on the tumour and including it completely. The SUV_{mean} was measured in the normal pancreas within a 1-cm^3 spherical volume of interest taking care to avoid eventual biliary stasis. Hence, the tumour/normal pancreas ratio was calculated as: tumour SUV_{max}/normal pancreas SUV_{mean}.

Gold standard

The normalization of blood glucose levels after resection of the pancreatic lesion, as well as the cytological and/or pathological diagnosis of insulinoma, were considered the diagnostic gold standard for solitary insulinoma. The diagnosis of nesidioblastosis was based on exclusion of an insulinoma and conclusive pathological examination of a segment of the pancreas. Malignant insulinoma was defined as the presence of nodal or visceral metastases.

Statistical analysis

Fisher's exact test was used to compare the diagnostic performance of the two imaging protocols (with and without CD premedication) carried out in two independent populations. The results of early and delayed ^{18}F-FDOPA PET/CT in the same population were compared using the McNemar test and the Sign test. Statistical significance was defined as $p<0.05$. Statistical analysis was performed using the Statistica (Statsoft) version 7 software package.

Results

^{18}F-FDOPA PET/CT findings in patients evaluated after carbidopa premedication

During the study period (2011 – 2013), 16 consecutive patients (10 women, 5 men; age range 20 – 81 years) with HH were evaluated using CD-assisted ^{18}F-FDOPA PET/CT before any pancreatic surgery (Table 1). One patient (patient 3) underwent a second PET/CT examination for recurrent HH after surgical excision of an insulinoma. Therefore, 17 ^{18}F-FDOPA PET/CT studies were finally performed.

Multiphasic CT and MRI were positive concordant or positive discordant for a pancreatic lesion with typical feature of NET in five and five patients, respectively. Conventional imaging failed to identify any pancreatic abnormality in the seven remaining patients. EUS performed in 13 patients and showed focal pancreatic abnormalities suggestive of solitary insulinoma in 8 of them. In three patients, EUS was positive with normal CT or MRI results. One patient had metastatic disease (nodal and liver involvement) with unresectable primary pancreatic tumour and was subsequently treated with diazoxide to control severe hypoglycaemia. Malignancy was defined by histologically proven liver metastases.

The final diagnosis was benign insulinoma in 11 patients (65 %) and malignant insulinoma in one patient. In the remaining five patients, the tumour remained occult in all imaging studies. Normal pancreatic parenchyma was only faintly visible in all the patients, suggesting the effective inhibitory influence of CD on normal acinar ^{18}F-FDOPA uptake.

PET/CT was positive in 8 of 11 patients (73 %) with histologically proven solitary insulinoma (Fig. 1) and in one patient with malignant insulinoma. PET/CT failed to detect three solitary insulinomas measuring 12, 25 and 26 mm. The median size of the ^{18}F-FDOPA PET/CT-positive benign tumours was 16 mm (range 4 – 40 mm). Among the eight insulinomas accurately detected on early images, three (13, 15 and 16 mm) were missed on delayed images (detection rate 45 %; Fig. 2). However, there was no statistically significant difference in tumour detection rate between early and delayed PET/CT studies.

Considering all patients with HH, including five without imaging evidence of disease, the primary lesion detection rate on ^{18}F-FDOPA PET/CT was 53 % (9/17 studies). In the 11 patients with histologically proven insulinoma (one malignant and ten benign tumours), ^{18}F-FDOPA PET/CT showed concordant positive findings in six and no concordant negative findings when compared with the CT and MRI results. In the patient with malignant insulinoma, PET/CT was positive for the primary tumour and metastases but failed to identify millimetric liver metastases revealed by MRI. In the remaining five patients, the results of PET/CT and conventional imaging were discordant: PET/CT was negative and conventional imaging positive in three patients, and PET/CT was positive and conventional imaging negative in the two remaining patients. The primary tumour remained occult on imaging by all modalities and EUS in five patients.

In positive ^{18}F-FDOPA PET/CT studies, the mean tumour/normal pancreas ratio was 3.0±1.4 (range 1.3 – 4.9) and 2.7±1.0 (range 1.4 – 4.5) in early and delayed PET acquisitions, respectively (not significant).

^{18}F-FDOPA PET/CT findings in patients evaluated without carbidopa premedication

Before 2011, eight consecutive patients (five women, three men; age range 16 – 81 years) with HH were evaluated before any pancreatic surgery using ^{18}F-FDOPA PET/CT without CD administration (Table 2). In all selected patients, the imaging work-up performed before PET/CT consisted of a variable combination of contrast-enhanced three-phase thoracoabdominal CT, pancreatic MRI and EUS.

The final diagnosis was benign insulinoma in four patients (50 %) and nesidioblastosis in one other patient. In the remaining three patients, no lesion was detected. Normal pancreatic parenchyma always showed a physiological, diffuse and intense ^{18}F-FDOPA uptake (Fig. 3). PET/CT was positive in none of the four patients with histologically proven insulinoma, showing no pancreatic focal radiotracer uptake higher than normal pancreas. Moreover, no regional uptake was seen in patients with nesidioblastosis. Finally, ^{18}F-FDOPA PET/CT failed to detect any tumour in the eight patients without CD premedication.

Comparison between ^{18}F-FDOPA PET/CT protocols

The results can be summarized as follows:

1. ^{18}F-FDOPA PET/CT with CD premedication was positive in 8 of 11 patients with histologically proven solitary insulinoma, a detection rate of 73 %. In the control patients who underwent PET/CT without CD premedication, none of the confirmed lesions (four insulinomas, one nesidioblastosis) was detected ($p<10^{-3}$).
2. Among all patients with HH, including those without imaging evidence of disease, the detection rate of the primary lesions by ^{18}F-FDOPA PET/CT with and without CD premedication was 53 % (9/17) and 0 %, respectively ($p<10^{-3}$).

Discussion

^{18}F-FDOPA PET has been shown to be able to distinguish focal from diffuse β-cell hyperplasia in newborns with HH

Table 1 Patients with hyperinsulinaemic hypoglycaemia evaluated with carbidopa-assisted ^{18}F-FDOPA PET/CT

Patient no.	Age (years)	Sex	Conventional imaging[a]		EUS	Tumour			^{18}F-FDOPA		Medical treatment	Final diagnostic procedure	Final diagnosis
			Positive/ negative	Concordant/ discordant		No. of lesions	Size (mm)	Location	Early	Delayed			
1	20	F	+	Discordant (MRI >)	Not available	3	Largest 25	Tail	+	+	None	Pancreatic surgery	Insulinoma grade 2
2	50	F	−	Concordant	+	1	4	Tail	+	+	None	Pancreatic surgery	Insulinoma grade 1
3	44	M	+	Concordant	Not available	1	25	Body	−	−	Proglycem	Pancreatic surgery	Insulinoma grade 1
3[b]	45	M	+	Concordant	Not available	1	16	Body	+	−	None	Pancreatic surgery	Relapsing insulinoma grade 2
4	51	F	+	Concordant	Not available	1	78	Body/tail	+	+	Proglycem	Lymph node metastasis biopsy (+)	Malignant insulinoma
5	81	F	+	Concordant	−	1	20	Body/tail	+	+	Proglycem	Pancreatic surgery	Insulinoma grade 1
6	44	F	−	Concordant	−				−	−	None	Clinical follow-up	HH without structural disease
7	33	F	−	Concordant	−				−	−	Proglycem	Clinical follow-up	HH without structural disease
8	48	F	+	Discordant (MRI only)	+	1	13	Uncus	+	−	None	Pancreatic surgery	Insulinoma grade 1
9	47	M	−	Concordant	−				−	−	None	Clinical follow-up	HH without structural disease
10	43	F	−	Concordant	+	1	15	Isthmus	+	−	None	Pancreatic surgery	Insulinoma grade 2
11	68	F	+	Discordant (MRI >)	+	4	Largest 12	Head	−	−	None	US-guided cytology (+)	Insulinoma grade 1
12	70	M	+	Concordant	+	1	40	Uncus	+	+	None	Pancreatic surgery	Insulinoma grade 1
13	22	M	+	Discordant (MRI only)	+	1	19	Tail	+	+	None	Pancreatic surgery	Insulinoma grade 1
14	37	F	−	Concordant	−				−	−	None	Explorative laparotomy (−)	HH without structural disease
15	58	M	−	Concordant	+	1	25	Tail	−	−	None	US-guided cytology (−)	HH without structural disease
16	47	M	+	Discordant (MRI only)	+	1	26	Head	−	−	None	Pancreatic surgery	Insulinoma grade 2

[a] Conventional imaging: CT and MRI; *MRI >* more lesions detected by MRI than CT, *MRI only* lesion detected by MRI and CT negative

[b] Second PET/CT examination performed for relapsing HH about 1 year after surgical excision of a benign insulinoma

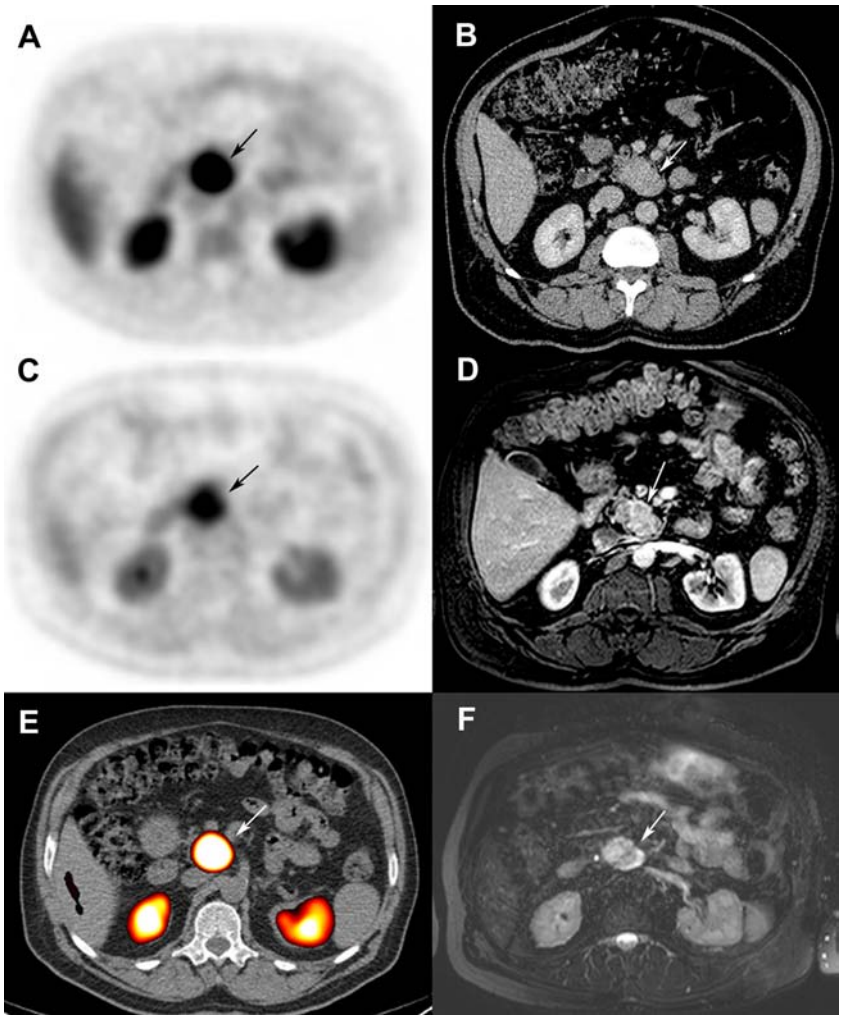

Fig. 1 Patient 10 (42-year-old woman; Table 1). **a** Attenuation-corrected axial carbidopa-assisted ^{18}F-FDOPA PET image (early acquisition) shows focal uptake; **c** attenuation-corrected axial ^{18}F-FDOPA PET image (delayed acquisition) shows focal uptake; **e** axial ^{18}F-FDOPA PET/CT fusion image; **b**, **d** CT images; **f** MRI image. Final diagnosis: insulinoma located in the uncinate process

due to the lower tracer uptake by immature acinar cells (low AADC expression) [24–29]. The main limitation of the use of ^{18}F-FDOPA PET/CT in adults is related to the intense and prolonged ^{18}F-FDOPA uptake by the mature exocrine pancreas (decarboxylation properties of zymogen granules), resulting in a low tumour-to-background uptake ratio [13].

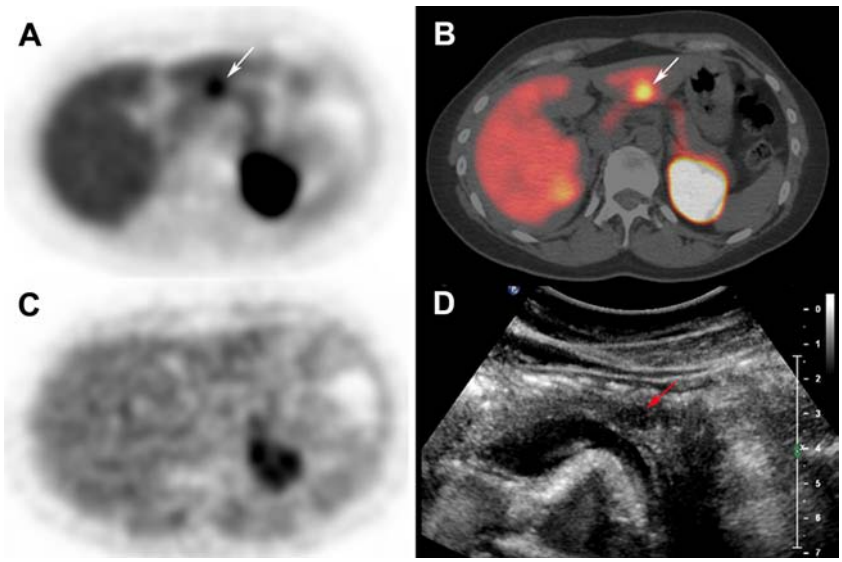

Fig. 2 Patient 5 (81-year-old woman; Table 1). **a** Attenuation-corrected axial carbidopa-assisted ^{18}F-FDOPA PET image (early acquisition) shows focal uptake; **b** axial ^{18}F-FDOPA PET/CT fusion image; **c** attenuation-corrected axial ^{18}F-FDOPA PET image (delayed acquisition) is negative; **d** contrast-enhanced US (delayed image) shows a hypoechogenic nodule. Final diagnosis: insulinoma located in the isthmus

Table 2 Control population with hyperinsulinaemic hypoglycaemia evaluated by ^{18}F-FDOPA PET/CT without carbidopa premedication

Patient no.	Age (years)	Sex	Conventional imaging[a]		EUS	Tumour			^{18}F-FDOPA	Medical treatment	Final diagnostic procedure	Final diagnosis
			Positive/negative	Concordant/discordant		No. of lesions	Size (mm)	Location				
1[b]	55	M	+	Concordant	+	1	13	Body/tail	–	None	Pancreatic surgery	Insulinoma
2[b]	54	M	+	Concordant	+	1	25	Tail	–	None	Pancreatic surgery	Insulinoma
3[b]	16	F	+	Discordant (MRI only)[c]	+	1	10 – 25	Head	–	None	Pancreatic surgery	Nesidioblastosis
4[b]	78	F	+	Concordant	Not available	1	20	Body	–	None	Pancreatic surgery	Insulinoma
5	33	F	+	Concordant	Not available	1	20	Body/tail	–	None	Pancreatic surgery	Insulinoma
6	81	F	–	Concordant	–				–	None	Clinical follow-up	HH without structural disease
7	38	M	–	Concordant	–				–	None	Clinical follow-up	HH without structural disease
8	33	F	–	Concordant	–				–	None	Clinical follow-up	HH without structural disease

[a] Conventional imaging: CT and MRI; *MRI only* lesion detected by MRI and CT negative

[b] Patients previously reported [13]

[c] CT, MRI and EUS were discordant: CT was negative, and MRI and EUS showed a head lesion, but of different sizes (25 and 10 mm, respectively)

This drawback can be circumvented by the use of CD premedication that reduces pancreatic uptake via inhibition of AADC. Our study suggests that the combination of CD premedication and early acquisition results in a higher detection rate of insulinoma than delayed PET/CT images alone with or without CD premedication.

It is well established that CD (a peripheral AADC inhibitor) decreases whole pancreatic uptake [30]. Insulinomas are probably less sensitive to the CD inhibitory effect than acinar cells, resulting in an increased lesion-to-background uptake ratio. Negativization of ^{18}F-FDOPA focal pancreatic hot spots has been reported after CD administration in patients with HH [18, 25, 29]. In the present series, we could not exclude the possibility that the use of CD may have induced negative findings in a few patients due to inhibition of tumoral AADC. However, in our opinion this possible drawback is counterbalanced by the increased sensitivity of PET imaging. The two patients with negative findings were treated with diazoxide at the time of the PET study. It is uncertain whether diazoxide interferes with ^{18}F-FDOPA uptake, but PET studies are usually performed 72 h after drug withdrawal in newborns with HH [29]. If possible, this withdrawal period should also be applied in adults.

Because some insulinomas are known to overexpress somatostatin receptor 2, they have been investigated with somatostatin receptor scintigraphy (SRS) during the past decades and more recently with ^{68}Ga-labelled somatostatin analogues (^{68}Ga-SSTa). These radiopharmaceuticals should be used if ^{18}F-FDOPA PET/CT imaging is not available, in patients with negative ^{18}F-FDOPA PET/CT or in patients with malignant insulinoma due to its high expression of somatostatin. The indications for the use of ^{68}Ga-SSTa will also rapidly evolve with the clinical use of peptide receptor radionuclide therapy to select good candidates for this therapy. Interestingly, insulinoma negative with ^{18}F-FDOPA could be positive on SRS or with ^{68}Ga-labelled somatostatin analogues [31]. This imaging pattern may correspond to a specific tumour phenotype since discordance between imaging based on somatostatin receptor and GLP1R has already been shown [32].

The timing of acquisition may also be important in the localization of insulinoma. In three patients, insulinoma was only detected on early images. In the population studied, early images showed 8 of 11 proved solitary insulinomas compared to delayed images that showed only 5 lesions, without reaching statistical significance. This could be attributed to the small size of our study population and to the fact that delayed acquisitions were performed earlier than in classical protocols for ^{18}F-FDOPA PET imaging (30 min vs. 60 min). Based on the present study, we recommend combining pharmacological modulation by CD and early PET/CT acquisitions. In patients with no history of MEN1 or MEN1-related syndromic manifestations and small tumours detected on early

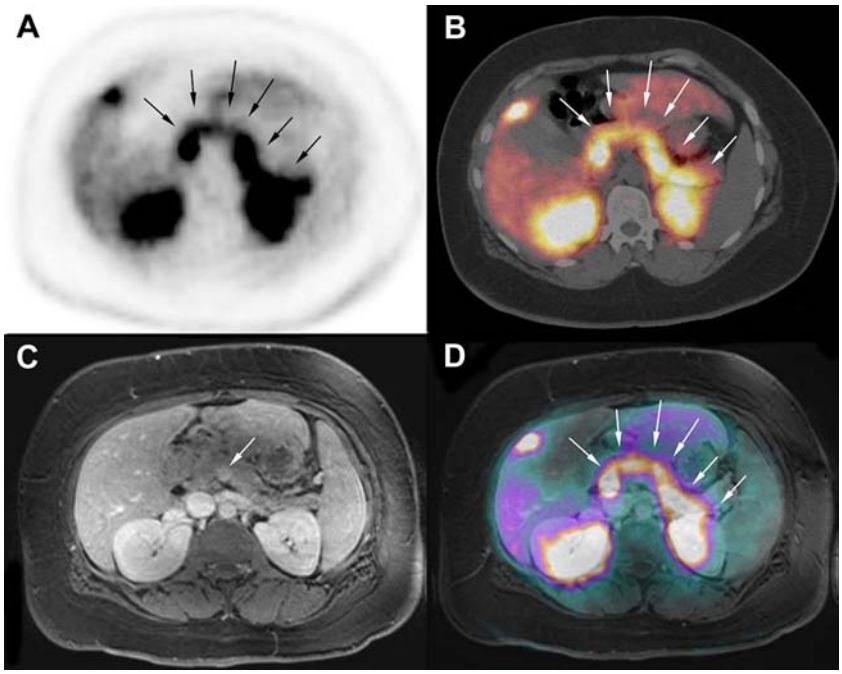

Fig. 3 Patient 5 (33-year-old woman; Table 2). **a**, **b** Attenuation-corrected axial ^{18}F-FDOPA PET (**a**) and PET/CT (**b**) images without carbidopa premedication acquired about 60 min after radiotracer injection show physiological, diffuse and intense pancreatic uptake. **c** T_1-weighted gadolinium-contrast-enhancement axial MRI image (**c**) shows a 20-mm tumour at the body–tail pancreatic junction masked from the normally high pancreatic uptake on PET/MRI. **d** Fused image. Insulinoma was histologically confirmed after surgery

acquisition, the role of whole-body acquisition remains questionable.

Based on our longstanding clinical experience, a decrease in tracer uptake is often seen in secreting and nonsecreting pancreatic NETs (unpublished observations). In our opinion, ^{18}F-FDOPA PET/CT protocols need to be tailored to individual clinical situations. It has been shown that in medullary thyroid carcinoma (MTC), tumour uptake decreases by 40 % between early and delayed images (starting after 60 min). Early acquisition (during the first 15 min) in patients with MTC with persistent/recurrent hypercalcitoninaemia is therefore recommended [33]. The imaging phenotype of insulinoma differs from that of carcinoids or paragangliomas/phaeochromocytomas in that it usually exhibits prolonged tracer retention. Both tumour types overexpress both large neutral amino acid transporters (i.e. LAT1 or LAT2) and AADC, a key enzyme involved in both serotonin and catecholamine biosynthesis. Quantification of LAT expression and AADC expression and activity in insulinoma could be of particular interest in the understanding of ^{18}F-FDOPA PET/CT findings.

We acknowledge several limitations to this study: its retrospective design, the involvement of two independent institutions with different patient populations, and the absence of a head-to-head comparison of the two protocols in the same patient. However, a clinical trial based on a dual-imaging protocol (with and without CD) in each patient could raise ethical issues related to the very low sensitivity of the classical ^{18}F-FDOPA PET/CT protocol for detecting insulinomas. In the present study, we used the same radiopharmaceutical and the same imaging protocol in both institutions. The two groups were also evaluated by different imaging protocols (early image centred over the pancreas in the study group vs. delayed whole-body evaluation in the control group). However, we have previously shown that there is early and intense tracer uptake in normal pancreas [13]. Therefore, we consider that early images without CD would have also missed insulinomas. Besides these limitations, the present study is one of the largest studies investigating ^{18}F-FDOPA PET/CT in patients with HH and CD premedication.

CD-assisted ^{18}F-FDOPA PET/CT leads to a low residual pancreatic ^{18}F-FDOPA activity with preservation of tumour uptake and enables detection of insulinoma in more than half of adult patients with HH. If ^{18}F-FDOPA PET/CT is indicated, we strongly recommend combining CD premedication and early PET/CT acquisition centred over the pancreas. This approach should be performed in the absence of available GLP1R-based imaging. The role of CD-assisted ^{18}F-FDOPA PET/CT in the detection of insulinoma will need to be compared to that of newly introduced and promising agents such as GLP-1 analogues.

Conflicts of interest None.

References

1. Cryer PE, Axelrod L, Grossman AB, Heller SR, Montori VM, Seaquist ER, et al. Evaluation and management of adult hypoglycemic disorders: an Endocrine Society Clinical Practice Guideline. J Clin Endocrinol Metab. 2009;94:709–28. doi:10.1210/jc.2008-1410.

2. Zimmer T, Stolzel U, Bader M, Koppenhagen K, Hamm B, Buhr H, et al. Endoscopic ultrasonography and somatostatin receptor scintigraphy in the preoperative localisation of insulinomas and gastrinomas. Gut. 1996;39:562–8.
3. Reubi JC, Waser B. Concomitant expression of several peptide receptors in neuroendocrine tumours: molecular basis for in vivo multireceptor tumour targeting. Eur J Nucl Med Mol Imaging. 2003;30:781–93. doi:10.1007/s00259-003-1184-3.
4. Grant CS. Insulinoma. Best Pract Res Clin Gastroenterol. 2005;19:783–98. doi:10.1016/j.bpg.2005.05.008.
5. Guettier JM, Kam A, Chang R, Skarulis MC, Cochran C, Alexander HR, et al. Localization of insulinomas to regions of the pancreas by intraarterial calcium stimulation: the NIH experience. J Clin Endocrinol Metab. 2009;94:1074–80.
6. Kaltsas GA, Besser GM, Grossman AB. The diagnosis and medical management of advanced neuroendocrine tumors. Endocr Rev. 2004;25:458–511.
7. Kwekkeboom DJ, Krenning EP, Scheidhauer K, Lewington V, Lebtahi R, Grossman A, et al. ENETS Consensus Guidelines for the Standards of Care in Neuroendocrine Tumors: somatostatin receptor imaging with (111)In-pentetreotide. Neuroendocrinology. 2009;90:184–9. doi:10.1159/000225946.
8. Sharma P, Arora S, Karunanithi S, Khadgawat R, Durgapal P, Sharma R, et al. Somatostatin receptor based PET/CT imaging with 68Ga-DOTA-Nal3-Octreotide for localisation of clinically and biochemically suspected insulinoma. Q J Nucl Med Mol Imaging. 2014.
9. Christ E, Wild D, Forrer F, Brandle M, Sahli R, Clerici T, et al. Glucagon-like peptide-1 receptor imaging for localization of insulinomas. J Clin Endocrinol Metab. 2009;94:4398–405. doi:10.1210/jc.2009-1082.
10. Wild D, Macke H, Christ E, Gloor B, Reubi JC. Glucagon-like peptide 1-receptor scans to localize occult insulinomas. N Engl J Med. 2008;359:766–8.
11. Brom M, Oyen WJ, Joosten L, Gotthardt M, Boerman OC. 68Ga-labelled exendin-3, a new agent for the detection of insulinomas with PET. Eur J Nucl Med Mol Imaging. 2010;37:1345–55. doi:10.1007/s00259-009-1363-y.
12. Kauhanen S, Seppanen M, Minn H, Gullichsen R, Salonen A, Alanen K, et al. Fluorine-18-L-dihydroxyphenylalanine (18F-DOPA) positron emission tomography as a tool to localize an insulinoma or beta-cell hyperplasia in adult patients. J Clin Endocrinol Metab. 2007;92:1237–44.
13. Tessonnier L, Sebag F, Ghander C, De Micco C, Reynaud R, Palazzo FF, et al. Limited value of 18F-F-DOPA PET to localize pancreatic insulin-secreting tumors in adults with hyperinsulinemic hypoglycemia. J Clin Endocrinol Metab. 2010;95:303–7. doi:10.1210/jc.2009-1357.
14. Orlefors H, Sundin A, Lu L, Oberg K, Langstrom B, Eriksson B, et al. Carbidopa pretreatment improves image interpretation and visualisation of carcinoid tumours with 11C-5-hydroxytryptophan positron emission tomography. Eur J Nucl Med Mol Imaging. 2006;33:60–5. doi:10.1007/s00259-005-1891-z.
15. Neels OC, Koopmans KP, Jager PL, Vercauteren L, van Waarde A, Doorduin J, et al. Manipulation of [11C]-5-hydroxytryptophan and 6-[18F]fluoro-3,4-dihydroxy-L-phenylalanine accumulation in neuroendocrine tumor cells. Cancer Res. 2008;68:7183–90. doi:10.1158/0008-5472.CAN-08-0095.
16. Imperiale A, Rust E, Gabriel S, Detour J, Goichot B, Duclos B, et al. 18F-fluorodihydroxyphenylalanine PET/CT in patients with neuroendocrine tumors of unknown origin: relation to tumor origin and differentiation. J Nucl Med. 2014;55:367–72. doi:10.2967/jnumed.113.126896.
17. Koopmans KP, Neels OC, Kema IP, Elsinga PH, Sluiter WJ, Vanghillewe K, et al. Improved staging of patients with carcinoid and islet cell tumors with 18F-dihydroxy-phenyl-alanine and 11C-5-hydroxy-tryptophan positron emission tomography. J Clin Oncol. 2008;26:1489–95. doi:10.1200/JCO.2007.15.1126.
18. Kauhanen S, Seppanen M, Nuutila P. Premedication with carbidopa masks positive finding of insulinoma and beta-cell hyperplasia in [18F]-dihydroxy-phenyl-alanine positron emission tomography. J Clin Oncol. 2008;26:5307–8. doi:10.1200/JCO.2008.18.8581. author reply 8–9.
19. Kauhanen S, Seppanen M, Minn H, Nuutila P. Clinical PET imaging of insulinoma and beta-cell hyperplasia. Curr Pharm Des. 2010;16:1550–60.
20. Hoegerle S, Altehoefer C, Ghanem N, Koehler G, Waller CF, Scheruebl H, et al. Whole-body 18F dopa PET for detection of gastrointestinal carcinoid tumors. Radiology. 2001;220:373–80. doi:10.1148/radiology.220.2.r01au25373.
21. Beuthien-Baumann B, Strumpf A, Zessin J, Bredow J, Kotzerke J. Diagnostic impact of PET with 18F-FDG, 18F-DOPA and 3-O-methyl-6-[18F]fluoro-DOPA in recurrent or metastatic medullary thyroid carcinoma. Eur J Nucl Med Mol Imaging. 2007;34:1604–9. doi:10.1007/s00259-007-0425-2.
22. Koopmans KP, de Groot JW, Plukker JT, de Vries EG, Kema IP, Sluiter WJ, et al. 18F-dihydroxyphenylalanine PET in patients with biochemical evidence of medullary thyroid cancer: relation to tumor differentiation. J Nucl Med. 2008;49:524–31. doi:10.2967/jnumed.107.047720.
23. Koopmans KP, de Vries EG, Kema IP, Elsinga PH, Neels OC, Sluiter WJ, et al. Staging of carcinoid tumours with 18F-DOPA PET: a prospective, diagnostic accuracy study. Lancet Oncol. 2006;7:728–34. doi:10.1016/S1470-2045(06)70801-4.
24. Barthlen W, Blankenstein O, Mau H, Koch M, Hohne C, Mohnike W, et al. Evaluation of [18F]fluoro-L-DOPA positron emission tomography-computed tomography for surgery in focal congenital hyperinsulinism. J Clin Endocrinol Metab. 2008;93:869–75. doi:10.1210/jc.2007-2036.
25. de Lonlay P, Simon-Carre A, Ribeiro MJ, Boddaert N, Giurgea I, Laborde K, et al. Congenital hyperinsulinism: pancreatic [18F]fluoro-L-dihydroxyphenylalanine (DOPA) positron emission tomography and immunohistochemistry study of DOPA decarboxylase and insulin secretion. J Clin Endocrinol Metab. 2006;91:933–40. doi:10.1210/jc.2005-1713.
26. Hardy OT, Hernandez-Pampaloni M, Saffer JR, Suchi M, Ruchelli E, Zhuang H, et al. Diagnosis and localization of focal congenital hyperinsulinism by 18F-fluorodopa PET scan. J Pediatr. 2007;150:140–5.
27. Otonkoski T, Nanto-Salonen K, Seppanen M, Veijola R, Huopio H, Hussain K, et al. Noninvasive diagnosis of focal hyperinsulinism of infancy with [18F]-DOPA positron emission tomography. Diabetes. 2006;55:13–8.
28. Ribeiro MJ, Boddaert N, Bellanne-Chantelot C, Bourgeois S, Valayannopoulos V, Delzescaux T, et al. The added value of [18F]fluoro-L-DOPA PET in the diagnosis of hyperinsulinism of infancy: a retrospective study involving 49 children. Eur J Nucl Med Mol Imaging. 2007;34:2120–8. doi:10.1007/s00259-007-0498-y.
29. Ribeiro MJ, De Lonlay P, Delzescaux T, Boddaert N, Jaubert F, Bourgeois S, et al. Characterization of hyperinsulinism in infancy assessed with PET and 18F-fluoro-L-DOPA. J Nucl Med. 2005;46:560–6.
30. Timmers HJ, Hadi M, Carrasquillo JA, Chen CC, Martiniova L, Whatley M, et al. The effects of carbidopa on uptake of 6-18F-fluoro-L-DOPA in PET of pheochromocytoma and extraadrenal abdominal paraganglioma. J Nucl Med. 2007;48:1599–606.
31. Treglia G, Inzani F, Campanini N, Rindi G, Agnes S, Giordano A, et al. A case of insulinoma detected by 68Ga-DOTANOC PET/CT and missed by 18F-dihydroxyphenylalanine PET/CT. Clin Nucl Med. 2013;38:e267–70. doi:10.1097/RLU.0b013e31825b222f.

32. Wild D, Christ E, Caplin ME, Kurzawinski TR, Forrer F, Brandle M, et al. Glucagon-like peptide-1 versus somatostatin receptor targeting reveals 2 distinct forms of malignant insulinomas. J Nucl Med. 2011;52:1073–8. doi:10.2967/jnumed.110.085142.

33. Soussan M, Nataf V, Kerrou K, Grahek D, Pascal O, Talbot JN, et al. Added value of early 18F-FDOPA PET/CT acquisition time in medullary thyroid cancer. Nucl Med Commun. 2012;33:775–9. doi:10.1097/MNM.0b013e3283543304.

Metabolomic profile of the adrenal gland: from physiology to pathological conditions

Alessio Imperiale[1,2], Karim Elbayed[2], François-Marie Moussallieh[1,2], Nathalie Reix[2,3], Martial Piotto[2,4], Jean-Pierre Bellocq[5], Bernard Goichot[6], Philippe Bachellier[7] and Izzie-Jacques Namer[1,2]

[1]Department of Biophysics and Nuclear Medicine, Strasbourg University Hospitals, Hôpital de Hautepierre, 1, Avenue Molière, 67098 Strasbourg Cedex, France
[2]ICube, University of Strasbourg/CNRS (UMR 7357), FMTS – Faculty of Medicine, Strasbourg, France
[3]Laboratory of Hormonology, Strasbourg University Hospitals, Strasbourg, France
[4]Bruker Biospin, Wissembourg, France
[5]Department of Pathology, Strasbourg University Hospitals, Strasbourg, France
[6]Department of Internal Medicine, Diabetes and Metabolic Disorders, Strasbourg University Hospitals, Strasbourg, France
[7]Department of Visceral Surgery and Transplantation, Strasbourg University Hospitals, Strasbourg, France

Correspondence should be addressed to A Imperiale
Email
alessio.imperiale@chru-strasbourg.fr

Abstract

In this study, we i) assessed the metabolic profile of the normal adrenal cortex and medulla of adult human subjects by means of ^{1}H-high-resolution magic-angle spinning nuclear magnetic resonance (HRMAS NMR) spectroscopy; ii) compared the biochemical profile of adenoma (Ad), adrenal cortical carcinoma (ACC), and pheochromocytoma (PCC) samples with that of healthy adrenal tissue samples; and iii) investigated the metabolic differences between ACCs and Ads as well as between ACCs and PCCs. Sixty-six tissue samples (13 adrenal cortical tissue, eight medullary tissue, 13 Ad, 12 ACC, and 20 PCC samples) were analyzed. Adrenaline and noradrenaline were undetectable in cortical samples representing the metabolic signature of the tissue derived from neural crest. Similarity between the metabolic profile of Ads and that of the normal adrenal cortex was shown. Inversely, ACC samples clearly made up a detached group exhibiting the typical stigmata of neoplastic tissue such as choline-containing compounds, biochemical markers of anaerobic processes, and increased glycolysis. Significantly higher levels of lactate, acetate, and total choline-containing compounds played a major role in the differentiation of ACCs from Ads. Moreover, the high fatty acid content of ACCs contributed to the cluster identification of ACCs. Of the 14 sporadic PCC samples, 12 exhibited predominant or exclusive noradrenaline secretion. The noradrenaline: adrenaline ratio was inverted in the normal medullary tissue samples. Multiple endocrine neoplasia type 2- and NF1-related PCC samples exhibited both adrenaline and noradrenaline secretion. In the von Hippel–Lindau disease-related PCC samples, only noradrenaline secretion was detected by HRMAS NMR spectroscopy. This study is one of the first applications of metabolomics to adrenal pathophysiology and it is the largest study to report HRMAS NMR data related to the adrenal cortex and adrenal cortical tumors.

Key Words
- pheochromocytoma
- adrenal cortical carcinoma
- adrenal adenoma
- HRMAS
- metabolomics

Endocrine-Related Cancer (2013) **20**, 705–716

http://erc.endocrinology-journals.org
DOI: 10.1530/ERC-13-0232

Published by Bioscientifica Ltd.

Introduction

The adrenal gland is a fascinating organ with two functionally distinct structures called the adrenal cortex and medulla, each with its own embryonic origin. While the adrenal cortex derives from mesoderm, the adrenal medulla is composed of chromaffin cells originating from neural crest tissue.

Tumors originating from the adrenal cortex are commonly classified as functional or nonfunctional with a variable degree of malignancy. The most clinically relevant adrenocortical pathologies are adenomas (Ads) and adrenal cortical carcinomas (ACCs). While ACCs are relatively rare and extremely aggressive tumors, Ads are more frequently found and always benign. There is no evidence that Ads degenerate into malignant lesions (Young 2007, Lloyd 2011). The rarity of the disease and the presence of special variants (pediatric, oncocytic, myxoid, and sarcomatoid) complicate the pathological diagnosis of ACCs. Accurate discrimination between atypical adrenal cortical Ads and malignant ACCs in patients without gross evidence of malignancy can be difficult (Roman 2006). Nowadays, ACCs are being diagnosed based on the recognition of at least three of nine morphological parameters using light microscopy, according to the Weiss scoring system (Weiss *et al*. 1989, Papotti *et al*. 2011). Nevertheless, diagnostic accuracy could be reduced in borderline cases with only one or two Weiss criteria, particularly for nonexpert pathologists.

In adults, tumors originating from the adrenal medulla are mainly functional and called pheochromocytomas (PCCs). Although it is well established that the malignancy rate depends on the patient's genetic background, presently no marker of malignant potential is completely defined. The presence of metastases is indispensable to identify patients with malignant disease who require a more aggressive therapeutic approach. Finally, the combination of various clinical, biochemical, and/or histological markers can indicate an aggressive tumor behavior (Korevaar & Grossman 2011).

Briefly, for both cortical and medullary neoplasms, the degree of malignancy is estimated according to the histological features clinical stage (particularly size) of the tumors and functional tests (McNicol 2011). Genetic and molecular alterations have been the subject of several studies, without, however, definitive conclusions being reached (Stratakis 2003, 2005, Lombardi *et al*. 2006).

^{1}H-high-resolution magic-angle spinning nuclear magnetic resonance (HRMAS NMR) spectroscopy can characterize the metabolic phenotype of intact cells, tissues, and organs from the analysis of an intact tissue sample (Nicholson & Wilson 2003). HRMAS NMR spectroscopy provides biochemical information related to the regulation of specific gene transcripts that are altered in the tumoral genome (Griffin & Shockor 2004), generating great interest on the part of both the scientific and medical communities, particularly in oncology (Claudino *et al*. 2012, O'Connell 2012). At present, very limited data are available concerning the adrenal tissue. A few applications of HRMAS NMR spectroscopy to pediatric neuroblastomas have been described in the literature (Peet *et al*. 2007, Wilson *et al*. 2009, Imperiale *et al*. 2011). More recently, Timmers' team has reported an *in vitro* ^{1}H-NMR spectroscopic study exploring the genotype-specific abnormalities in mitochondrial function associated with distinct profiles of energy metabolism and catecholamine content in PCCs and paragangliomas (Rao *et al*. 2013). To date, to the best of our knowledge, no other HRMAS NMR investigations concerning healthy adrenal tissue and the related pathologies have been reported, particularly regarding the adrenal cortex.

In this study, we first assessed the metabolic profile of both normal adrenal cortex and medulla of adult human subjects using HRMAS NMR spectroscopy. Then, we compared the biochemical pattern of healthy tissue with the profiles obtained from the Ad, ACC, and PCC samples. Finally, we investigated the differences between ACCs and Ads as well as between ACCs and PCCs.

Subjects and methods

Tissue samples analyzed

Among all the adrenal specimens collected in the tumor bank of the Strasbourg University Hospital until January 2010, 66 tissue samples including normal adrenal cortical and medullary tissue, Ad, ACC, and PCC samples were retrospectively selected for this study according to the following criteria: i) final diagnosis according to the pathological standards; ii) absence of both medical and surgical treatment before obtaining the tumor sample for HRMAS analysis; iii) tissue specimens collected after surgery and snap-frozen in liquid nitrogen before storage at −80 °C; and iv) tissue samples not contaminated by the histopathological fixing medium.

Of the 66 tissue specimens analyzed, 13 normal adrenal cortical and eight normal medullary tissue samples were obtained from subjects who underwent

http://erc.endocrinology-journals.org
DOI: 10.1530/ERC-13-0232

Published by Bioscientifica Ltd.

both nephrectomy and adrenalectomy for localized and early-stage renal cell carcinoma. The other 45 tissue samples included 13 Ad, 12 ACC, and 20 PCC samples.

In the Ad group, four samples were aldosterone-secreting Ads. No hormonal hypersecretion was associated with the remaining nine cases. The mean size of Ads determined during pathological examination was 3.3 cm (range 1.5–6 cm). The mean age of the patients during adrenal surgery was 53 years (range 43–76 years).

In the ACC group, six of the 12 samples were secreting tumors. The mean size of ACCs determined during pathological examination was 12 cm (range 6–24 cm). In all the cases, the Weiss score was ≥ 4. Seven patients exhibited a locoregional involvement associated with nodal metastases. In the remaining five cases, ACC was confined to the adrenal gland at the time of surgery. Of these, three patients exhibited a systemic metastatic spread about 1 year later and two patients were free of disease during the first 5 years of postsurgical follow-up. The mean age of the patients during adrenal surgery was 62 years (range 32–80 years).

Finally, in the PCC group, all the 20 samples were secreting tumors. In 14 of the 20 patients, no somatic mutation associated with multiple endocrine neoplasia type 2 (MEN2) and von Hippel–Lindau (VHL) disease was identified at the time of diagnosis. Moreover, no mutations in any of the succinate dehydrogenase complex subunit genes were identified in these patients. No case had a positive family history of nonsyndromic PCCs or paragangliomas. Hence, PCCs were considered as sporadic in 14 cases. On the other hand, PCCs were associated with MEN2 in two patients, Recklinghausen's disease (NF1) in two patients, and VHL disease in the remaining two cases. In all the 20 included patients, no metastatic spread was observed both at diagnosis and during a follow-up of at least 5 years after surgery. The mean size of the PCCs determined during pathological examination was 6.2 cm (range 1.5–14 cm). The mean age of the patients during adrenal surgery was 36 years (range 29–63 years). The tumor secretion profile was determined according to the results of the presurgical biochemical tests for plasma free metanephrines and/or urinary fractionated metanephrines and catecholamines.

Tissue sample preparation for HRMAS NMR spectroscopy

The amount of tissue used for the HRMAS analysis ranged from 15 to 20 mg. For each sample, the percentage of tumor cells and the percentage of necrosis with regard to the total surface were calculated based on frozen sections using a mirror sample stored in the tissue bank. Samples containing at least 30% tumor cells and $<50\%$ necrosis were used for this study. Each tissue sample was introduced into a 30 µl disposable insert. Ten microliters of D_2O were added to the rotor to provide a lock frequency for the NMR spectrometer. The exact weight of the sample used was determined by weighing the empty insert and the insert containing the tissue sample. The insert was stored at -80 °C and placed in a 4 mm ZrO_2 rotor just before the HRMAS analysis.

HRMAS NMR spectroscopy technical features

HRMAS NMR spectra were recorded on a Bruker Advance III 500 spectrometer operating at a proton frequency of 500.13 MHz and equipped with a 4 mm double-resonance (^{1}H and ^{13}C) gradient HRMAS probe. A Bruker cooling unit was used to regulate the temperature by cooling down the bearing air flowing into the probe. To minimize the effects of tissue degradation, all *ex vivo* spectra were acquired at a temperature of 4 °C. This value was calibrated exactly using a 100% methanol sample. To keep the rotation sidebands out of the spectral region of interest and to minimize sample degradation, all NMR experiments were conducted on samples spinning at 3502 Hz. For each sample, a one-dimensional (1D) proton spectrum using a Carr–Purcell–Meiboom–Gill (CPMG) pulse sequence with presaturation of the water signal was acquired as reported previously (Piotto *et al.* 2009). To eliminate signal losses due to B_1 inhomogeneity, the inter-pulse delay between the 180° pulses of the CPMG pulse train was synchronized with the sample and set to 285 µs (Piotto *et al.* 2001, Elbayed *et al.* 2005). The number of loops was set to 328, thus giving the CPMG pulse train a total length of 93 ms. The parameters for the CPMG experiment were set as follows: sweep width, 14.2 p.p.m.; number of points, 32k; relaxation delay, 2 s; and acquisition time, 2.3 s. A total of 128 free induction decays were acquired, resulting in an acquisition time of 10 min. Spectra were referenced by setting the lactate doublet chemical shift to 1.33 p.p.m. In order to confirm resonance assignments, 2D homonuclear and heteronuclear experiments were also carried out immediately after the acquisition of 1D spectra. Because the duration of these experiments was long, they were conducted on only a few samples representative of each class of tissues and exclusively for signal assignment. Significant tissue degradation occurs during this long measurement time; therefore, ^{1}H CPMG experiments were completed before the 2D signal assignment experiments. Data were zero-filled to a 2k×1k matrix and

http://erc.endocrinology-journals.org
DOI: 10.1530/ERC-13-0232

Published by Bioscientifica Ltd.

weighted with a shifted square sine-bell function before Fourier transformation. HRMAS NMR signals were bucketed into integral regions 0.01 p.p.m. wide (p.p.m. range 8.65–1) using the AMIX 3.8 Software (Bruker GmbH, Rheinstetten, Germany) and exported into SIMCA P (version 11.0, Umetrics AB, Umeå, Sweden). To accommodate the influence of metabolites present at both high and low concentrations, without emphasizing spectral noise, unit variance scaling was employed for all the analyses. Spectra were referenced for chemical shift according to the lactate peak.

Metabolite quantification procedure

Metabolites were quantified by means of a proprietary program based on a custom MATLAB algorithm in a Windows-based environment. The quantification procedure was based on the pulse length-based concentration measurement (PULCON) described previously by our team (Piotto *et al*. 2012). Spectra were normalized according to the weight of each sample and calibrated using the signal intensity of a 19.3 nmol reference solution of lactate, scanned under the same analytical conditions. The peak integral corresponding to each metabolite's region was normalized to the integral of the entire spectrum. For our experiments, only peaks that were well resolved in the 1D CPMG spectra were quantified. One pulse sequence was acquired in addition to the CPMG sequence for fatty acid (FA) estimation. Quantification results are expressed as nanomoles per milligram of tissue. Metabolites were assigned using standard metabolite chemical shift tables available in the literature (Martinez-Bisbal *et al*. 2004, Wishart *et al*. 2007).

To assess adrenaline concentrations in the tissue samples, the signal resulting from the N-methyl radical selected at 2.75 p.p.m. was considered. The 3,4-dihydroxybenzene group of both adrenaline and noradrenaline generates a spectral complex between about 6.85 and 6.98 p.p.m. The integral of the region corresponding to the ^{1}H in position 5 of the aromatic ring (IUPAC nomenclature) was selected to quantify the amount of adrenaline plus noradrenaline in each tissue sample. Finally, noradrenaline concentrations were determined by subtracting adrenaline concentrations from adrenaline plus noradrenaline concentrations. A negative value of noradrenaline indicates that there was no physical quantity, so the 0 value was assigned to noradrenaline for the statistical analysis. Dopamine could contribute to peaks in the region between 6.85 and 6.98 p.p.m. However, no triplets at 2.85 and 3.22 p.p.m., representing the spectral signature of dopamine, were detected in HRMAS NMR spectra, suggesting the absence or an undetectable amount of dopamine in the analyzed tissue samples.

The above approach has been tested and confirmed (data not shown) previously using the quantification NMR analysis of adrenaline and noradrenaline standard solutions that were first separated and subsequently mixed (1/1, v/v).

Statistical analysis

The standardized metabolite concentration values are expressed as median and range. As has been widely suggested (Sitter *et al*. 2009, Beckonert *et al*. 2010), a combination of principal component analysis (PCA) and partial least-squares discriminant analysis (PLS-DA) was employed.

A PCA was carried out to quickly evaluate the quality of the data and to identify possible outliers (Ebbels & Cavill 2009). Then, a PLS-DA was employed to optimize the separation between groups in each of the following six models: i) normal adrenal cortex vs medulla; ii) normal adrenal cortex vs Ads; iii) normal adrenal cortex vs ACCs; iv) ACCs vs Ads; v) normal adrenal medulla vs PCCs; and vi) ACCs vs PCCs. PLS-DA was initially carried out for the whole set of variables (i.e. metabolites) in order to select those with a real discriminating power. These metabolites were determined using the regression coefficient plot with 95% jackknifed CIs. Metabolites with a variable importance for projection (VIP) value ≥ 0.9 were selected and labeled VIP metabolites. Afterwards, a second PLS-DA, based on the VIP metabolites, was carried out to classify the samples. Cross-validation was used in each PLS-DA model to determine the number of components and to avoid overfitting the data because of the small number of samples. Two measurements of model quality were reported for PLS-DA: R^2Y and Q^2, representing respectively the goodness of fit (i.e. data variation) and the goodness of prediction, as estimated by cross-validation. A value of $Q^2 \geq 0.5$ is generally considered a good predictor for PLS-DA components. The relationships between variables were assessed using the Spearman's rank test. Comparisons were computed using the nonparametric Mann–Whitney *U* test. The STATISTICA 7 (STATSOFT; www.statsoft.com) package was used for statistical data analysis. A P value <0.05 was considered statistically significant.

Results

The representative 1D HRMAS CPMG spectra of the normal adrenal cortical and medullary tissue, Ad, ACC,

http://erc.endocrinology-journals.org
DOI: 10.1530/ERC-13-0232

Published by Bioscientifica Ltd.

and PCC samples are shown in Figs 1 and 2. A total of 24 identified metabolites were quantified from the spectra obtained from all the 66 tissue samples within the range of 8.65–1 p.p.m. (Table 1). Apart from peaks due to small water-soluble molecules, the acquired spectra displayed consistent broad resonances, which were attributed to three different FA moieties defined as a, b, and c (Martinez-Bisbal *et al*. 2004). Finally, five additional resolved signals that peaked at 1.14, 2.20, 3.36, 4.30, and 8.50 p.p.m. were visualized in the CPMG spectra without definitive metabolite attribution and therefore called $X_{1.14}$, $X_{2.20}$, $X_{3.36}$, $X_{4.30}$, and $X_{8.50}$.

Normal adrenal cortex vs normal medulla

Thirteen normal adrenal cortical and eight normal medullary tissue samples were included in the analysis. A two-component PLS-DA based on VIP metabolites was characterized by a faithful representation of the Y data ($R^2Y=0.8$) and a good cumulative confidence criterion of prediction ($Q^2=0.7$). The score plot of the PLS-DA model showed a separation of the two sets of samples (Fig. 3). Normal medulla was characterized by a significantly higher abundance of adrenaline, noradrenaline, myo-inositol, glutamate, glutathione, lactate, succinic and ascorbic acids, creatine, scyllo-inositol, glutamine, taurine, glycine, total choline-containing compounds, and $X_{4.30}$, $X_{3.36}$, and $X_{8.50}$. The adrenal cortex was characterized by a higher level of FA (a) and (b). Both adrenaline and noradrenaline complexes were undetectable in all the cortical samples.

Normal adrenal cortex vs cortical Ads

Thirteen normal adrenal cortical tissue and 13 Ad samples were considered. According to visual analysis, spectra belonging to adrenal cortical tissue and Ad samples were mostly related. The two-component PLS-DA model based on VIP metabolites showed only incomplete separation between the two sets of samples (Fig. 3) and was characterized by a low goodness-of-prediction value ($Q^2=0.4$). Valine, alanine, aspartic acid, γ-aminobutyric

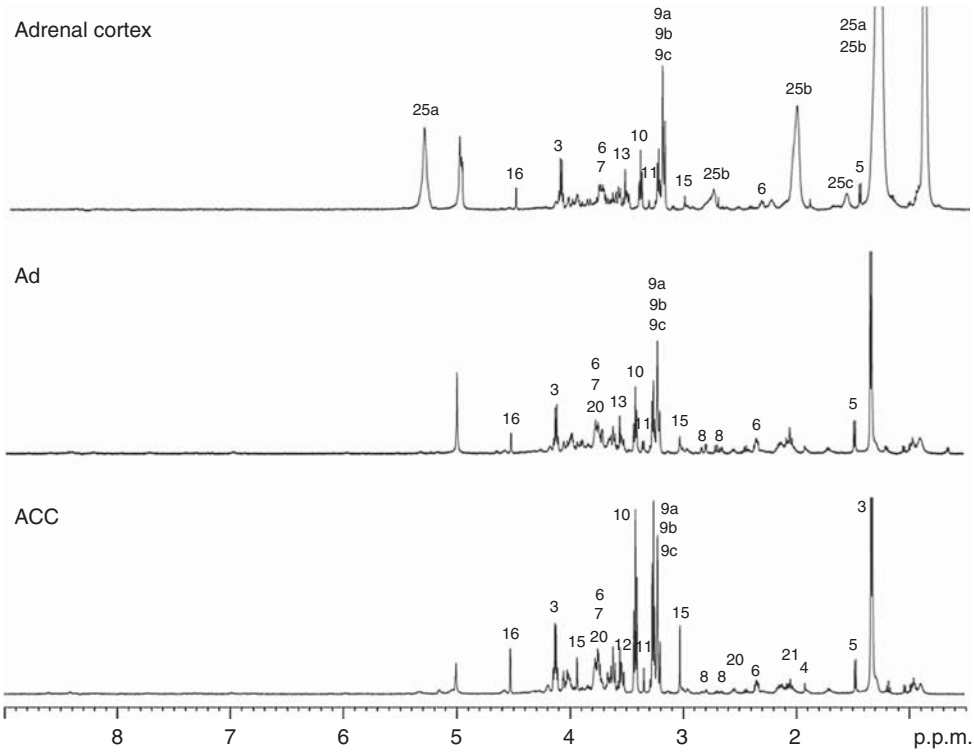

Figure 1

Representative 1D ^{1}H CPMG HRMAS spectra of healthy adrenal cortical tissue, Ad, and ACC samples. Partial metabolite assignment is indicated. The numbers refer to the metabolites listed in Table 1. The metabolic content of healthy and cancerous tissues can be directly compared since the intensity of each spectrum was normalized with respect to the weight of the sample.

Published by Bioscientifica Ltd.

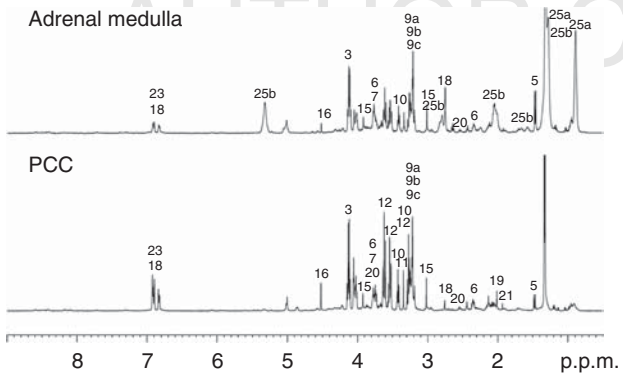

Figure 2
Representative 1D ^{1}H CPMG HRMAS spectra of both healthy adrenal medullary tissue and PCC samples. Partial metabolite assignment is indicated. The numbers refer to the metabolites listed in Table 1. The metabolic content of healthy and cancerous tissues can be directly compared since the intensity of each spectrum was normalized with respect to the weight of the sample.

acid (GABA), isoleucine, N-acetyl aspartate (NAA), acetate, lysine, $X_{2.20}$, and FA (a), (b), and (c) were significantly more abundant in the cortical samples. Succinic acid and $X_{3.36}$ were slightly more abundant in Ad samples, without, however, reaching statistical significance.

A two-component PLS-DA model based on VIP metabolites was built from Ad samples according to hormonal secretion (Fig. 4A; $R^2Y=0.72$ and $Q^2=0.44$). scyllo-Inositol and $X_{3.36}$ and $X_{4.30}$ characterized non-secreting Ad samples. On the other hand, glutamate, glutamine, GABA, $X_{2.20}$, and succinate were more abundant in secreting Ad samples. A statistically significant difference was found for $X_{3.36}$ and $X_{2.20}$, scyllo-inositol, GABA, and glutamate.

Normal adrenal cortex vs ACCs

Thirteen normal adrenal cortical tissue and 12 ACC samples were analyzed. The two tissue classes were clearly separated by a two-component PLS-DA based on VIP metabolites (Fig. 3), showing an accurate representation of the data and good cumulative confidence criterion of fit ($R^2Y=0.9$) and prediction ($Q^2=0.85$). The statistically significant abundance of glutathione, lactate, myo-inositol, glycine, total choline-containing compounds, creatine, glutamate, glutamine, scyllo-inositol, and $X_{8.50}$ was found to be a discriminator of ACCs. The adrenal cortex was characterized by a higher level of NAA, isoleucine, FA (a) and (b), and $X_{4.30}$ and $X_{1.14}$. A two-component PLS-DA model based on VIP metabolites was built from ACC samples according to hormonal secretion (Fig. 4B; $R^2Y=0.71$ and $Q^2=0.44$). Glutamine, glutamate, acetate, lysine, valine, and succinate were more abundant in nonsecreting tumors, without reaching statistical significance. Secreting ACC samples exhibited a higher abundance of aspartate, FA (b), $X_{1.14}$, and total choline-containing compounds. However, no significant difference was observed for any of these metabolites.

Finally, when PLS-DA was built according to clinical aggressivity, the ten patients with metastatic ACCs were not successfully discriminated from the remaining two with confined disease at diagnosis and without systemic spread during the first 5 years of postsurgical follow-up.

ACCs vs cortical Ads

Twelve ACC and 13 Ad samples were included in the analysis. A two-component PLS-DA model based on VIP metabolites was characterized by $R^2Y=0.9$ and $Q^2=0.85$, showing a good differentiation of Ad and ACC samples (Fig. 3). A significantly higher abundance of lactate, GABA, creatine, NAA, acetate, alanine, glutamate, glutamine, valine, myo-inositol, glycine, glutathione, isoleucine, lysine, ethanolamine, FA, total choline-containing compounds, and $X_{2.20}$, and $X_{8.50}$ was found to be a discriminator of ACCs.

Normal adrenal medulla vs PCCs

Eight normal medullary tissue and 20 PCC samples were compared. When a two-component PLS-DA model was built using only data points corresponding to VIP metabolites, the following results were obtained: $R^2Y=0.8$ and $Q^2=0.7$. Figure 3 presents the score plot of the PLS-DA showing a clear separation between the two sets of samples. A significantly higher abundance of taurine, alanine, aspartate, GABA, glutathione, noradrenaline, ascorbic acid, total choline-containing compounds, and $X_{4.30}$ was observed in PCC samples than in the normal medullary tissue samples.

According to the presurgical biological evaluation, ten of the 14 sporadic PCC samples exhibited predominant noradrenaline secretion, two exclusive noradrenaline secretion and two predominant adrenaline secretion (Fig. 5). For all the examined sporadic PCC samples, HRMAS NMR spectroscopy revealed the presence of a greater amount of noradrenaline than of adrenaline. On the other hand, in the normal medullary tissue samples, adrenaline was more abundant than noradrenaline (Table 2). The abundance of noradrenaline was

http://erc.endocrinology-journals.org
DOI: 10.1530/ERC-13-0232

Published by Bioscientifica Ltd.

Table 1 ^{1}H-NMR resonance assignments of the metabolites identified and quantified in the 66 adrenal samples examined

Numbers	Metabolite	Group	^{1}H chemical shift (p.p.m.)
1	Isoleucine	δCH_3	0.94
		γCH_3	1.01
		γCH_2	1.51
		αCH	3.65
2	Valine	γCH_3	0.98
		$\gamma' CH_3$	1.04
		βCH	2.30
3	Lactate	CH_3	1.33
		CH	4.12
4	Lysine	γCH_2	1.43
		δCH_2	1.71
		βCH_2	1.89
		εCH_2	3.01
5	Alanine	βCH_3	1.48
		αCH	3.78
6	Glutamate	βCH_2	2.05
		γCH_2	2.34
		αCH	3.76
7	Glutamine	βCH_2	2.14
		γCH_2	2.44
		αCH_2	3.77
8	Aspartic acid	βCH_2(u)	2.70
		βCH_2(d)	2.80
		αCH	3.90
9a	Choline	$-N^+-(CH_3)_3$	3.21
		βCH_2	3.52
		αCH	4.06
9b	Phosphorylcholine	$-N^+-(CH_3)_3$	3.22
		βCH_2	3.60
		αCH	4.16
9c	Glycerophosphocholine	$-CH_2-NH_3^+$	3.23
		αCH_2	4.32
		βCH_2	3.69
		CH_2-HPO_4(d)	3.88
		CH_2OH	3.91
		CH_2-HPO_4(u)	3.95
10	Taurine	$-CH_2-NH_3^+$	3.26
		$-CH_2-SO_3^-$	3.42
11	scyllo-Inositol	All Hs	3.35
12	myo-Inositol	C5H	3.27
		C1H, C3H	3.54
		C4H, C6H	3.61
		C2H	4.06
13	Glycine	αCH	3.56
14	β-Glucose	C4H	3.43
		C3H, C5H	3.47
		C6H(u)	3.75
		C6H(d)	3.89
		C1H	4.65
15	Creatine	CH_3	3.03
		CH_2	3.93
16	Ascorbic acid	-CHOH-	4.02
		C4H	4.52
17	Succinic acid	(α,β CH_2)	2.40
18	Adrenaline	CH_3-NH	2.75
		C4H	6.84
		C3H	6.92
		C6H	6.93
19	N-acetyl aspartate (NAA)	CH_3	2.04
		αCH	4.37
20	Glutathione	CH_2-CONH	2.54
		CH_2-SH	2.95
		CH-NH_2	3.78
21	Acetate	CH_3	1.92
		$3CH_2$	1.90
22	γ-Aminobutyric acid (GABA)	$4CH_2$	2.28
		$2CH_2$	3.01
23	Noradrenaline	C4H	6.84
		C3H	6.92
		C6H	6.93
24	Ethanolamine	$-CH_2-NH_3^+$	3.13
		CH_2OH	3.82
25a	Fatty acids (a)	CH_3	0.90
		(2)CH_2	1.29
		(1)CH_2	1.31
25b	Fatty acids (b)	(2)CH_2	2.03
		CH_2	2.80
		(2)CH	5.33
		(1)CH	5.33
25a,b	Fatty acids (a) and (b)	(n)CH_2	1.29
25c	Fatty acids (c)	(2)CH_2	1.60

Spectra were referenced by setting the lactate doublet chemical shift to 1.33 p.p.m. Metabolites were assigned using standard metabolite chemical shift tables available in the literature (Martinez-Bisbal *et al.* 2004, Wishart *et al.* 2007).

significantly higher in PCC samples than in the normal medullary tissue samples ($P=0.04$). Adrenaline was moderately more abundant in PCC samples than in the normal tissue samples, without, however, reaching statistical significance.

In patients with VHL disease-related PCCs, only noradrenaline was detected by HRMAS NMR spectroscopy. MEN2- and NF1-related PCC samples showed an elevation of the levels of both adrenaline and noradrenaline (Table 2).

ACCs vs PCCs

Twelve ACC and 20 PCC samples were included in the analysis. A two-component PLS-DA based on VIP metabolites (Fig. 3) was characterized by a good representation of the Y data ($R^2Y=0.8$) and a good cumulative confidence criterion of prediction ($Q^2=0.6$). Statistically significant differences between ACC and PCC samples were found in 14 of the 24 metabolites identified. A higher abundance of adrenaline, noradrenaline, aspartate, scyllo-inositol, GABA, myo-inositol, and ascorbic acid was found to be a significant discriminator of PCCs. On the other hand, ACC

http://erc.endocrinology-journals.org
DOI: 10.1530/ERC-13-0232

Published by Bioscientifica Ltd.

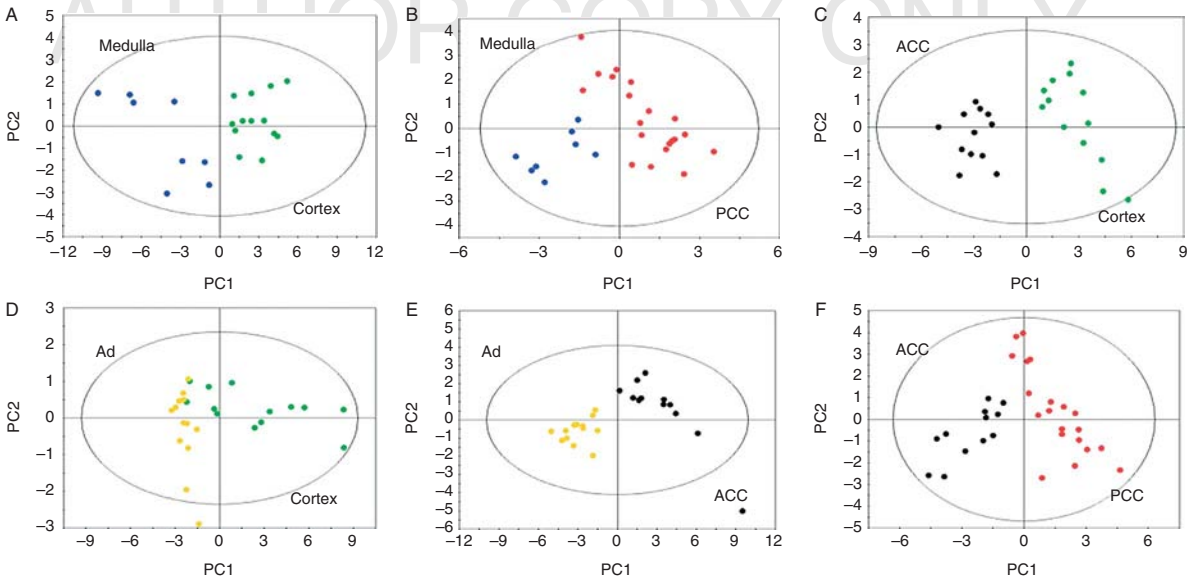

Figure 3

Results of PLS-DA models built according to histological classification: (A) normal adrenal cortex vs normal adrenal medulla, (B) normal adrenal medulla vs PCC, (C) normal adrenal cortex vs ACC, (D) normal adrenal cortex vs Ad, (E) ACC vs Ad, and (F) ACC vs PCC.

samples contained a larger amount of glycine, alanine, taurine, creatine, ethanolamine, total choline-containing compounds, and FA (b).

Discussion

In this study, we analyzed 66 tissue samples of normal and pathological adrenal tissues of adult human subjects by means of HRMAS NMR spectroscopy. The first objective was to characterize the global metabolic profile differentiating normal adrenal cortex from medulla. Afterwards, the biochemical pattern of healthy tissue was compared with that of pathological tissue of the same embryological origin. Finally, the differences between ACCs and both Ads and PCCs were investigated. To the best of our knowledge, no previous study has reported the metabolic fingerprint of the normal adult human adrenal gland and adrenal cortical pathologies such as Ads and ACCs.

The visual comparison of spectra obtained from the cortical tissue samples demonstrated a significant similarity between Ad and normal adrenal cortical tissue samples (Fig. 1), afterwards confirmed by the results of a multivariate analysis. PLS-DA scatter plots evidenced a continuum-like distribution of Ad and normal adrenal cortical tissue samples. Inversely, despite the common embryological origin, ACC samples clearly represented a detached group, reflecting the substantial malignant properties of ACCs. Interestingly, other authors (Rechache *et al.* 2012) who have conducted genome-wide DNA methylation profiling of adrenocortical tumor and normal adrenal cortical tissue samples have recently reported similar PCA results. Moreover, in a recent article by the same team, Jain *et al.* (2012) proposed a working model of the molecular pathogenesis of ACCs showing a malignancy progression from normal cortex to ACCs through cortical hyperplasia and Ads.

Predictably, when compared with the normal adrenal cortical samples, ACC samples exhibited the typical stigmata of neoplastic tissue. The metabolic fingerprint of ACC samples was characterized by the general metabolic markers of malignancy such as choline-containing compounds, which are linked to increased phospholipid turnover. Biochemical markers representative of anaerobic processes and increased glycolytic activity such as lactate levels were also present. The abundance of amino acid resonance peaks suggested an increase in amino acid production via nonoxidative pathways. The increased rate of protein degradation related to cell death, which is particularly evident in large and necrotic tumors, or the deregulation of the Krebs cycle may explain the altered amino acid concentration observed in ACC samples.

Significantly higher levels of lactate, acetate, and total choline-containing compounds play a major role in the differentiation of ACCs from Ads. Moreover, the large FA content of ACC samples contributed to the cluster

Published by Bioscientifica Ltd.

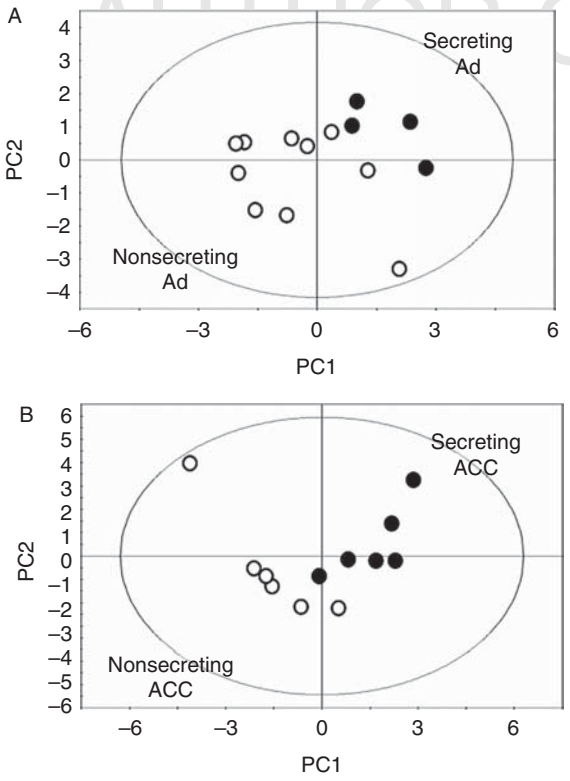

Figure 4
Results of PLS-DA models built respectively from Ad (A) and ACC (B) samples according to tumoral secreting properties. Both classes of PLS-DA models show a separation between secreting and nonsecreting lesions.

identification of ACCs. The esterification of acetate to form acetyl CoA as a major precursor in β-oxidation for FA synthesis is believed to be the main mechanism of acetate incorporation in tumors. Nevertheless, alternative biochemical pathways of acetate intake or accumulation may include the Krebs cycle and the synthesis of cholesterol through citrate.

According to the secreting properties, good results were obtained by PLS-DA models built from both ACC and Ad samples. Unfortunately, when considering the natural history of ACCs, patients with aggressive ACCs (metastatic spread at diagnosis or within 1 year of surgery) were not successfully separated by PLS-DA from patients without metastatic ACCs at diagnosis and during the first 5 years of postsurgical follow-up. However, both the small size and the asymmetry of groups are limiting factors potentially influencing the final results. Further investigations with a larger population are necessary to assess a potential metabolic fingerprint specific for a poor prognosis.

To date, only one recent paper mainly focused on PCCs and paragangliomas (Rao *et al.* 2013) is available concerning the application of NMR spectroscopy for adrenal pathology investigation. Compared with Rao's study, in which liquid NMR spectroscopy was used to analyze homogenized and centrifuged tissue preparations, we studied intact tissue samples using HRMAS NMR spectroscopy. While the inferior sensitivity compared with that of the liquid-state NMR spectroscopy may be a disadvantage, HRMAS NMR spectroscopy allows for a good spectral quality, avoiding laborious procedures for tissue preparation prior to the analysis. Moreover, the tissue sample can be stored again after the acquisition of spectra and is therefore available for pathological analysis when a discrepancy arises between the metabolic and histopathological data of the mirror sample. In Rao's work, the relationships between genotype-specific differences in mitochondrial function and catecholamine content in paragangliomas (PGLs) have been established. These authors also demonstrated for the first time the feasibility of detecting catecholamines by NMR spectroscopy in PCC and paraganglioma samples, confirming our previous findings obtained from the analysis of normal adrenal medullary tissue samples (Imperiale *et al.* 2011).

Of the 14 sporadic PCC samples analyzed, 12 exhibited predominant or exclusive noradrenaline secretion. In sporadic PCC samples, HRMAS NMR spectroscopy revealed a greater amount of noradrenaline than of adrenaline. In contrast, in the normal medullary tissue samples, adrenaline was more abundant than noradrenaline. As is well known, the synthesis of adrenaline depends on the presence of phenylethanolamine-*N*-methyltransferase (PNMT). The levels of *PNMT* mRNA have been found to be lower in PCC samples than in the normal medulla (Lehnert 1998). This disparity is probably responsible for the difference in catecholamine content between tumors and normal adrenal medulla, leading to higher noradrenaline secretion in PCC samples examined in the present study. Unfortunately, the data concerning PNMT tumor activity in the PCC samples examined are not available for further correlations.

In patients with hereditary PCCs, the results of HRMAS NMR investigation matched the biological findings. MEN2- and NF1-related PCC samples exhibited the presence of both adrenaline and noradrenaline. In the VHL disease-related PCC samples, only noradrenaline was detected by HRMAS NMR spectroscopy. The low noradrenaline value measured in the VHL disease-related PCC samples contrasts with the high catecholamine production and the elevated rate constants of catecholamine secretion in this PCC genotype. The small quantity of starting material for the NMR analysis may be a potential bias in the assessment of the amount of noradrenaline.

http://erc.endocrinology-journals.org
DOI: 10.1530/ERC-13-0232

Published by Bioscientifica Ltd.

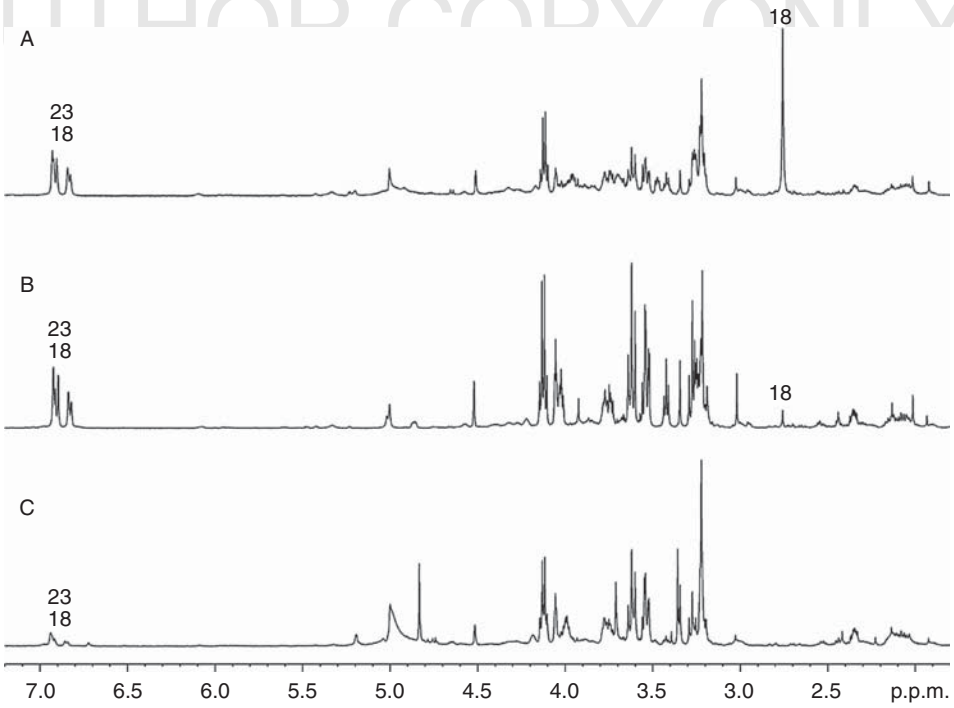

Figure 5

One-dimensional ^{1}H CPMG HRMAS spectra obtained from three sporadic PCC samples with different catecholamine-secreting patterns: (A) predominant adrenaline secretion, (B) predominant noradrenaline secretion, and (C) exclusive noradrenaline secretion. The intensity of each spectrum was normalized with respect to the weight of the tissue sample. The numbers refer to the metabolites listed in Table 1.

Unfortunately, the size of the samples analyzed does not allow us to draw any definitive conclusion. However, these results are in agreement with the findings of Rao *et al.* (2013), who investigated a larger cohort of patients with hereditary paragangliomas.

A higher quantity of GABA discriminated PCC samples from the normal medullary tissue and ACC samples, suggesting a role in PCC pathophysiology. Interestingly, in the early 1980s, Hatanaka *et al.* (1980) described a clonal cell line (PC 12) established from a rat PCC model able to synthesize GABA together with catecholamine and acetylcholine.

Ascorbic acid is critical in the biochemical cascade of catecholamine production (Lehnert 1998). In the present series, ascorbic acid was identified as a significant discriminator of PCCs than of the normal medulla and ACCs. In 1977, a clonal line of rat PCC cells was used as

Table 2 Catecholamine quantification results obtained from the HRMAS NMR analysis of eight normal medullary tissue and 20 PCC samples

	Number of samples	NA (nmol/mg)	Adrenaline (nmol/mg)
Normal medulla	8	0.6 (0–1.8)[a]	1.6 (0.7–4.4)[a]
Sporadic PCC	14	2.4 (0–11.6)[a]	1.8 (0–5.3)[a]
VHL disease-related PCC	1	1	ND
	1	0.4	ND
NF1-related PCC	1	2.8	2.1
	1	1.6	1.1
MEN2-related PCC	1	5.8	2.3
	1	0.8	3.9

NA, noradrenaline; ND, undetectable.
[a]Median (range).

Published by Bioscientifica Ltd.

a model of noradrenergic tissue to study ascorbic acid transport (Spector & Greene 1977). In these cells, ^{14}C-ascorbic acid was concentrated by an energy-dependent transport system. Moreover, the optimal production of noradrenaline required ascorbate in the medium. In our 20 PCC samples, ascorbic acid was significantly correlated (Spearman's correlation test, $P<0.05$) to the amount of noradrenaline ($R=0.56$). The level of noradrenaline in PCC samples could also be biased from the lack of PNMT. However, the correlation existing also between ascorbic acid and adrenaline amounts ($R=0.55$) and the sum of noradrenaline plus adrenaline amounts ($R=0.64$) underlines the role played by ascorbate in catecholamine biosynthetic pathway.

The 3,4-dihydroxybenzene group, common to both adrenaline and noradrenaline, generates a clear signal between 6.8 and 6.9 p.p.m. This signal, unaffected by any significant pollution, is hence easy to recognize and quantify. According to these considerations, the 3,4-dihydroxybenzene group resonance assumes a diagnostic significance and may have an impact on clinical practice. Interesting results were reported on this topic by Kim *et al.* (2009), who used *in vivo* MRS to describe a signal at 6.8 p.p.m. in PCC samples probably representing catecholamines not observed in cortical Ad samples. Indeed, further developments of *in vivo* magnetic resonance spectroscopy (MRS) focusing on catecholamine spectral regions could be an interesting and useful axis of clinical research in patients with atypical adrenal masses that are challenging to characterize by preoperative investigations.

Despite these interesting results, this study has the inherent limitations of any retrospective observational case series including a relatively limited number of patients because it was focused on a rare condition. Consequently, the small number of samples makes this study a preliminary investigation. In addition, malignant PCCs, which are the most clinically important tumors with a particularly poor prognosis, are not adequately represented. Nevertheless, this study represents one of the first applications of metabolomics to adrenal pathophysiology and it is the largest study to report HRMAS data related to the adrenal cortex and adrenal cortical tumors, laying the foundations for future, more complex investigations also including data from molecular biology and other omics procedures.

Declaration of interest

The authors declare that there is no conflict of interest that could be perceived as prejudicing the impartiality of the research reported.

Funding

This work is part of the CARMeN project and was supported by grants from Région Alsace, Oséo, Communauté Urbaine de Strasbourg, Conseil Départemental du Bas-Rhin, Bruker BioSpin, University of Strasbourg, and Strasbourg University Hospital.

Author contribution statement

A I wrote the manuscript and was responsible for study design, data analysis, bibliographic research, and manuscript review; F-M M was responsible for HRMAS NMR data acquisition, spectral analysis, and manuscript review; K E was responsible for experimental design, spectral analysis, and manuscript review; N R was involved in patient biological exploration and manuscript review; M P had responsibility for experimental design and manuscript review; J-P B conducted the histopathological analysis; B G was involved in patient clinical management and manuscript review; P B was responsible for patient surgical management and manuscript review; and I-J N was involved in experimental design, data analysis, and manuscript review. All the authors read and approved the final manuscript.

Acknowledgements

The Tumor Bio-bank (Centre de Ressources Biologiques) personnel of the Strasbourg University Hospital are gratefully acknowledged for their technical assistance.

References

Beckonert O, Coen M, Keun HC, Wang Y, Ebbels TM, Holmes E, Lindon JC & Nicholson JK 2010 High-resolution magic-angle-spinning NMR spectroscopy for metabolic profiling of intact tissues. *Nature Protocols* **5** 1019–1032. (doi:10.1038/nprot.2010.45)

Claudino WM, Goncalves PH, di Leo A, Philip PA & Sarkar FH 2012 Metabolomics in cancer: a bench-to-bedside intersection. *Critical Reviews in Oncology/Hematology* **84** 1–7. (doi:10.1016/j.critrevonc.2012.02.009)

Ebbels T & Cavill R 2009 Bioinformatic methods in NMR-based metabolic profiling. *Progress in Nuclear Magnetic Resonance Spectroscopy* **55** 361–374. (doi:10.1016/j.pnmrs.2009.07.003)

Elbayed K, Dillmann B, Raya J, Piotto M & Engelke F 2005 Field modulation effects induced by sample spinning: application to high-resolution magic angle spinning NMR. *Journal of Magnetic Resonance* **174** 2–26. (doi:10.1016/j.jmr.2004.11.017)

Griffin JL & Shockor JP 2004 Metabolic profiles of cancer cells. *Nature Reviews. Cancer* **4** 551–561. (doi:10.1038/nrc1390)

Hatanaka H, Tanaka M & Amano T 1980 A clonal rat pheochromocytoma cell line possesses synthesizing ability of γ-aminobutyric acid together with catecholamine and acetylcholine. *Brain Research* **183** 490–493. (doi:10.1016/0006-8993(80)90487-4)

Imperiale A, Elbayed K, Moussallieh FM, Neuville A, Piotto M, Bellocq JP, Lutz P & Namer IJ 2011 Metabolomic pattern of childhood neuroblastoma obtained by ^{1}H-high-resolution magic angle spinning (HRMAS) NMR spectroscopy. *Pediatric Blood & Cancer* **56** 24–34. (doi:10.1002/pbc.22668)

Jain M, Rechache N & Kebebew E 2012 Molecular markers of adrenocortical tumors. *Journal of Surgical Oncology* **106** 549–556. (doi:10.1002/jso.23119)

Kim S, Salibi N, Hardie AD, Xu J, Lim RP, lee VS & Taouli B 2009 Characterization of adrenal pheochromocytoma using respiratory-triggered proton MR spectroscopy: initial experience. *AJR. American Journal of Roentgenology* **192** 450–454. (doi:10.2214/AJR.07.4027)

Published by Bioscientifica Ltd.

Korevaar TI & Grossman AB 2011 Pheochromocytomas and paragangliomas: assessment of malignant potential. *Endocrine* **40** 354–365. (doi:10.1007/s12020-011-9545-3)

Lehnert H 1998 Regulation of catecholamine synthesizing enzyme gene expression in human pheochromocytoma. *European Journal of Endocrinology* **138** 363–367. (doi:10.1530/eje.0.1380363)

Lloyd RV 2011 Adrenal cortical tumors, pheochromocytomas and paragangliomas. *Modern Pathology* **24** S58–S65. (doi:10.1038/modpathol.2010.126)

Lombardi CP, Raffaelli M, Pani G, Maffione A, Princi P, Traini E, Galeotti T, Rossi ED, Fadda G & Bellantone R 2006 Gene expression profiling of adrenal cortical tumors by cDNA macroarray analysis. Results of a preliminary study. *Biomedicine & Pharmacotherapy* **60** 186–190. (doi:10.1016/j.biopha.2006.03.006)

Martinez-Bisbal MC, Marti-Bonmati L, Piquer J, Revert A, Ferrer P, Llacer JL, Piotto M, Assemat O & Celda B 2004 1H and 13C HR-MAS spectroscopy of intact biopsy samples *ex vivo* and *in vivo* 1H MRS study of human high grade gliomas. *NMR in Biomedicine* **17** 191–205. (doi:10.1002/nbm.888)

McNicol AM 2011 Update on tumours of the adrenal cortex, phaeochromocytoma and extra-adrenal paraganglioma. *Histopathology* **58** 155–168. (doi:10.1111/j.1365-2559.2010.03613.x)

Nicholson JK & Wilson ID 2003 Understanding 'global' systems biology; metabonomics and the continuum of metabolism. *Nature Reviews. Drug Discovery* **2** 668–676. (doi:10.1038/nrd1157)

O'Connell TM 2012 Recent advances in metabolomics in oncology. *Bioanalysis* **4** 431–451. (doi:10.4155/bio.11.326)

Papotti M, Libé R, Durengon E, Volante M, Bertherat J & Tissier F 2011 The Weiss score and beyond – histopathology for adrenocortical carcinoma. *Hormones & Cancer* **2** 333–340. (doi:10.1007/s12672-011-0088-0)

Peet AC, McConville C, Wilson M, Levine BA, Reed M, Dyer SA, Edwards EC, Strachan MC, McMullan DJ, Wilkes TM *et al.* 2007 1H MRS identifies specific metabolite profiles associated with MYCN-amplified and non-amplified tumour subtypes of neuroblastoma cell lines. *NMR in Biomedicine* **20** 692–700. (doi:10.1002/nbm.1181)

Piotto M, Bourdonneau M, Furrer J, Bianco A, Raya J & Elbayed K 2001 Destruction of magnetization during TOCSY experiments performed under magic angle spinning: effect of radial B1 inhomogeneities. *Journal of Magnetic Resonance* **149** 114–118. (doi:10.1006/jmre.2001.2287)

Piotto M, Moussallieh FM, Dillmann B, Imperiale A, Neuville A, Brigand C, Bellocq JP, Elbayed K & Namer IJ 2009 Metabolic characterization of primary human colorectal cancers using high resolution magic angle spinning 1H magnetic resonance spectroscopy. *Metabolomics* **5** 292–301. (doi:10.1007/s11306-008-0151-1)

Piotto M, Moussallieh FM, Imperiale A, Benahmed MA, Detour J, Bellocq JP, Namer IJ & Elbayed K 2012 Reproducible sample preparation and spectrum acquisition techniques for metabolic profiling of human tissues by proton high-resolution magic angle spinning nuclear magnetic resonance. In *Methodologies for Metabolomics: Experimental Strategies and Techniques*, pp 496–524. Ed P Lutz. UK: Cambridge University Press.

Rao JU, Engelke U, Rodenburg R, Wevers R, Pacak K, Eisenhofer G, Qin N, Kuster B, Goudswaard A, Lenders JW *et al.* 2013 Genotype-specific abnormalities in mitochondrial function associate with distinct profiles of energy metabolism and catecholamine content in pheochromocytoma and paraganglioma. *Clinical Cancer Research* **30** 3787–3795. (doi:10.1158/1078-0432.CCR-12-3922)

Rechache NS, Wang I, Stevenson HS, Killian JK, Edelman DC, Merino M, Zhang L, Nilubol N, Stratakis CA, Meltzer PS *et al.* 2012 DNA methylation profiling identifies global methylation differences and markers of adrenocortical tumors. *Journal of Clinical Endocrinology and Metabolism* **97** E1004–E1013. (doi:10.1210/jc.2011-3298)

Roman S 2006 Adrenocortical carcinoma. *Current Opinion in Oncology* **18** 36–42. (doi:10.1097/01.cco.0000198976.43992.14)

Sitter B, Bathen TF, Tessem MB & Gribbestad IS 2009 High-resolution magic angle spinning (HR MAS) MR spectroscopy in metabolic characterization of human cancer. *Progress in Nuclear Magnetic Resonance Spectroscopy* **54** 239–254. (doi:10.1016/j.pnmrs.2008.10.001)

Spector R & Greene LA 1977 Ascorbic acid transport by a clonal line of pheochromocytoma cells. *Brain Research* **136** 131–140. (doi:10.1016/0006-8993(77)90137-8)

Stratakis CA 2003 Genetics of adrenocortical tumors: gatekeepers, landscapers and conductors in symphony. *Trends in Endocrinology and Metabolism* **14** 404–410. (doi:10.1016/j.tem.2003.08.005)

Stratakis CA 2005 Applications of genomic medicine in endocrinology and post-genomic endocrine research. *Hormones* **4** 38–44.

Weiss LM, Medeiros LJ & Vickery AL Jr 1989 Pathologic features of prognostic significance in adrenocortical carcinoma. *American Journal of Surgical Pathology* **13** 202–206. (doi:10.1097/00000478-198903000-00004)

Wilson M, Davies NP, Brundler MA, McConville C, Grundy RG & Peet AC 2009 High resolution magic angle spinning 1H NMR of childhood brain and nervous system tumours. *Molecular Cancer* **8** 6–17. (doi:10.1186/1476-4598-8-6)

Wishart DS, Tzur D, Knox C, Eisner R, Chi Guo A, Young N, Cheng D, Jewell K, Arndt D, Sawhney S *et al.* 2007 HMDB: Human Metabolome Database. *Nucleic Acids Research* **35** D521–D526. (doi:10.1093/nar/gkl923)

Young WF 2007 Incidentally discovered adrenal mass. *New England Journal of Medicine* **356** 601–610. (doi:10.1056/NEJMcp065470)

Received in final form 25 July 2013
Accepted 6 August 2013
Made available online as an Accepted Preprint
6 August 2013

Published by Bioscientifica Ltd.

NEOPLASIA
www.neoplasia.com

Volume 17 Number 1 January 2015 pp. 55–65 55

Metabolome Profiling by HRMAS NMR Spectroscopy of Pheochromocytomas and Paragangliomas Detects SDH Deficiency: Clinical and Pathophysiological Implications[1,2]

Alessio Imperiale[*,†], François-Marie Moussallieh[†], Philippe Roche[‡], Stéphanie Battini[*,†], A. Ercument Cicek[§], Frédéric Sebag[‖], Laurent Brunaud[¶], Anne Barlier[#], Karim Elbayed[†], Anderson Loundou[**], Philippe Bachellier[††], Bernard Goichot[‡‡], Constantine A. Stratakis[§§], Karel Pacak[‖‖], Izzie-Jacques Namer[*,†] and David Taïeb[¶¶]

*Department of Biophysics and Nuclear Medicine, Hautepierre Hospital, University Hospitals of Strasbourg, Strasbourg, France; [†]ICube, UMR 7357, University of Strasbourg/CNRS and FMTS, Faculty of Medicine, Strasbourg, France; [‡]Integrative Structural and Chemical Biology (iSCB) and INT-3D Molecular Modeling Platform, Cancer Research Centre of Marseille, CNRS UMR7258, INSERM U1068, Institut Paoli Calmettes, Aix-Marseille University UM105, Marseille, France; [§]Lane Center for Computational Biology, School of Computer Science, Carnegie Mellon University, Pittsburgh, PA, USA; [‖]Department of Endocrine Surgery, La Timone University Hospital, Aix-Marseille University, Marseille, France; [¶]Department of Digestive, Hepato-Biliary and Endocrine Surgery, Brabois University Hospital, Nancy, France; [#]Laboratory of Biochemistry and Molecular Biology, Conception Hospital, Aix-Marseille University, Marseille, France; **Department of Public Health, Aix-Marseille University, Marseille, France; [††]Department of Visceral Surgery and Transplantation, Hautepierre Hospital, University Hospitals of Strasbourg, Strasbourg, France; [‡‡]Department of Internal Medicine, Diabetes and Metabolic Disorders, Hautepierre Hospital, University Hospitals of Strasbourg, Strasbourg, France; [§§]Section on Genetics and Endocrinology (SEGEN), Program on Developmental Endocrinology and Genetics (PDEGEN), Eunice Kennedy Shriver National Institute of Child Health and Human Development, National Institutes of Health, Bethesda, MD, USA; [‖‖]Program in Reproductive and Adult Endocrinology, Eunice Kennedy Shriver National Institute of Child Health and Human Development, National Institutes of Health, Bethesda, MD, USA; [¶¶]La Timone University Hospital, European Center for Research in Medical Imaging, Aix-Marseille University, Marseille, France

Abbreviations: GSH, glutathione; HRMAS, ^{1}H high-resolution magic angle spinning; NMR, nuclear magnetic resonance; PGL, paraganglioma; PHEO, pheochromocytoma; *SDH*, succinate dehydrogenase

Address all correspondence to: Alessio Imperiale, MD, PhD, Department of Biophysics and Nuclear Medicine, Hautepierre University Hospital, 1, Avenue Molière, 67098 Strasbourg Cedex, France.
E-mail: alessio.imperiale@chru-strasbourg.fr

[1] This article refers to supplementary materials, which are designated by Supplementary Tables 1 to 4 and Supplementary Figures 1 and 2 and are available online at www.neoplasia.com.

[2] This work is part of the CARMeN project and was supported by grants from Région Alsace, Oséo, Communauté Urbaine de Strasbourg, Conseil Départemental du Bas-Rhin, Bruker BioSpin, University of Strasbourg, and Strasbourg University Hospital. Competing interests: The authors have declared no competing interests. Author contributions: A.I.—writer, study design, spectra and data analysis, bibliographic research, and manuscript review; F.-M.M.—HRMAS-NMR data acquisition, spectra analysis and metabolites quantification; P.R.—modeling, data analysis; S.B.—statistical analysis; A.E.C.—network analysis; F.S.—patient surgical management; L.B.—patient surgical management; A.B.—molecular biology analysis, data analysis; K.E.—spectra analysis and metabolites quantification; A.L.—statistical analysis, data analysis; P.B.—patient surgical management; B.G.—patient clinical management, data analysis; C.S.—writer, manuscript review; K.P.—writer, data analysis, manuscript review; I.-J.N.—experimental design, data analysis, manuscript review. D.T.—writer, study design, data analysis, bibliographic research, and manuscript review. All authors have read and approved the final manuscript.
Received 3 September 2014; Revised 23 October 2014; Accepted 27 October 2014

1476-5586/15
http://dx.doi.org/10.1016/j.neo.2014.10.010

Abstract

Succinate dehydrogenase gene (SDHx) mutations increase susceptibility to develop pheochromocytomas/paragangliomas (PHEOs/PGLs). In the present study, we evaluate the performance and clinical applications of ^{1}H high-resolution magic angle spinning (HRMAS) nuclear magnetic resonance (NMR) spectroscopy–based global metabolomic profiling in a large series of PHEOs/PGLs of different genetic backgrounds. Eighty-seven PHEOs/PGLs (48 sporadic/23 SDHx/7 von Hippel-Lindau/5 REarranged during Transfection/3 neurofibromatosis type 1/1 hypoxia-inducible factor 2α), one SDHD variant of unknown significance, and two Carney triad (CTr)–related tumors were analyzed by HRMAS-NMR spectroscopy. Compared to sporadic, SDHx-related PHEOs/PGLs exhibit a specific metabolic signature characterized by increased levels of succinate ($P < .0001$), methionine ($P = .002$), glutamine ($P = .002$), and myoinositol ($P < .0007$) and decreased levels of glutamate ($P < .0007$), regardless of their location and catecholamine levels. Uniquely, ATP/ascorbate/glutathione was found to be associated with the secretory phenotype of PHEOs/PGLs, regardless of their genotype ($P < .0007$). The use of succinate as a single screening test retained excellent accuracy in distinguishing SDHx *versus* non–SDHx-related tumors (sensitivity/specificity: 100/100%). Moreover, the quantification of succinate could be considered a diagnostic alternative for assessing SDHx-related mutations of unknown pathogenicity. We were also able, for the first time, to uncover an SDH-like pattern in the two CTr-related PGLs. The present study demonstrates that HRMAS-NMR provides important information for SDHx-related PHEO/PGL characterization. Besides the high succinate–low glutamate hallmark, SDHx tumors also exhibit high values of methionine, a finding consistent with the hypermethylation pattern of these tumors. We also found important levels of glutamine, suggesting that glutamine metabolism might be involved in the pathogenesis of SDHx-related PHEOs/PGLs.

Neoplasia (2015) 17, 55–65

Introduction

Pheochromocytomas/paragangliomas (PHEOs/PGLs) are characterized by high genetic heterogeneity—more than 14 different well-studied genes have been linked to the development of these tumors. Current genetic testing identifies pathogenic mutations in one third or more of cases. Of all the known genetic mutations, deleterious mutations in any of the *succinate dehydrogenase* (*SDH*) genes (collectively named *SDHx*-associated tumors) are currently the leading genetic cause of head and neck PGLs and account for more than 30% of all hereditary cases. The four *SDHx* genes encode the four subunits of the SDH enzyme (also named mitochondrial complex II). This membrane complex catalyzes the oxidation of succinate to fumarate in the tricarboxylic acid (TCA) cycle and the respiratory chain. In *SDHx* mutation carriers, tumorigenesis requires a second hit process (biallelic inactivation) that invariably results in decreased SDH activity and/or a significant reduction or complete absence of its protein. For the index cases, genetic testing is often needed to implement personalized medical approaches [1]. A great benefit of genetic testing also comes from evaluating family members since they are potentially at risk of developing tumors, often multiple and metastatic ones.

Until present, the choice of which genes to be tested has been guided by clinical presentation and *ex vivo* biomarkers. Immunohistochemistry can be very well used to show the presence or absence of protein products [2,3]. Metabolomics, or global metabolite profiling, which is a new technology of functional genomics, can be used for investigating metabolite changes associated with some gene mutations [4]. Currently, well-recognized tools for metabolomics are nuclear magnetic resonance (NMR) spectroscopy and gas chromatography–mass spectrometry (GC-MS) or liquid chromatography (LC)–MS. GC-MS and LC-MS are more widely represented in the technical platforms referred to as metabolomics, mainly due to their high sensitivity [5]. These technologies generate massive amounts of data that can be interpreted and used for building predictive models. For this purpose, machine-learning algorithms represent potent and useful instruments to reduce the complexity of the data analysis. Among NMR techniques, ^{1}H high-resolution magic angle spinning (HRMAS) NMR spectroscopy technology is especially suited to analyze a small volume of intact tissue samples while avoiding any chemical extraction procedures or sample manipulation, which are necessary for both MS and liquid-state NMR or well-established immunohistochemistry. HRMAS NMR enables rapid (3-4 minutes for tissue sample preparation followed by 10 minutes of spectra acquisition) and reliable identification and quantification of several metabolites from spectra with excellent resolution and signal-to-noise ratio. Recently, metabolomics has proven to be a promising tool in the characterization PHEO/PGL [6–10].

The aim of the present study was to investigate the HRMAS NMR-based metabolomic profiling of PHEOs/PGLs to 1) confirm the accuracy of the previously described metabotype pattern based on

four selected metabolites [i.e., succinate, glutamate, glutathione (GSH), and ATP] in the diagnosis of SDH-related PHEO/PGL in a large cohort of tumors with different genetic backgrounds, 2) define the global metabolomic profile of the SDH-related PHEOs/PGLs in comparison to sporadic tumors, and 3) identify metabolites that could be used as clinical predictors of SDH deficiency even in PHEOs/PGLs without any germline or somatic susceptibility gene mutations.

Materials and Methods

Patients and Tumors

Eighty-seven specimens of PHEOs and PGLs of sympathetic origin obtained from 79 unrelated patients were retrospectively selected in this study according to the following criteria:

1. Histologic diagnosis of PGL/PHEO
2. Genetic screening for germline mutations in the SDH subunits B/C/D (*SDHB/C/D*) (including large gene rearrangements of all the *SDH* genes), von Hippel-Lindau (*VHL*) (including large gene rearrangements), neurofibromatosis type 1 (*NF1*) (in the presence of clinical features), REarranged during Transfection (*RET*) (in the presence of hypercalcitoninemia), transmembrane-encoding gene *TMEM127*, and MYC-associated factor X genes
3. Absence of systemic anticancer therapy before surgery
4. Tissue specimens collected during surgery just after tumor removal and snap-frozen in liquid nitrogen before storage at −80°C.

The tumors were obtained from three different institutions in France (Strasbourg, Marseille, and Nancy University Hospitals) and were distributed as follows: 48 sporadic (42 PHEOs, 6 sympathetic PGLs), 23 *SDHx* (5 PHEOs, 18 sympathetic PGLs), 7 *VHL* (5 PHEOs, 2 sympathetic PGLs), 5 *RET* (PHEOs), 3 *NF1* (PHEOs), and 1 hypoxia-inducible factor 2α (*EPAS1/HIF2A*) (sympathetic PGL). The 23 samples of *SDHx* tumors were obtained from 23 distinct tumors belonging to 15 patients and were distributed as follows: 9 *SDHB* and 14 *SDHD*.

Data were acquired under regular clinical care conditions, with Ethics Committee approval obtained for the use of these data for scientific purposes. Written informed consent was obtained from all patients included in the present study.

HRMAS NMR Spectroscopy

HRMAS NMR spectra were recorded on a Bruker Avance III 500 spectrometer operating at a proton frequency of 500.13 MHz, installed at the Pathological Department of Strasbourg University Hospital. The amount of frozen tissue used for NMR analysis ranged from 15 to 20 mg. A one-dimensional (1D) proton spectrum using a Carr-Purcell-Meiboom-Gill (CPMG) pulse sequence with presaturation of the water signal was acquired for each sample. 1D HRMAS NMR spectra were bucketed into integral regions 0.01 ppm wide (ppm range, 1-8.65) using AMIX 3.8 software (Bruker GmbH, Rheinstetten, Germany) and exported into SIMCA P (version 11.0; Umetrics AB, Umeå, Sweden).

To confirm resonance assignments, two-dimensional (2D) heteronuclear (^{1}H-^{13}C) experiments were also recorded immediately after the end of 1D spectra acquisition. Because the duration of these experiments is long and tissue degradation occurs during NMR acquisition, only a few representative samples were analyzed by 2D experiments. Metabolites were assigned using standard metabolite chemical shift tables available in the literature [11,12].

Metabolite quantification has been previously described [6]. Briefly, quantification was performed using an external reference standard of sodium lactate, scanned under the same analytical conditions. Spectra were normalized according to sample weight. Peaks of interest were automatically defined by an in-house program using MATLAB 7.0 (Mathworks, Natick, MA). Peak integration was then compared to the one obtained with the lactate reference and was corrected according to the number of protons. For our experiments, only peaks that were well resolved in 1D CPMG spectra were quantified. Quantification results were expressed as nmol/mg of tissue.

Statistical Analysis

A combination of principal component analysis (PCA) and orthogonal partial least square discriminant analysis (OPLS-DA) was herein adopted. The PCA was performed to evaluate the quality of the data and to identify possible outliers [13]. Then, the OPLS-DA was employed to optimize the separation between tumor subgroups. The following two-class models of OPLS-DA were built in this study:

1. SDHx (n = 23) *versus* non-SDHx PHEOs/PGLs (n = 64) including sporadic, *VHL*, *RET*, *NF1*, and *HIF2A* tumors. This analysis was performed to confirm our previous results achieved in a smaller cohort of patients [7] and obtained from the analysis of spectral intervals corresponding exclusively to four selected metabolites with a possible key role in tumoral development. Accordingly, succinate, glutamate, GSH, and ATP were identified and used in the model. Succinate amount was estimated by integrating the area comprised between 2.39 and 2.43 ppm, glutamate quantity between 2.32 and 2.38 ppm, GSH amount between 2.93 and 2.98 ppm, and ATP amount within the range of 6.07 to 6.11 ppm.
2. SDHx (n = 23) *versus* sporadic PHEOs/PGLs (n = 48). Seventy-one selected tumor samples were included in this model to assess the global metabolic fingerprint of *SDHx*-related PHEOs/PGLs in an exploratory and untargeted manner. Accordingly, the full spectrum that ranged from 1 to 8.65 ppm was analyzed and considered in the statistical model. In this case, the OPLS-DA was performed on the whole set of metabolites (variables) to select those with a real discriminating power. Metabolites corresponding to variable importance for projection (VIP) value ≥1 were selected and labeled VIP metabolites. Two measurements of model quality were reported for OPLS-DA: R^2Y and Q^2 representing, respectively, the goodness of fit (i.e., data variation) and the goodness of prediction, as estimated by cross-validation. $Q^2 \geq 0.5$ can be considered as a good predictor [14].

Cross-validation was used in each OPLS-DA model to determine the number of components and to avoid overfitting the data. A cross-validation embedded in a Monte Carlo resampling approach [15,16] was used during the construction of the model to build a confusion matrix that allowed a direct visualization of the performances of the model in terms of classification power [sensitivity (Se), specificity (Sp), positive predictive value (PPV), negative predictive value (NPV), and global accuracy]. The SIMCA P (version 11.0; Umetrics AB) package was used for statistical data analysis.

Continuous variables are expressed as mean ± SD. Statistical analysis was performed using IBM SPSS Statistics version 20 (IBM SPSS Inc, Chicago, IL). The Spearman non-parametric test was performed to determine the correlation between metabolites. Comparisons of tumor metabolite concentrations between *SDHx*-related and sporadic tumors were performed using a Mann-Whitney U test. The receiver operating characteristic (ROC) curves were used to evaluate the clinical utility of metabolite quantification in the diagnosis of *SDHx* mutation. Areas under the ROC curve, sensitivity, and specificity were determined using MedCalc version 13.2.2 (MedCalc Software, Ostend, Belgium). According to the ROC curve, values exhibiting the best accuracies were chosen as the threshold for a screening test. Linear regression model was used to examine the association between metabolite levels and genetic status with adjustment for tumor location and total catecholamine levels

as explanatory variables. For multiple testings, adjusted P values were calculated using the false discovery rate (FDR) procedure with the SAS PROC MULTTEST statement [17]. PCA was performed to visualize and analyze correlations between metabolite concentrations and *SDHx* status. PCA was done using the package FactoMiner (Multivariate Exploratory Data Analysis and Data Mining with R). Values of $P < .05$ were considered to be statistically significant.

Network Analysis

The Algorithm to Determine Expected Metabolite Level Alterations Using Mutual Information (ADEMA) has been applied [18]. Instead of analyzing metabolites one by one, the algorithm assesses the changes in groups of metabolites, between the case and the control. It incorporates the metabolic network topology to determine the groups of metabolites. ADEMA uses mutual information to 1) find out if those metabolites are biomarkers when considered together and 2) predict the expected direction of change per metabolite, when metabolic network topology is considered.

Figure 2 shows the simplified metabolic subnetwork we have used to relate metabolites. The network was constructed using Kyoto Encyclopedia of Genes and Genomes (KEGG) [19,20] and the work of Selway et al. [21] On the basis of the network, the following metabolite groups were obtained:

- aspartate, succinate, glutamate, glutamine, ATP
- methionine, myoinositol, ascorbate, noradrenaline, adrenaline, ATP
- myoinositol, ascorbate, methionine, taurine, ATP
- noradrenaline, adrenaline, total catecholamines, ATP
- myoinositol, ascorbate, noradrenaline, adrenaline, total catecholamines, ATP.

For discretization of metabolite observations, we have set number of levels (M) as 6 and number possible levels an observation assigned to (k) as 4. Missing metabolite observations were amputated using the average measurement value for that metabolite. Using the abovementioned metabolite groups and parameters, an expected metabolite level for case and for control is obtained per metabolite. The direction of the expected change is obtained by comparing expected levels (e.g., *SDHx vs* sporadic PHEOs/PGLs).

Results

SDHx versus Non-SDHx PHEOs/PGLs

At visual inspection, all the spectra obtained from the 87 analyzed tumor samples were of good quality without any prominent hallmarks of tissue necrosis or cystic components. The generated multivariate one-component OPLS-DA based on succinate, glutamate, GSH, and ATP allowed a clear separation of *SDHx* from non-*SDHx* PHEOs/PGLs showing accurate representation of the data and a good cumulative confidence criterion of fit ($R^2Y = 0.65$) and prediction ($Q^2 = 0.64$). These results are graphically represented in Figure 1.

Nineteen of 23 patients with *SDHx*-related PHEOs/PGLs were correctly identified. Moreover, all 64 patients with non–*SDHx*-related PHEOs/PGLs were accurately classified. To detect patients with *SDHx* germline mutations, the Se and Sp of the established model were 83% and 100%, respectively. PPV, NPV, and global accuracy were 100%, 94%, and 95%, respectively.

No significant spectrum overlap that prevented quantification of succinate, glutamate, GSH, and ATP was found. All NMR spectra from the *SDHx*-related PHEOs/PGLs showed significantly high levels of succinate (4.01 ± 2.45 nmol/mg *vs* 0.06 ± 0.06 nmol/mg, $P < .00001$) and lower concentration of glutamate (0.70 ± 0.41 nmol/mg *vs* 1.60 ± 0.76 nmol/mg, $P < .00001$) compared to those of sporadic tumors and PHEOs/PGLs related to *VHL*, *RET*, *NF1*, and *HIF2* mutations. Neither GSH nor ATP amount was significantly different between the *SDHx*- and *non–SDHx*-related PHEOs/PGLs (Figure 1). Interestingly, the four *SDHx*-related tumor samples, which were incorrectly classified by the previous OPLS-DA model, showed significantly lower amounts of succinate ($P = .003$) and higher concentrations of glutamate ($P = .003$) than the remaining 19 *SDHx*-related PHEOs/PGLs [7].

SDHx versus Sporadic PHEOs/PGLs

Twenty-three *SDHx*-related PHEOs/PGLs and 48 sporadic tumors were included in the analysis. A total of 24 metabolites was recognized from the spectra obtained from all 71 tumor samples within the range of 1 to 8.65 ppm (Supplementary Table 1). Besides peaks due to small water-soluble molecules, the acquired spectra display consistent broad resonances, which were attributed to three different fatty acid moieties defined as a, b, and c [22]. A two-component OPLS-DA showed a very clear separation of the two sets of samples, a faithful representation of the Y data ($R^2Y = 0.82$) and a good cumulative confidence criterion of prediction ($Q^2 = 0.7$). These results are graphically represented in Figure 1. When comparing sporadic to *SDHx*-related tumors, the OPLS-DA model accurately classified all samples. Examples of 1D HRMAS CPMG spectra obtained from sporadic and *SDHD*-related PGL are represented in Supplementary Figure 2.

According to the results of the OPLS-DA model, 12 VIP metabolites were identified. A higher level of succinate, myoinositol, methionine, glutamine, taurine, and ATP characterized *SDHx*-related PHEOs/PGLs, while sporadic tumors contained a larger amount of adrenaline, noradrenaline, glutamate, GSH, ascorbate, and aspartic acid (Figure 1). The quantity of the 12 metabolites previously listed was assessed and used for tumor comparison according to the genetic background. When compared to sporadic phenotypes, the metabolomic profile of *SDHx*-related tumors exhibits statistical significance in the following areas:

1. Increased levels of succinate (4.01 ± 2.45 nmol/mg *vs* 0.06 ± 0.06 nmol/mg, $P < .0001$), taurine (2.59 ± 1.35 nmol/mg *vs* 1.66 ± 1.43 nmol/mg, $P = .002$), methionine (0.09 ± 0.04 nmol/mg *vs* 0.04 ± 0.04 nmol/mg, $P < .0001$), glutamine (0.37 ± 0.24 nmol/mg *vs* 0.23 ± 0.16 nmol/mg, $P = .12$), and myoinositol (3.18 ± 1.43 nmol/mg *vs* 1.87 ± 1.49 nmol/mg, $P < .0001$).
2. Decreased levels of aspartate (0.32 ± 0.50 nmol/mg *vs* 0.50 ± 0.27 nmol/mg, $P < .0001$), glutamate (0.71 ± 0.41 nmol/mg *vs* 1.64 ± 0.78 nmol/mg, $P < .0001$), and adrenaline (0.10 ± 0.43 nmol/mg *vs* 1.17 ± 2.18, $P < .001$) (Supplementary Tables 2 and 3).

In spite of GSH, ATP, catecholamines, and ascorbate playing a role in tumor classification in the OPLS-DA model, their amounts were not statistically different between *SDHx*-related PHEOs/PGLs and sporadic tumors when compared using a standard non-parametric univariate test.

Interestingly, after adjustment for tumors, total catecholamine content, and tumor location (adrenal and extra-adrenal), succinate ($P < .0001$), methionine ($P = .002$), glutamate ($P < .0007$), glutamine ($P = .002$), and myoinositol ($P < .0007$) remained statistically different between the two groups (Supplementary Table 3). Correlations between variables are represented in Supplementary Table 4. The importance of the different metabolites regarding their correlations with the mutation status is illustrated in Supplementary Figures (Supplementary Figure 1).

When the data are analyzed using ADEMA, using the metabolic subnetwork depicted in Figure 2, the following results were obtained. ADEMA has predicted a higher level of succinate, myoinositol,

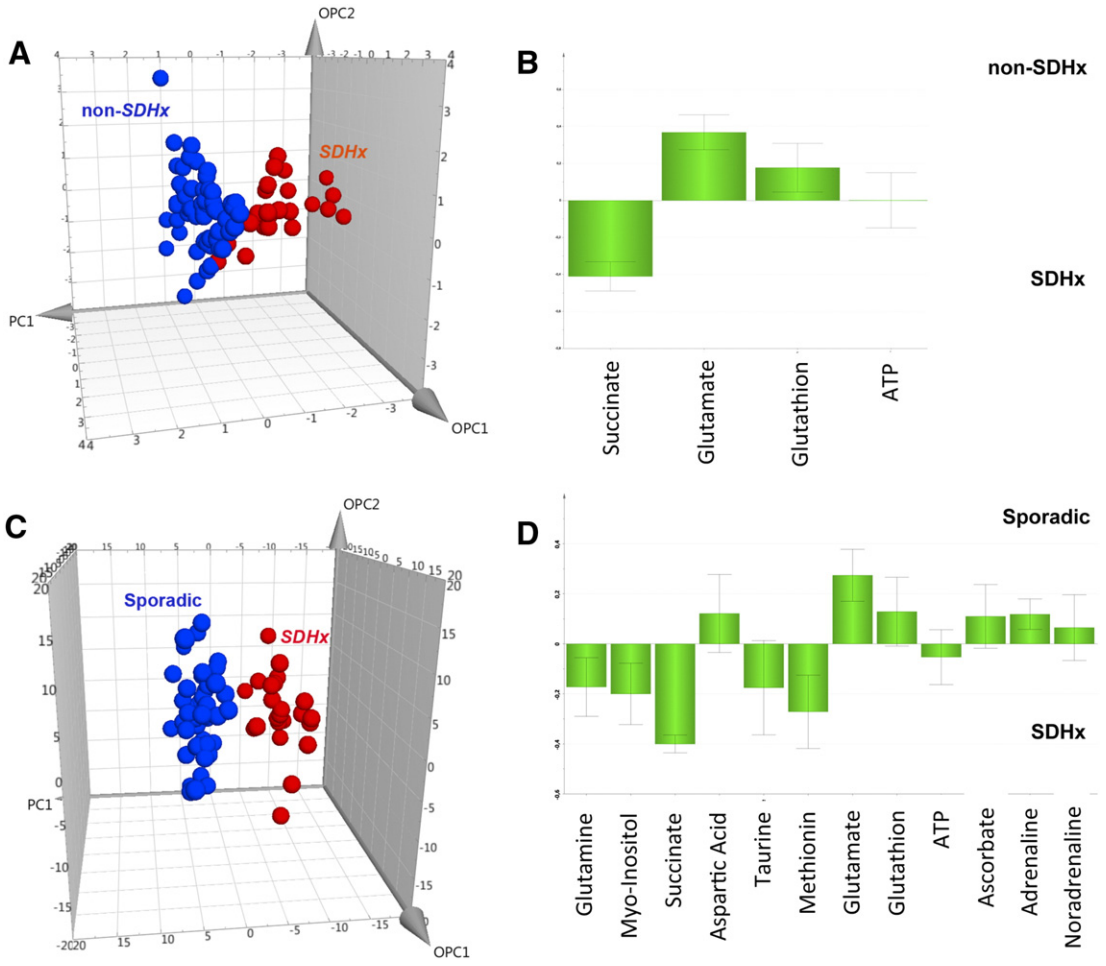

Figure 1. Results of three-component OPLS-DA models and the corresponding loading plots according to the patient's genotypes: (A and B) SDHx ($n = 23$) *versus* non-SDHx PHEOs/PGLs ($n = 64$), including sporadic, VHL, RET, NF1, and HIF2 tumors, and based on succinate, glutamate, GSH, and ATP; (C and D) SDHx ($n = 23$) *versus* sporadic PHEOs/PGLs ($n = 48$) and based on the whole tumoral metabolome. For this OPLS-DA model, the loading plot represents only the 12 metabolites with the higher discriminant power (VIP metabolites). A clear distinction between the different classes of tumors is shown in both models.

methionine, glutamine, and taurine in *SDHx*-related PHEOs/PGLs, while sporadic tumors contained a higher amount of adrenaline, glutamate, GSH, and total catecholamines (Figure 2). ATP, noradrenaline, ascorbate, GSH, and aspartate are predicted to be equivalent among cases and controls. Results show that network and mutual information-based analysis is in accordance with the statistical significance of changes shown above (Supplementary Table 3), with the exception of aspartate. Aspartate is predicted to be same in both groups by ADEMA.

Quantification of Succinate Concentration as a Screening Method for SDH Mutation

The use of succinate as a single screening test showed higher accuracy when compared to other metabolites and a combination of metabolites for distinguishing *SDHx versus* non–*SDHx*-related tumors (including sporadic, *VHL*, *MEN2*, and *HIF2A* tumors; Figure 3 and Table 1) and *SDHx*-related tumors *versus* sporadic ones (Figure 3 and Table 1). As shown in Figure 4, tumors with high succinate levels had a high probability of belonging to an *SDHx* patient. The optimal succinate cutoff was 0.253 nmol/mg for distinguishing *SDHx versus* any non-*SDHx* tumors and 0.096 nmol/mg to discriminate between *SDHx* and sporadic tumors. With these threshold points, Se and Sp were 100% in both situations. Interestingly, the four *SDHx*-related PHEOs/PGLs that were incorrectly classified by the OPLS-DA model built on the whole studied population showed a succinate value higher than the diagnostic threshold established by ROC curve analysis, leading to correct tumor identification. To discriminate *SDHx*-related from sporadic PHEOs/PGLs, ROC curves were also built using the quantitative values of glutamate, methionine, myoinositol, and methionine/glutamate ratio. However, the diagnostic accuracy obtained for each single metabolite was lower than the accuracy achieved by succinate as a single tumor biomarker. The cutoff of 0.742 nmol/mg for glutamate, 0.045 nmol/mg for methionine, and 2.383 nmol/mg for myoinositol provided suboptimal values of Se and Sp in both cases (Se = 86.9% and Sp = 89.5% for glutamate; Se = 95.6% and Sp = 62.5% for methionine; and Se = 73.9% and Sp = 81.2% for myoinositol). Finally, considering 0.0524 nmol/mg as the diagnostic threshold for methionine/glutamate ratio, Se and Sp were 91.3% and 89.6%, respectively (Figure 3 and Table 1).

Quantification of Succinate Concentration as a Functional Test for Evaluating SDHx Mutation of Unknown Pathogenicity

We report the case of a 55-year-old male who was evaluated for bilateral carotid body PGLs (CBPGLs). At the initial examination, there was no family history of any PGL. Plasma/urinary metanephrines and serum chromogranin A were normal. Both PGLs were

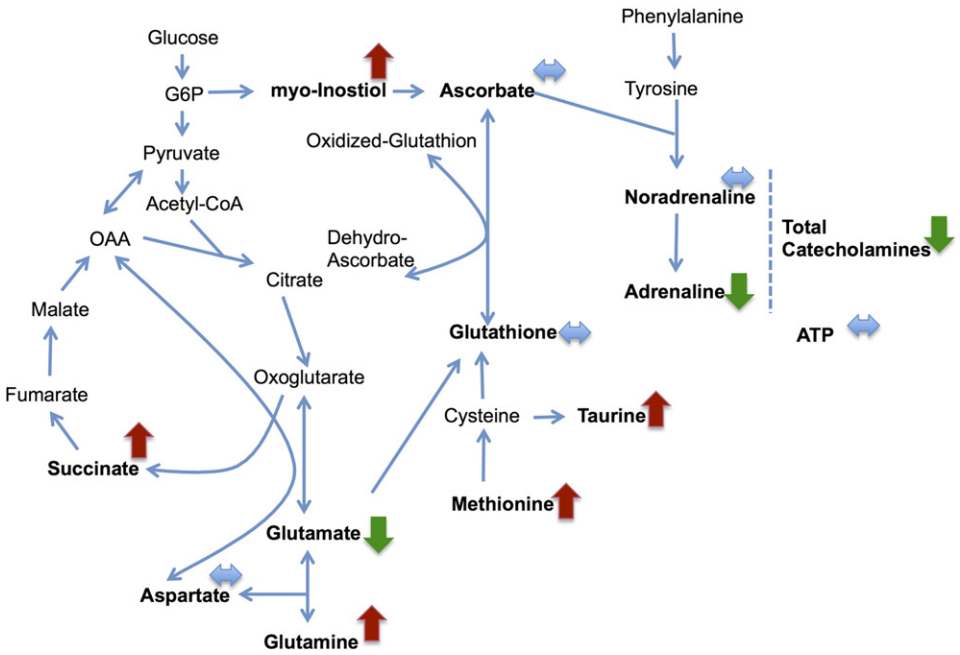

Figure 2. Metabolic subnetwork showing the results of the ADEMA analysis that compares *SDHx* ($n = 23$) *versus* sporadic PHEOs/PGLs ($n = 64$). Red arrows show metabolites that are predicted to increase, green arrows show metabolites that are predicted to decrease, and blue arrows show metabolites that are expected to stay the same, between two groups, respectively.

visualized by computed tomography (CT) and ^{18}F-fluorodihydroxyphenylalanine positron emission tomography/CT (Figure 4, *A* and *B*). Genetic testing revealed a deletion of six nucleotides in exon 4 of the *SDHD* gene (c.433_438del), resulting in a deletion of two amino acids (p.His145_Asp146del, Δ145,146). This allelic variant, never reported in the literature, was classified as of unknown significance according to *in silico* analysis. Both CBPGLs were removed and histopathology confirmed the diagnosis. Investigating the pathogenicity of this mutation, HRMAS NMR spectroscopy of an intact tissue sample showed an increased succinate concentration (0.378 nmol/mg) consistent with an SDH dysfunction (Figure 4*C*). Furthermore, SDHB immunohistochemistry (Figure 4*D*) and homology modeling with MODELLER (Figure 4*E*) further supported the pathogenicity of this mutation. After the diagnosis, the patient's sister was found to have bilateral PHEOs and HNPGLs, further supporting the diagnosis of a hereditary PGL in these family members.

Quantification of Succinate Concentration in a Case of Carney Triad

We report HRMAS NMR spectroscopy findings in two extra-adrenal PGLs obtained from a single Carney triad (CTr) patient. The clinical case was previously reported [23]. Briefly, the diagnosis of CT was based on the following criteria: young female patient (18 years at diagnosis), no family history, two extra-adrenal PGLs of sympathetic origin (one thoracic and one abdominal), multiple gastric Gastrointestinal Stromal Tumor (GIST), and an absence of mutations in any of the *SDH* genes (including large deletions). HRMAS NMR spectra obtained from the analysis of both PGLs are represented in Figure 5 and are uniquely consistent with an SDH mutation–like pattern, showing an important succinate peak corresponding to a succinate amount of 1.91 and 4.63 nmol/mg, respectively.

Discussion

The present study shows that HRMAS NMR spectroscopy is a very reliable method for classifying various PHEOs/PGLs according to their genetic background [7]. Such a metabolomics-based approach allows for the detection of metabolic changes (biomarkers) that are specifically related to a medical condition (e.g., *SDHx*-related mutation), resulting in diagnostic and potential prognostic implications. In our study, HRMAS NMR spectroscopy allowed for the exploratory investigation of the global metabolic phenotype of *SDHx*-related PHEOs/PGLs, leading to the identification of several specific biochemical alterations.

First, we described the whole metabolome findings of SDHx-related PHEOs/PGLs and found that several metabolites do not belong to the Krebs cycle, such as methionine/taurine, glutamate/aspartate, and myoinositol.

Moreover, we found that the assessment of succinate concentration can be clinically relevant as a single metabolic biomarker for discriminating *SDHx*-related tumors from sporadic and other hereditary PHEOs/PGLs. Thus, HRMAS NMR spectroscopy could be used as a reliable screening method for the indication of whether sequencing of one of the *SDH* genes should be initiated. Furthermore, the present study also documents that *SDHx* mutations with unknown pathogenicity could be reclassified by this approach. Finally, in PHEOs/PGLs where a genetic abnormality is highly expected, although leading to the disappearance of SDH protein (e.g., patients with Carney triad), HRMAS NMR spectroscopy can nicely point to such a protein abnormality and could lead to a narrow search for specific genes of this and other cancers.

The role of MS in the diagnosis of SDHx-related tumors and for functional analysis of SDH variants has been recently reported in a large population of patients [9]. Although MS is characterized by a superb sensitivity, it also has some disadvantages. The chemical extraction procedure before tissue sample examination represents a crucial question. Perchloric acid extraction should be avoided because of significant

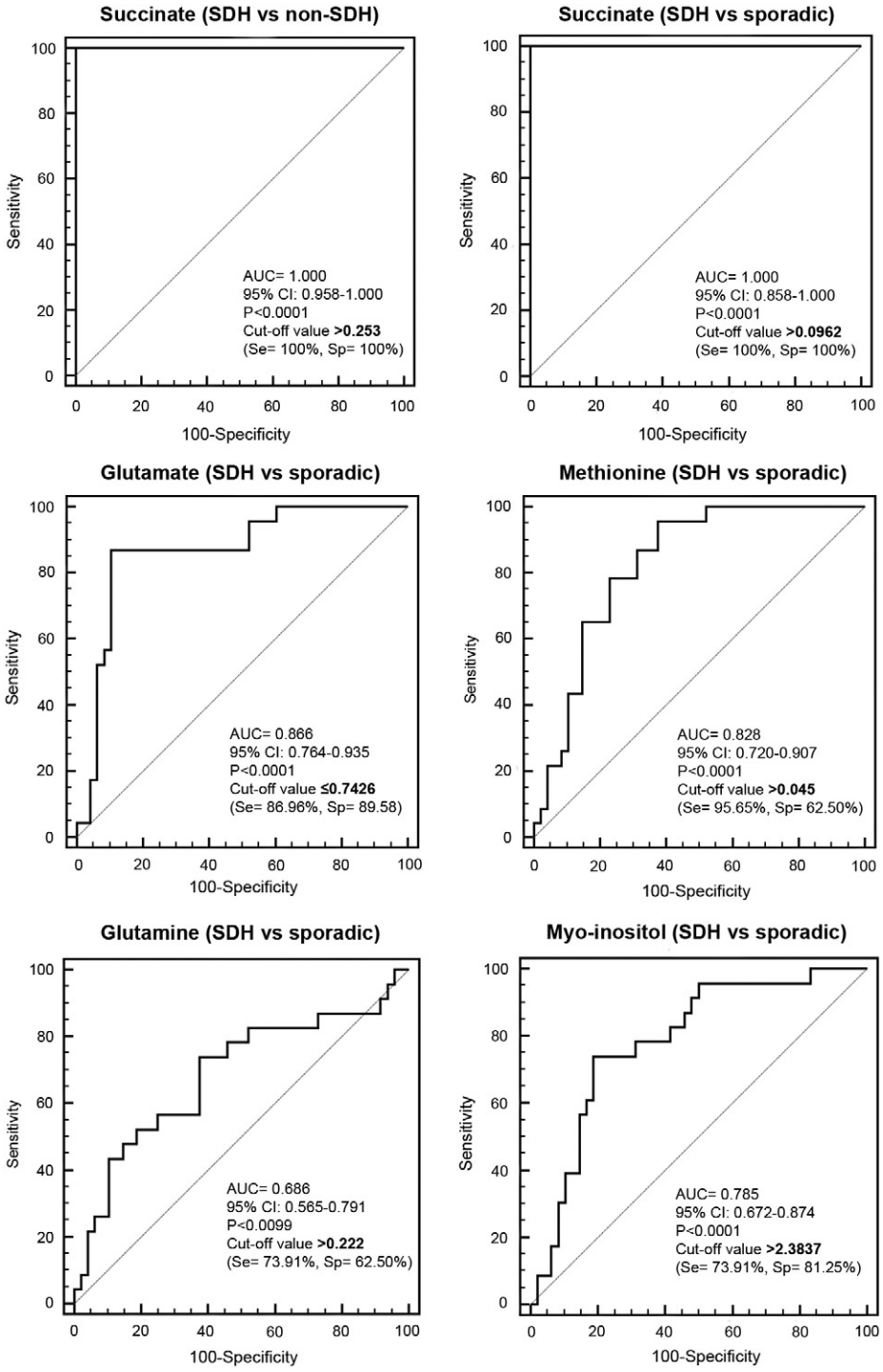

Figure 3. ROC curves obtained from analysis of the succinate, glutamate, methionine, glutamine, and myoinositol concentrations for the diagnosis of SDHx mutation. Detailed information about the area under the ROC curve, the cutoff values, sensitivity, and specificity are shown.

changes in the real metabolic profile. Moreover, LC-MS is neither as reproducible nor resolvable as GC and it is perhaps the slowest (1 to 2 days per sample) of all three methods, including GC-MS and NMR spectroscopy. Finally, LC-MS is not really quantitative and is often designed to simply detect the presence or absence of a molecule rather than to assess its concentration [24]. Furthermore, immunohistochemistry (IHC) for SDH tumors, although currently very popular and reliable, first requires sample processing and, second, an experienced technician and pathologist to minimize false-positive or false-negative interpretations. Moreover, this technique provides a limited view of a tumor's biology, usually assessing only one protein at a time and in a semiquantitative manner. In contrast, HRMAS NMR allows for rapid and reproducible quantification of several metabolites (proteins) from only 15 mg of intact tissue, requiring only about 1 hour to prepare the tissue sample, collect data, and analyze the results. Nevertheless, similar to other approaches, experienced staff are required to interpret results. However, compared to other methods mentioned above, HRMAS NMR spectroscopy provides new insights into the understanding of tumor

Table 1. Performances of Succinate, Methionine, and Glutamate Concentrations in the Diagnosis of SDHx Mutation

	Se (95% CI)	Sp	PPV	NPV	Accuracy
Succinate > 0.253 (*SDHx vs* non-*SDHx*)	100% (85.2-100)	100% (94.4-100)	100% (85.2-100)	100% (94.4-100)	100% (95.8-100)
Succinate > 0.0962 (*SDHx vs* sporadic)	100% (81.5-100)	100% (54.1-100%)	100% (81.5-100)	100% (54.1-100)	100% (86.2-100)
Glutamate ≤ 0.7426 (*SDHx vs* sporadic)	86.9% (66.4-97.2)	89.6% (77.3-96.5)	80.0% (60.9-91.1)	93.5 (82.5-97.8)	88.7 (79.3-91.2)
Methionine > 0.045 (*SDHx vs* sporadic)	95.7% (78.1-99.9)	62.5% (47.4-76.1)	55% (38.5-70.7)	96.8% (83.3-99.9)	73.2% (61.9-82.2)
Glutamine > 0.222 (*SDHx vs* sporadic)	73.9% (51.6-89.9)	62.5% (48.4-74.8)	48.6% (32.9-64.4)	83.3% (68.1-92.1)	66.2% (54.6-76.1)
Myoinositol > 2.3837 (*SDHx vs* sporadic)	73.9% (51.6-89.8)	81.3% (68.1-89.9)	65.4% (46.2-80.6)	86.7% (73.8-93.7)	78.9% (68.0-86.8)
Methionine/glutamate > 0.0524 (*SDHx vs* sporadic)	91.3% (72.0-98.9)	89.6% (77.3-96.5	80.8% (62.1-91.5)	95.6% (85.2-98.8)	90.1% (81.0-95.1)

CI, confidence interval.

biology by simultaneously identifying metabolites from fresh tissue associated with unique cancer metabolome and behavior, including SDHx mutations.

In the present study, except for well-known changes in tumor succinate levels, high methionine and low glutamate/aspartate were found to be associated with SDHx deficiency. Recently, it has been shown that SDHx-related tumors exhibited a hypermethylated phenotype [25]. Thus, a high methionine metabotype is consistent with a hypermethylation pattern. In the methionine cycle, methionine is converted to *S*-adenosyl methionine, which is a methyl donor for numerous reactions of methylation, including DNA. The mechanisms involved in the reduction of glutamate/aspartate in *SDHx*-mutated tumors are largely unknown and might be related to an inhibition of the membrane transport of these amino acids or a decrease in their synthesis due to a TCA defect. It has

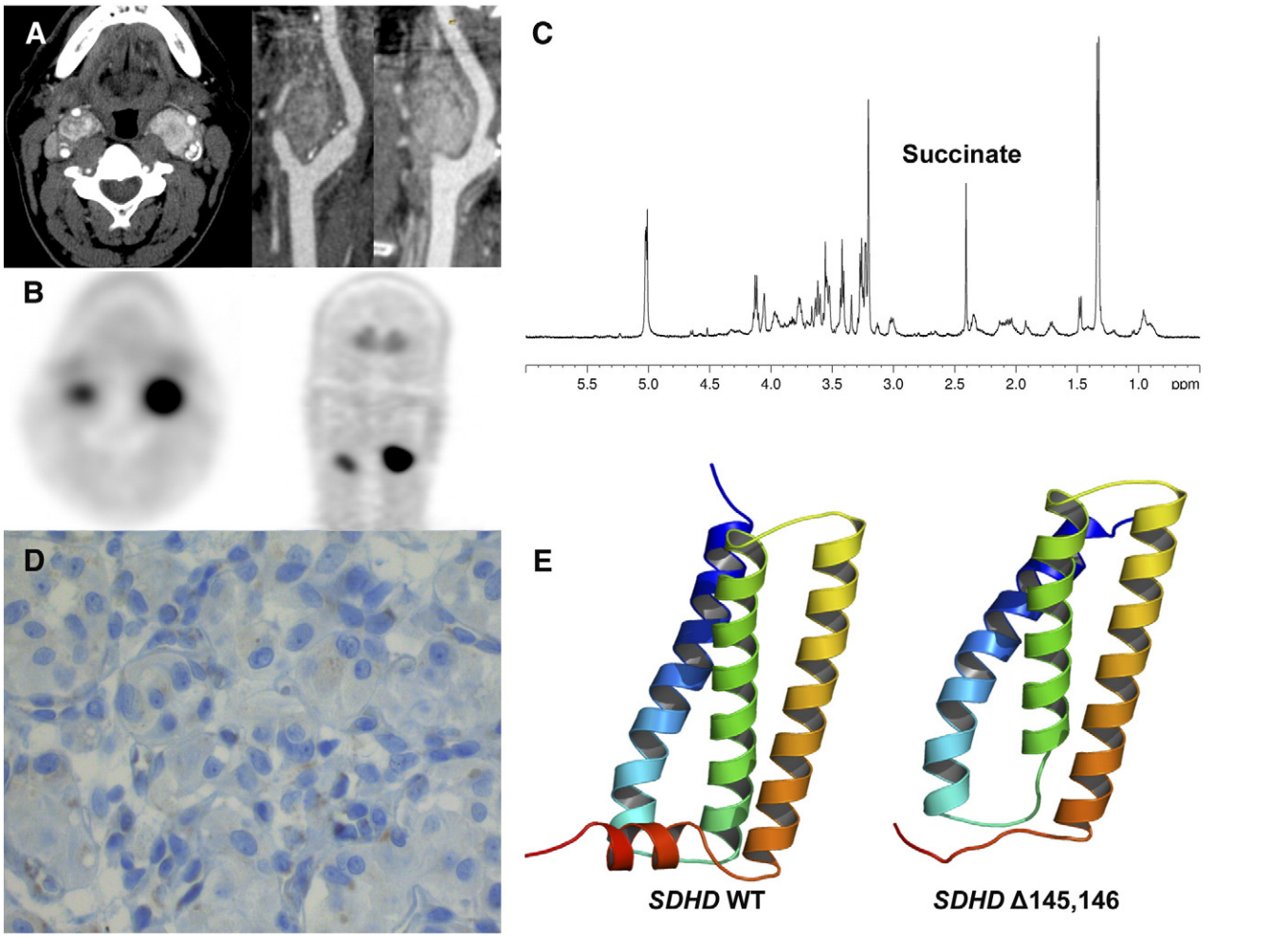

Figure 4. HRMAS NMR spectra from a tumor with SDHD mutation of unknown pathogenicity. Contrast-enhanced CT (A) and ^{18}F-fluorodihydroxyphenylalanine PET/CT (B) showing a CBPGL. Succinate peak on 1D HRMAS CPMG spectrum NMR spectroscopy (C). Absence of significant SDHB immunostaining on tumor cells (D). Cartoon representation of the 3D models of Wild Type (WT) (E, left) and deleted mutant (E, right) of human SDHD. The structures are rendered using a gradient color from blue to red, at the N terminus and C terminus of the protein, respectively. The Δ145,146 deletion occurs in a small loop between H3 (yellow orange) and H4 (reddish) helices and induces a possible destructuration of C-terminal helix H4. In WT SDHD, this alpha-helix interacts with alpha-helix H3 of subunit C and corresponds to the second binding site of ubiquinone. Models were generated with Modeller v9.13 using the crystal structure of porcine mitochondrial SDH as a template (PDB code 1ZP0). Panel E was generated with PyMOL program (www.pymol.org).

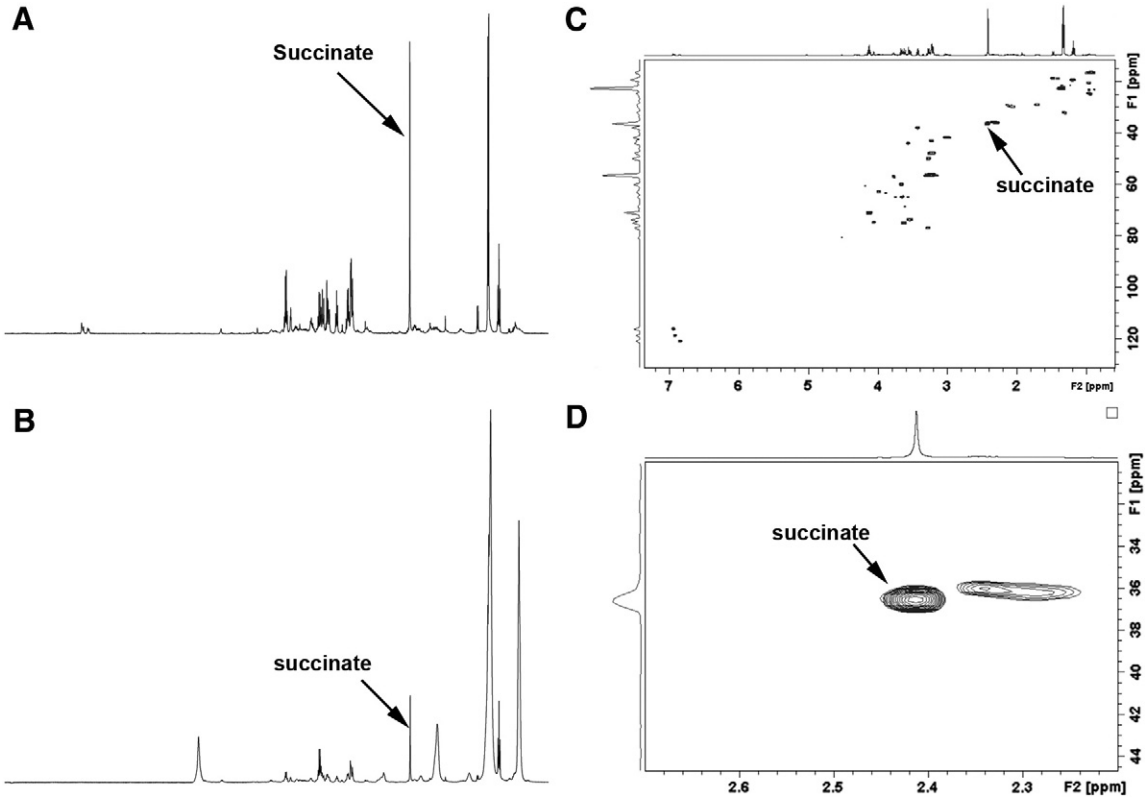

Figure 5. 1D and 2D HRMAS NMR spectra obtained from the analysis of Carney triad–related thoracic and abdominal PGLs developed in a single patient. The metabolic content in 1D spectra (A, B) can be directly compared since the intensity of each spectrum was normalized with respect to the weight of each examined sample. The two Carney triad–related tumors show an obvious peak of succinate-like SDHx-related PGL phenotype, suggesting a dysfunction of the SDH complex in both cases. The increase of lactate and fatty acids, which is pronounced in Carney triad–related PGLs, suggests necrotic involution of tumor, probably associated with a prolonged time of ischemia after surgery and is independent from succinate accumulation. 2D spectra (C) with zoom on the succinate region (D) were obtained from the thoracic PGL and confirm the important accumulation of succinate in tumoral tissue. Succinate assignment is indicated.

been shown that the rat PC12 PHEO cell line expresses different glutamate transporters, including the glutamate aspartate transporter. DNA methylation has also been shown as a potential mechanism for silencing the human glutamate transporter [26]. Evaluation of the expression of glutamate aspartate transporter and other glutamate transporters in SDHx-related PGL in comparison to sporadic cases would be of particular interest. We also found an increase of glutamine levels in SDHx-related tumors. The microarray study showed a significantly higher concentration of glutamine transporter SLC3A2 mRNA. We suggest that glutamine metabolism is involved in the pathogenesis of *SDHx*-related PHEOs/PGLs [27].

Glutaminolysis is an anaplerotic pathway of the TCA cycle and supports the production of antioxidant molecules [28–30]. Myoinositol was found to be associated with SDH status and catecholamine levels. Myoinositol is a six-carbon alcohol easily detected in HRMAS NMR spectra. Therefore, it could be potentially used as a biomarker. The relationship between SDH and myoinositol is largely unknown, but it is possible that SDHx-related tumors participate in the activation of myoinositol signaling pathways.

When compared to sporadic phenotypes, the metabolomic profile of *SDHx*-related tumors exhibits decreased levels of adrenaline. *SDHx*-related tumors have been previously found to be associated with lower catecholamine content.

ATP, ascorbate, and GSH were found to be associated with the secretory phenotype. This secretory machinery, which includes neurotransmitter uptake and storage in vesicles and exocytosis, requires ATP—a finding that has been found on NMR spectra. A high rate of glucose uptake might be necessary to fulfill this high ATP demand. Interestingly, ATP production is not impaired in the presence of SDH deficiency. It is therefore possible that TCA remains partially functional and enables, together with glycolysis, the production of NADH. The electrons, born on NAD1 (nicotinamide-adenine dinucleotide), are transferred to respiratory complex I (NADH dehydrogenase) and then to coenzyme Q10. From coenzyme Q10, the electrons are passed to complex III. Therefore, ATP production remains possible through the electron transport chain (ETC) despite inactivation of complex II of the respiratory chain.

PHEOs/PGLs may also highly accumulate ascorbate since human cells do not synthesize it. Ascorbate accumulation in cells can occur through two different mechanisms. The sodium-dependent vitamin C transporters can transport ascorbate in a sodium-dependent fashion. In adrenal tissues, only sodium-dependent vitamin C transporter 2 is present [31]. The other possibility is that dehydroascorbic acid (DHA) can be accumulated through various glucose transporters (GLUT1, for example). DHA undergoes rapid reduction in the intracellular environment (through GSH, thioredoxin, or other NADPH-dependent processes), leading to ascorbate accumulation. However, significant oxidation of ascorbate in the extracellular environment would need to be present to generate the DHA necessary to explain the high intracellular ascorbate levels found in the tumors. It is unclear whether there is a direct

explanation for the high ascorbate levels in some tumors. In the present study, we found that ascorbate was correlated with total catecholamine concentrations. This finding could be explained by the role of ascorbate as a cofactor in the conversion of dopamine to norepinephrine. Oxygen is also a co-factor in that reaction, consistent with the idea that the tumors are not hypoxic.

GSH is the most abundant endogenous antioxidant protein and therefore plays a critical role in the regulation of oxidative stress. We have found GSH to be correlated with total catecholamine levels. *o*-Quinones are physiological oxidation products of catecholamines that contribute to redox cycling, toxicity, and apoptosis. Therefore, GSH conjugation of these oxidized metabolites (*o*-quinones) through GSH transferases is a detoxification reaction that prevents redox cycling, thus indicating that GSH and GSH transferases have a cytoprotective role involving elimination of reactive chemical species originating from the oxidative metabolism of catecholamines [32].

When we have analyzed our observations using a mutual information and metabolic network–based analysis, called ADEMA, we have seen that the algorithm has predicted changes that are in accordance with the hypotheses given above. This shows that the results are also robust with respect to the dependencies within the topology of the metabolic network.

Metabolomics may also illustrate the SDH dysfunction that may occur in the absence of an SDH mutation. This is the case for Carney triad. Carney triad, originally described by J. Aidan Carney in 1977, associates tumors in at least two of the five following organs in the same patient: stomach (gastric gastrointestinal stromal tumor), lungs (pulmonary chondroma), paraganglionic system (extra-adrenal PGL), adrenal cortex (adenoma), and esophagus (leiomyoma) [33]. At present, a specific genetic mutation has not been discovered with CT; however, very few patients were found to have SDHx genetic mutations. Recently, DNA methylation at the gene locus of the SDHC has been found in CT-related tumors, leading to loss of the SDHC protein [34]. In the present study, we found that Carney triad was associated with SDH deficiency. Therefore, in the presence of high succinate/no SDHx mutation, the possible diagnosis of CT should be raised and patients should undergo screening for other CT-related tumors, especially gastric gastrointestinal stromal tumor that may affect long-term survival in CT patients.

Conclusions

The present study, which includes a large number of PHEOs/PGLs, shows that HRMAS NMR spectroscopy provides unique and accurate information in the metabolomic classification of these tumors. Furthermore, this approach also advances our knowledge of the pathogenesis of PHEOs/PGLs. It is also expected that many of these metabolomic approaches, along with the latest improvements, will reveal new targets for future therapeutic options. Recent introduction of cryogenic probes has already improved spectral signal-to-noise ratios by up to a factor of five, reducing the gap between HRMAS NMR and MS [35]. In comparison to 1D ^{1}H-NMR spectroscopy, 2D techniques based on proton scalar coupling are further improving both detection sensitivity and metabolite identification, especially when specific metabolite-related picks are overlapped in 1D NMR acquisitions. Moreover, it is nowadays possible to quantify metabolites on 2D spectra [36]. However, the large centrifugal forces applied to the biologic sample during several hours of 2D NMR acquisition have a direct consequence on tissue integrity, which could potentially influence results [37].

The present study well justifies that, in the near future, functional genomics will allow for and perfect the identification of tumor-specific metabolic biomarkers as well as their genetics. It is expected that cancer metabolomes will be quickly implemented in new diagnostic and treatment options of various cancers as well as their prognosis.

Supplementary data to this article can be found online at http://dx.doi.org/10.1016/j.neo.2014.10.010.

Acknowledgements

The laboratory personnel of the Tumor Bio-Bank (Centre de Ressources Biologiques) of the Strasbourg University Hospital are gratefully acknowledged for their technical assistance.

References

[1] Taïeb D, Kaliski A, Boedeker CC, Martucci V, Fojo T, Adler Jr JR, and Pacak K (2014). Current approaches and recent developments in the management of head and neck paragangliomas. *Endocr Rev* . http://dx.doi.org/10.1210/er.2014-1026.

[2] van Nederveen FH, Gaal J, Favier J, Korpershoek E, Oldenburg RA, de Bruyn EM, Sleddens HF, Derkx P, Riviere J, and Dannenberg H, et al (2009). An immunohistochemical procedure to detect patients with paraganglioma and phaeochromocytoma with germline SDHB, SDHC, or SDHD gene mutations: a retrospective and prospective analysis. *Lancet Oncol* **10**, 764–771.

[3] Korpershoek E, Favier J, Gaal J, Burnichon N, van Gessel B, Oudijk L, Badoual C, Gadessaud N, Venisse A, and Bayley JP, et al (2011). SDHA immunohistochemistry detects germline SDHA gene mutations in apparently sporadic paragangliomas and pheochromocytomas. *J Clin Endocrinol Metab* **96**, E1472-1476.

[4] Reitman ZJ, Jin G, Karoly ED, Spasojevic I, Yang J, Kinzler KW, He Y, Bigner DD, Vogelstein B, and Yan H (2011). Profiling the effects of isocitrate dehydrogenase 1 and 2 mutations on the cellular metabolome. *Proc Natl Acad Sci U S A* **108**, 3270–3275.

[5] Griffin JL (2003). Metabonomics: NMR spectroscopy and pattern recognition analysis of body fluids and tissues for characterisation of xenobiotic toxicity and disease diagnosis. *Curr Opin Chem Biol* **7**, 648–654.

[6] Imperiale A, Elbayed K, Moussallieh FM, Reix N, Piotto M, Bellocq JP, Goichot B, Bachellier P, and Namer IJ (2013). Metabolomic profile of the adrenal gland: from physiology to pathological conditions. *Endocr Relat Cancer* **20**, 705–716.

[7] Imperiale A, Moussallieh FM, Sebag F, Brunaud L, Barlier A, Elbayed K, Bachellier P, Goichot B, Pacak K, and Namer IJ, et al (2013). A new specific succinate-glutamate metabolomic hallmark in SDHx-related paragangliomas. *PLoS One* **8**, e80539.

[8] Rao JU, Engelke UF, Rodenburg RJ, Wevers RA, Pacak K, Eisenhofer G, Qin N, Kusters B, Goudswaard AG, and Lenders JW, et al (2013). Genotype-specific abnormalities in mitochondrial function associate with distinct profiles of energy metabolism and catecholamine content in pheochromocytoma and paraganglioma. *Clin Cancer Res* **19**, 3787–3795.

[9] Richter S, Peitzsch M, Rapizzi E, Lenders JW, Qin N, de Cubas AA, Schiavi F, Rao JU, Beuschlein F, and Quinkler M, et al (2014). Krebs cycle metabolite profiling for identification and stratification of pheochromocytomas/paragangliomas due to succinate dehydrogenase deficiency. *J Clin Endocrinol Metab* . http://dx.doi.org/10.1210/jc.2014-2151.

[10] Canu L, Rapizzi E, Zampetti B, Fucci R, Nesi G, Richter S, Qin N, Giache V, Bergamini C, and Parenti G, et al (2014). Pitfalls in genetic analysis of pheochromocytomas/paragangliomas—case report. *J Clin Endocrinol Metab* **99**, 2321–2326.

[11] Wishart DS, Jewison T, Guo AC, Wilson M, Knox C, Liu Y, Djoumbou Y, Mandal R, Aziat F, and Dong E, et al (2013). HMDB 3.0—the Human Metabolome Database in 2013. *Nucleic Acids Res* **41**, D801–D807.

[12] Wishart DS, Tzur D, Knox C, Eisner R, Guo AC, Young N, Cheng D, Jewell K, Arndt D, and Sawhney S, et al (2007). HMDB: the Human Metabolome Database. *Nucleic Acids Res* **35**, D521–D526.

[13] Ebbels TMD and Cavill R (2009). Bioinformatic methods in NMR-based metabolic profiling. *Prog Nucl Magn Reson Spectrosc* **55**, 361–374.

[14] Wold S, Ruhe A, Wold H, and Dunn WJJ (1984). The collinearity problem in linear regression. The partial least squares (PLS) approach to generalized inverses. *SIAM J Sci Stat Comput* **5**, 735–743.

[15] Picard RR and Cook RD (1984). Cross-validation of regression models. *J Am Stat Assoc* **79**, 575–583.
[16] Xu QS and Liang YZ (2001). Monte Carlo cross validation. *Chemom Intell Lab Syst* **56**, 1–11.
[17] Benjamini Y and Hochberg Y (1995). Controlling the false discovery rate: a practical and powerful approach to multiple testing. *J R Stat Soc Ser B* **57**, 289–300.
[18] Cicek AE, Bederman I, Henderson L, Drumm ML, and Ozsoyoglu G (2013). ADEMA: an algorithm to determine expected metabolite level alterations using mutual information. *PLoS Comput Biol* **9**, e1002859.
[19] Kanehisa M and Goto S (2000). KEGG: Kyoto encyclopedia of genes and genomes. *Nucleic Acids Res* **28**, 27–30.
[20] Kanehisa M, Goto S, Sato Y, Kawashima M, Furumichi M, and Tanabe M (2014). Data, information, knowledge and principle: back to metabolism in KEGG. *Nucleic Acids Res* **42**, D199–D205.
[21] Selway ZZ (2014). Metabolism at a Glance. . 3rd edn.Malden, MI: Blackwell Publishing; 2014.
[22] Martínez-Bisbal MC, Martí-Bonmatí L, Piquer J, Revert A, Ferrer P, Llacer JL, Piotto M, Assemat O, and Celda B (2004). ^{1}H and ^{13}C HR-MAS spectroscopy of intact biopsy samples ex vivo and in vivo 1H MRS study of human high grade gliomas. *NMR Biomed* **17**, 191–205.
[23] Taïeb D, Sebag F, Sarde E, Berdah S, Doddoli C, Palazzo F, Barlier A, Neumann H, and Mundler O (2012). First report of harlequin syndrome as the presenting feature of Carney Triad: a diagnostic and imaging challenge. *J Clin Oncol* **30**, e168–e171.
[24] Wishart DS (2013). Exploring the human metabolome by nuclear magnetic resonance spectroscopy and mass spectroscopy, vol. 627. Cambridge, United Kingdom: Cambridge University Press; 2013.
[25] Letouzé E, Martinelli C, Loriot C, Burnichon N, Abermil N, Ottolenghi C, Janin M, Menara M, Nguyen AT, and Benit P, et al (2013). SDH mutations establish a hypermethylator phenotype in paraganglioma. *Cancer Cell* **23**, 739–752.
[26] Zschocke J, Allritz C, Engele J, and Rein T (2007). DNA methylation dependent silencing of the human glutamate transporter *EAAT2* gene in glial cells. *Glia* **55**, 663–674.
[27] Vicha A, Taieb D, and Pacak K (2014). Current views on cell metabolism in SDHx-related pheochromocytoma and paraganglioma. *Endocr Relat Cancer* **21**, R261-277.
[28] Dang CV (2010). Glutaminolysis: supplying carbon or nitrogen or both for cancer cells? *Cell Cycle* **9**, 3884–3886.
[29] Eng CH and Abraham RT (2010). Glutaminolysis yields a metabolic by-product that stimulates autophagy. *Autophagy* **6**, 968–970.
[30] Yuneva M (2008). Finding an "Achilles' heel" of cancer: the role of glucose and glutamine metabolism in the survival of transformed cells. *Cell Cycle* **7**, 2083–2089.
[31] Bornstein SR, Yoshida-Hiroi M, Sotiriou S, Levine M, Hartwig HG, Nussbaum RL, and Eisenhofer G (2003). Impaired adrenal catecholamine system function in mice with deficiency of the ascorbic acid transporter (SVCT2). *FASEB J* **17**, 1928–1930.
[32] Baez S, Segura-Aguilar J, Widersten M, Johansson AS, and Mannervik B (1997). Glutathione transferases catalyse the detoxication of oxidized metabolites (*o*-quinones) of catecholamines and may serve as an antioxidant system preventing degenerative cellular processes. *Biochem J* **324**(Pt 1), 25–28.
[33] Carney JA (2013). Carney triad. *Front Horm Res* **41**, 92–110.
[34] Haller F, Moskalev EA, Faucz FR, Barthelmess S, Wiemann S, Bieg M, Assie G, Bertherat J, Schaefer IM, and Otto C, et al (2014). Aberrant DNA hypermethylation of SDHC: a novel mechanism of tumor development in Carney triad. *Endocr Relat Cancer* **21**(4), 567–577.
[35] Lindon JC and Nicholson JK (2008). Spectroscopic and statistical techniques for information recovery in metabonomics and metabolomics. *Annu Rev Anal Chem (Palo Alto, Calif)* **1**, 45–69.
[36] Righi V, Andronesi O, Mintzopoulos D, and Tzika AA (2009). Molecular characterization and quantification using state of the art solid-state adiabatic TOBSY NMR in burn trauma. *Int J Mol Med* **24**, 749–757.
[37] Esteve V, Martinez-Granados B, and Martinez-Bisbal MC (2014). Pitfalls to be considered on the metabolomic analysis of biological samples by HR-MAS. *Front Chem* **2**, 33.

In vivo detection of catecholamines by magnetic resonance spectroscopy: A potential specific biomarker for the diagnosis of pheochromocytoma

Alessio Imperiale, MD, PhD,[a,b] Stephanie Battini, PhD Stud,[b] Gerlinde Averous, MD,[c] Didier Mutter, MD, PhD,[d] Bernard Goichot, MD, PhD,[e] Philippe Bachellier, MD, PhD,[f] Karel Pacak, MD, PhD,[g] David Taïeb, MD, PhD,[h,i] *and* **Izzie-Jacques Namer, MD, PhD,[a,b]** *Strasbourg, Marseille, and Calmettes, France, and Bethesda, MD*

From the Department of Biophysics and Nuclear Medicine,[a] University Hospitals of Strasbourg; ICube, UMR (Unité Mixte de Recherche) 7357 University of Strasbourg/CNRS (Centre National de la Recherche Scientifique) & FMTS (Fédération de Médecine Translationnelle de Strasbourg),[b] Faculty of Medicine of Strasbourg; Department of Pathology,[c] University Hospitals of Strasbourg; Department of General, Digestive and Endocrine Surgery,[d] IRCAD-IHU, University Hospitals of Strasbourg; Department of Internal Medicine, Diabetes and Metabolic Disorders,[e] University Hospitals of Strasbourg; Department of Visceral Surgery and Transplantation,[f] University Hospitals of Strasbourg, Strasbourg, France; Program in Reproductive and Adult Endocrinology, Eunice Kennedy Shriver National Institute of Child Health and Human Development,[g] National Institutes of Health, Bethesda, MD; Department of Nuclear Medicine,[h] La Timone University Hospital, CERIMED, Aix-Marseille University, Marseille, France; and Inserm UMR1068 Marseille Cancerology Research Center,[i] Institut Paoli-Calmettes, Marseille, France

Pheochromocytoma (PHEO) is a catecholamine-secreting tumor that originates from the chromaffin cells of the adrenal medulla. The diagnosis of pheochromocytoma relies on an increase of plasma or urinary metanephrines. Concomitant disease as kidney failure, however, may be associated with false-positive results.[1] Moreover, nonsecreting PHEOs are not exceptional.[2,3]

Medical imaging plays a crucial role in the evaluation of PHEO. Magnetic resonance imaging (MRI) has high sensitivity but limited specificity.[4,5] Radionuclide imaging also may contribute to the characterization of adrenal masses with high specificity but uses ionizing radiation.[6]

Catecholamines can be detected by ex vivo analysis of intact tumor samples by the use of ^{1}H high-resolution magic-angle spinning nuclear magnetic resonance (^{1}H-HRMAS NMR) spectroscopy. The 3,4-dihydroxybenzene group characteristic of both adrenaline and noradrenaline generates an NMR signal that can be easily recognized and quantified.[7]

The objective of this study was to evaluate the clinical reliability of catecholamine in vivo detection by proton magnetic resonance spectroscopy (1H-MRS). In 2014, 2 patients were referred to the Medical Imaging Department of the University Hospitals of Strasbourg for evaluation of adrenal masses. The first patient, a 52-year-old man, had typical symptoms of PHEO with increased 24-hour urinary normetanephrine (6,439 nmol/24 hr, upper reference limit <2,293) and metanephrine (3,646 nmol/24 hr, upper reference limit <1,515) values. Results of an MRI scan revealed a right adrenal tumor measuring 50 mm in diameter with atypical features (Fig 1, *A*). The second patient, a 32-year-old man, presented with a nonsecreting adrenal incidentaloma. Results of an MRI scan revealed a 40-mm right adrenal tumor with typical features of adenoma (Fig 2, *A*). Respiratory-triggered single-voxel 1H-MRS was performed in addition to standard MRI acquisition before the injection of gadolinium on both tumors (Fig 1, *B*, and Fig 2, *B*). According to previous reports,[7,8] spectral analysis also was

Accepted for publication March 17, 2015.

Reprint requests: Alessio Imperiale, MD, PhD, Service de Biophysique et de Médecine Nucléaire - Hôpital de Hautepierre, 1, Avenue Molière, 67098 Strasbourg Cedex, France. E-mail: alessio.imperiale@chru-strasbourg.fr.

Surgery 2015;■:■-■.

0039-6060/$ - see front matter

http://dx.doi.org/10.1016/j.surg.2015.03.012

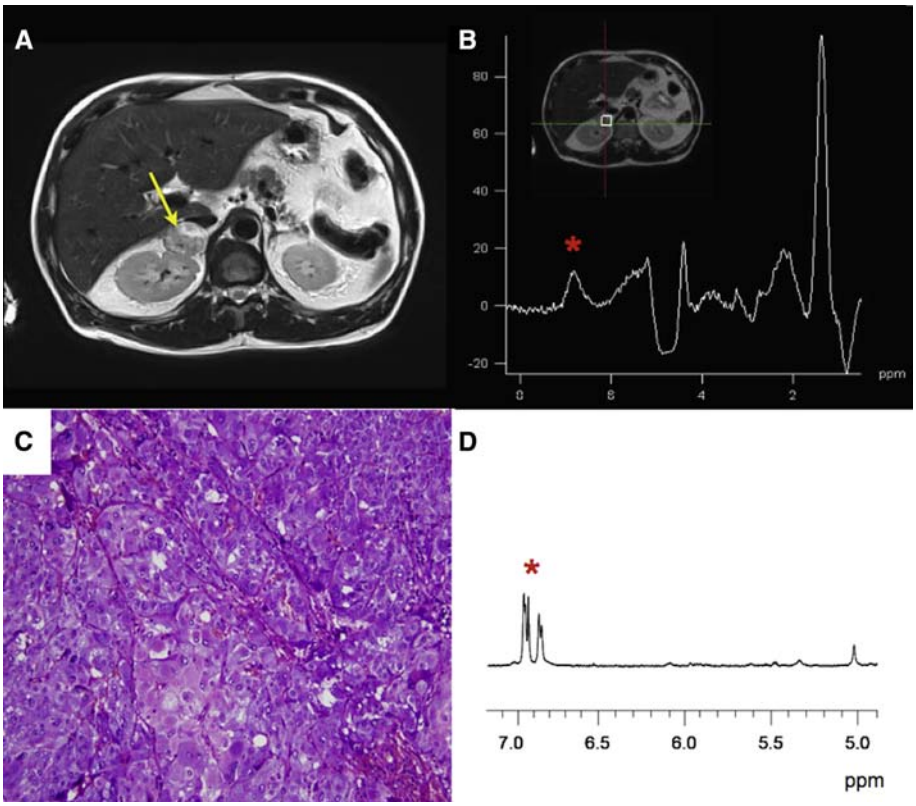

Fig 1. Results of upper abdomen MRI (*A*), in vivo respiratory-triggered proton single-voxel ^{1}H-MRS (*B*), and ex vivo ^{1}H-HRMAS NMR (*D*), respectively, performed in a pheochromocytoma (*C*). The signal detected at about 7 ppm (*) corresponds to the spectral signature of the catecholamine-specific 3,4-dihydroxybenzene group detected in pheochromocytoma by respiratory triggered single voxel ^{1}H-MRS then confirmed by ^{1}H-HRMAS NMR.

in the 4.7–9 ppm range for catecholamine assessment.

As expected, the tumor from the first patient exhibited a clear signal on respiratory triggered single voxel 1H-MRS study at approximately 7 ppm (Fig 1, *B*), corresponding to the spectral signature of the catecholamine-specific 3,4-dihydroxybenzene group, thus pointing towards the presence of PHEO. These findings were then confirmed by histopathology (Fig 1, *C*) as well as ex vivo ^{1}H-HRMAS NMR spectroscopy (Fig 1, *D*). In the second case, no tumor catecholamine content was detected on either in vivo (Fig 2, *B*) and ex vivo spectroscopy (Fig 2, *D*) and the histopathologic diagnosis confirmed the presence of adrenocortical adenoma (Fig 2, *C*).

This is the first report demonstrating a head-to-head comparison between in vivo and ex vivo NMR spectroscopy for the detection of catecholamine-secreting tumors. It also suggests that in vivo assessment of tumoral catecholamines might play a unique role in the differential diagnosis of adrenal tumors to confirm or rule out the presence of PHEO, especially in unusual situations.[1,9] It is also expected that this new approach will play an important role in the assessment of therapeutic responses of PHEO by monitoring catecholamine content in these tumors.

In conclusion, respiratory-triggered proton ^{1}H-MRS could be represent a functional, noninvasive, and nonionizing technique in the diagnosis of PHEO; however, the clinical utility of respiratory triggered single voxel ^{1}H-MRS needs to be further evaluated in a larger series of patients with adrenal incidentalomas that also includes more challenging situations such as cystic, hemorrhagic, and nonsecreting PHEOs, which are characterized from slightly high or completely absent of catecholamine secretion. Moreover, a comparison between respiratory-triggered single voxel ^{1}H-MRS and radionuclide imaging techniques (ie, ^{123}I-metaiodobenzylguanidine scintigraphy, ^{18}F-fluorodihydroxyphenylalanine positron emission tomography) would be of particular interest for a definitive validation.

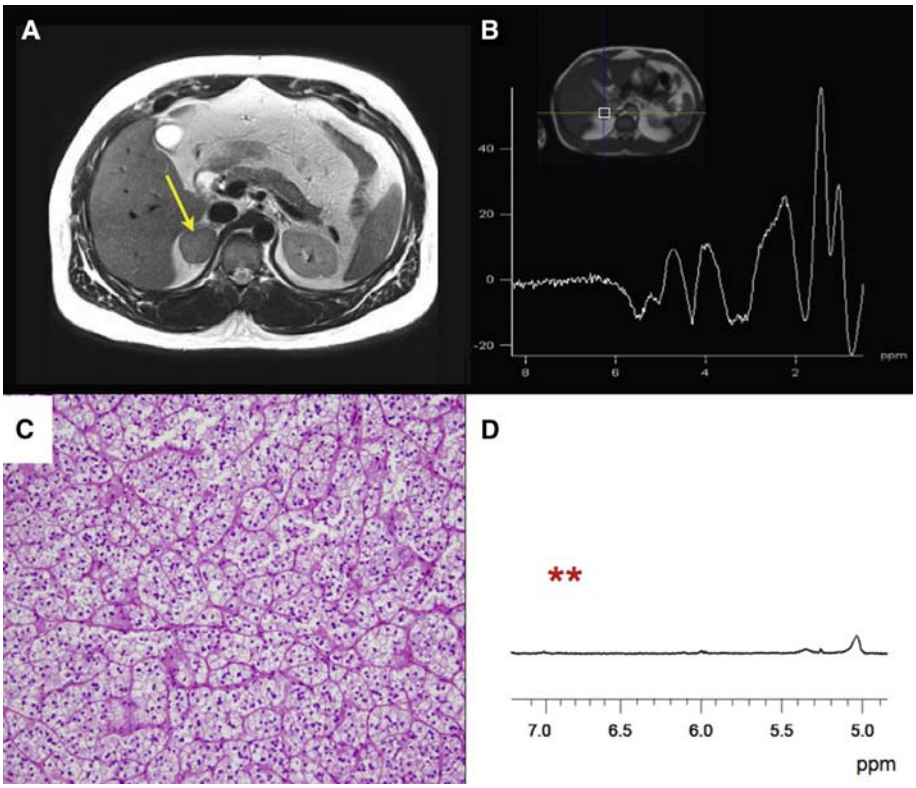

Fig 2. Results of upper abdomen MRI (*A*), in vivo respiratory-triggered single-voxel ^{1}H-MRS (*B*), and ex vivo ^{1}H-HRMAS NMR (*D*), respectively, performed in adrenocortical adenoma (*C*). No catecholamine-specific signal was detectable neither by ^{1}H-MRS nor by ^{1}H-HRMAS NMR (**) at about 7 ppm.

REFERENCES

1. Eisenhofer G, Huysmans F, Pacak K, Walther MM, Sweep FC, Lenders JW. Plasma metanephrines in renal failure. Kidney Int 2005;67:668-77.
2. Mannelli M, Pupilli C, Lanzillotti R, Ianni L, Amorosi A, Credi G, et al. A nonsecreting pheochromocytoma presenting as an incidental adrenal mass. Report on a case. J Endocrinol Invest 1993;16:817-22.
3. Kimura N, Miura Y, Nagatsu I, Nagura H. Catecholamine synthesizing enzymes in 70 cases of functioning and nonfunctioning phaeochromocytoma and extra-adrenal paraganglioma. Virchows Arch A Pathol Histopathol 1992;421:25-32.
4. Jacques AE, Sahdev A, Sandrasagara M, et al. Adrenal phaeochromocytoma: correlation of MRI appearances with histology and function. Eur Radiol 2008;18:2885-92.
5. Blake MA, Kalra MK, Maher MM, Sahani DV, Sweeney AT, Mueller PR, et al. Pheochromocytoma: an imaging chameleon. RadioGraphics 2004;24:S87-99.
6. Taieb D, Timmers HJ, Hindie E, Guillet BA, Neumann HP, Walz MK, et al. EANM 2012 guidelines for radionuclide imaging of phaeochromocytoma and paraganglioma. Eur J Nucl Med Mol Imaging 2012;39:1977-95.
7. Imperiale A, Elbayed K, Moussallieh FM, Reix N, Piotto M, Bellocq JP, et al. Metabolomic profile of the adrenal gland: from physiology to pathological conditions. Endocr Relat Cancer 2013;20:705-16.
8. Kim S, Salibi N, Hardie AD, Xu J, Lim RP, Lee VS, et al. Characterization of adrenal pheochromocytoma using respiratory-triggered proton MR spectroscopy: initial experience. AJR Am J Roentgenol 2009;192:450-4.
9. Eisenhofer G, Peitzsch M. Laboratory evaluation of pheochromocytoma and paraganglioma. Clin Chem 2014;60:1486-99.

Curriculum Vitae

Alessio IMPERIALE

Service de Biophysique et Médecine Nucléaire
Hôpitaux Universitaires de Strasbourg

ICube, UMR 7357, Université de Strasbourg/CNRS

Strasbourg, Mai 2016

ETAT CIVIL

NOM, Prénom : IMPERIALE, Alessio
Lieu et Date de naissance : Lecce (Italie), 21 janvier 1975
Nationalité : Italienne
Situation de famille : marié, 2 enfants
Domicile : 58, Avenue de la Foret Noire, 67000 Strasbourg
Tél. : +33 3 88 61 75 09
+33 6 71 86 58 24
Courriel : alessio.imperiale@chru-strasbourg.fr

SITUATION PROFESSIONNELLE

- Praticien Hospitalier (depuis 2005, RPPS : 10002464856), Service de Biophysique et Médecine Nucléaire, Hôpitaux Universitaires de Strasbourg [1,2] (Pr. I.J. Namer)

  [1] Hôpital de Hautepierre
  1, Avenue Molière 67098 Strasbourg CEDEX 9, France
  Tel. +33 3 88 12 75 52 / +33 3 88 12 75 46

  [2] Nouvel Hôpital Civil
  1, Place de l'Hôpital 67000 Strasbourg, France
  Tel. +33 3 69 55 04 13 / +33 3 69 54 97 70

- Réfèrent Médical pour l'Imagerie Oncologique Nucléaire (depuis 2011), Hôpitaux Universitaires de Strasbourg

- Affiliation permanente (depuis 2014) au Laboratoire ICube, UMR 7357, Université de Strasbourg/CNRS

DIPLOMES ET TITRES UNIVERSITAIRES

2000 : Diplôme d'État de Docteur en Médecine. «*Evaluation de la perfusion cérébrale par technique SPECT dans la pathologie démentielle neuro-dégénérative*»

Directeur de thèse: Pr R. Palumbo, Département de Sciences Radiologiques, Division de Médicine Nucléaire, Faculté de Médecine de l'Université de Pérouse, Italie)

2004 : Diplôme d'Études Spécialisées en Médecine Nucléaire. «*Evaluation du drainage pyélo-urétéral chez les enfants présentant une hydronéphrose congénitale par scintigraphie rénale au ^{123}I-Hippuran avec test au Captopril*»

Directeur de thèse: Pr G. La Cava, Département de Physiopathologie Clinique, Division de Médicine Nucléaire, Faculté de Médecine de l'Université de Florence, Italie)

2014 : Doctorat d'Université. «Métabolomique par spectroscopie RMN à haute résolution en rotation à l'angle magique (HRMAS) appliquée à la pathologie tumorale surrénalienne»

Directeur de thèse: Pr I.J. Namer (Co-Directeur : K. Elbayed), Service de Biophysique et Médecine Nucléaire, Faculté de Médecine de l'Université de Strasbourg

2015 : DIU de Pédagogie Médicale. Université de Strasbourg

2016 (en cours) : HDR. Université de Strasbourg

EXPERIENCE PROFESSIONNELLE

2000-2004 : Internat en DES de Médecine Nucléaire, Faculté de Médecine et Chirurgie, Firenze, Italie.

Depuis 2005 : Praticien Hospitalier, Service de Biophysique et Médecine Nucléaire, Hôpitaux Universitaires de Strasbourg (7^{éme} échelon).

ACTIVITE HOSPITALIERE

Expérience en médecine nucléaire diagnostique monophotonique :

- examens scintigraphiques osseux ;
- examens scintigraphiques thyroïdiens, parathyroïdiens ;
- examens scintigraphiques pulmonaires ;
- scintigraphies rénales ;
- explorations cardiaques ;
- oncologie nucléaire ;
- marquages cellulaires : leucocytes, hématies ;
- explorations digestives.

Expérience en médecine nucléaire diagnostique positonique :

- examens TEP-TDM au ^{18}F-FDG : oncologie, cardiologie, médecine interne.
- examens TEP-TDM à la ^{18}F-fluoro-choline, à la ^{18}F-fluoro-DOPA : oncologie.

Expérience en médecine nucléaire thérapeutique :

- Radio immunothérapie (ZEVALIN®)
- Radio embolisation Hépatique (SIRSPHERES®)

Repérage isotopique :

- ganglion sentinelle (Cancer mammaire et ORL)
- repérage tumoral peropératoire : ganglion sentinelle (Cancer Colique)

SOCIETES SAVANTES

- Membre de la Société Française de Médecine Nucléaire et Imagerie Moléculaire (SFMN)
- Membre actif du groupe de travail ENDOCRINOLOGIE au sein de la SFMN
- Affiliation à la Société Européenne de Médecine Nucléaire (European Association of Nuclear Medicine, EANM) en cours

ACTIVITE D'ENSEIGNEMENT

PREMIER CYCLE

a. Biophysique

Enseignements dirigés :

- PACES (UE3B) : Radioactivité (22,5 heures/an depuis 2015/2016)

b. Médecine Nucléaire

Cours magistraux :

- DFGSM3 (UE G1A) : Médecine Nucléaire en Oncologie (2 heures/an depuis 2014/2015)

Enseignements dirigés :

- DFASM4 (Stage de Radiologie) : Présentation de cas cliniques en Médecine Nucléaire (15 heures/an depuis 2013/2014)

Travaux pratiques :

- DFGSM3 (UE G1A) : Médecine nucléaire (15 heures/an depuis 2013/2014)

DEUXIEME CYCLE

a. Encadrement clinique

Externes et internes du Service de Biophysique et Médecine Nucléaire, Hôpitaux Universitaires de Strasbourg (4 jours/semaine depuis 2005)

b. Thèse de Médecine

Encadrement :

- S. Cimarelli : Dysfonction ventriculaire gauche transitoire non ischémique : apport de l'imagerie fonctionnelle isotopique (Strasbourg, 2007)
- E. Rust : Intérêt de la TEP/TDM au FDG dans le diagnostic initial des cancers coliques présumes non métastatique : étude prospective (Strasbourg, 2011)
- D. Morland : Fiabilité de la TEP-TDM au ^{18}F-FDG dans l'évaluation ganglionnaire médiastinale des carcinomes bronchiques non à petites cellules dans l'optique

d'une chirurgie mini-invasive : évaluation rétrospective de 134 patients (Strasbourg, 2014)

- C. Heimburger : Evaluation comparative des performances diagnostiques de la TEP/TDM à la ^{18}F-FDOPA et de l'imagerie radiologique en coupes dans l'évaluation post thérapeutique des paragangliomes de la tète et du cou (Strasbourg, 2014)
- N. Muller : Impact de la TEP/TDM au ^{18}F-FDG dans la prise en charge des patients greffés d'organe avec suspicion de complication tumorale ou infectieuse: analyse rétrospective sur huit ans de pratique Clinique (Strasbourg, 2015)
- M. Helali (en cours, soutenance prévue en 2016, Strasbourg)

Co-encadrement :

- M. Foré : Intérêt du PETscan dans le suivi des patients atteints de sarcoïdose (Médaille d'or, Strasbourg, 2009)

c. Thèse de Pharmacie

Co-encadrement :

- A. Pierre : Etude in vitro de l'apport de la carbidopa dans l'exploration fonctionnelle des insulinomes par tomographie par émission de positons à la ^{18}F-FDOPA (Strasbourg, 2015)

TROISIEME CYCLE

a. Cours magistraux (DES, DU, DIU)

- Imagerie fonctionnelle des tumeurs neuroendocrines (DES d'Oncologie Médicale, 1 heure/an depuis 2010)
- Tomographie par Emission de Positons: l'examen TEP-TDM au FDG en oncologie broncho-pulmonaire (DU de Chirurgie thoracique, 1 heure/an depuis 2010)
- Lymphadénectomie sélective en chirurgie mammaire: le point de vue du médecin nucléaire (DU de Sénologie, 1 heure/an depuis 2015)

b. Encadrement mémoire de DES de Médecine Nucléaire

- S. Cimarelli : Explorations cardiologiques nucléaires dans la cardiomyopathie de Takotsubo (DES de Médecine Nucléaire, 2008)
- J. Keomany : Apport de la TEP-TDM à la ^{18}F-FDOPA dans le suivi thérapeutique des patients avec Carcinome médullaire de la thyroïde (DES de Médecine Nucléaire, 2010)

- E. Rust : Performances de la TEP-TDM à la 6-Fluoro-[18F]-L-Dihydroxyphénylalanine et de l'imagerie radiologique conventionnelle dans la prise en charge des patients avec maladie tumorale endocrine dont le primitif est inconnu (DES de Médecine Nucléaire, 2011)

c. Formation Doctorale (Thèse de science)

Co-encadrement :

- Etude métabolomique par spectroscopie RMN à haute résolution en rotation à l'angle magique (HRMAS) dans les pathologies des parathyroïdes et du pancréas (S. Battini, Directeur de thèse: Pr I.J. Namer; co-directeur: K. Elbayed)

AUTRES

a. Formation continue de l'Université de Strasbourg

Cours magistraux :

- 18F-FDG TEP-TDM: Indications et cas cliniques (Initiation à la TEP-TDM, 2 heures, en 2008 et 2009)
- Imagerie fonctionnelle en pathologie endocrinienne (Prise en charge médico-chirurgicale des pathologies endocriniennes courantes, 1 heure, en 2009)
- TEP-TDM au ^{18}F-FDG. Les critères d'activités d'une tuberculose: du diagnostic à l'évaluation de l'efficacité du traitement (Imagerie de la Tuberculose, 2 heures/an depuis 2014)

b. D.T.S. Imagerie Médicale et Radiologie Thérapeutique (Strasbourg)

Cours magistraux :

- Tomographie par Emission de Positons. Quelles indications en routine clinique ? (6 heures/an depuis 2013)

ACTIVITE DE RECHERCHE

Recherche Clinique

Caractérisation à l'aide de plusieurs techniques d'imagerie isotopique et optimisation diagnostique et thérapeutique des tumeurs neuroendocrines (TNE) avec attention particulière aux tumeurs pancréatiques et digestives. Participation à nombreux projets de recherche clinique nationaux multicentriques en tant que investigateur principal ou associé.

Recherche Fondamentale

Caractérisation métabolique (métabolomique) par spectroscopie par résonance magnétique à partir de biopsies tissulaires (*ex vivo*) des TNE digestives et des tumeurs de la glande surrénale (pheochromocytoma/paragangliome, corticosurrénalome malin, adénome). Une collaboration avec les équipes de Marseille, Nancy et du NIH (Bethesda, USA) a permis d'établir la signature métabolique des paragangliomes/phéochromocytomes, de différencier des tumeurs selon leur profil sécrétoire biologique et génotypiquement différentes, et d'établir un modèle statistiquement robuste pour prédire la présence de mutations agressives. Nous avons pu développer la spectroscopie RMN *in vivo* afin de caractériser des masses surrénaliennes et cervicales avant la chirurgie, avec des conséquences potentielles sur la prise en charge thérapeutique du patient.

Travaux en cours

Développement d'un axe de recherche translationnelle autour des TNE intégrant la dimension cellulaire, l'expérimentation animale, le développement de l'imagerie préclinique par microTEP ainsi que la spectroscopie par résonance magnétique *ex vivo* et *in vivo.*

Indices de productivité

Auteur et co auteur de 79 publications internationales et de 9 publications nationales dans des journaux à comité de lecture (1358 points SIGAPS) : 31 fois 1^{ér} auteur, 21 fois 2ème auteur, 15 fois dernier auteur, 4 fois avant dernier auteur.

PUBLICATIONS

a. Publications internationales dans des revues à comité de lecture

1. Imperiale C, **Imperiale A**. Some fast mono multi-processor configurations for a single multi-parameter multichannel analyzer. Measurement. 2000;27:257-75.
2. Imperiale C, **Imperiale A**. On nuclear spectrometry pulses digital shaping and processing. Measurement. 2001; 30: 49-73.
3. La Cava G, **Imperiale A**, Olianti C, Gheri RG, Ladu C, Mannelli M, Pupi A. SPECT semiquantitative analysis of adrenocortical ^{131}I-6-beta iodomethyl-norcholesterol uptake to discriminate subclinical and preclinical functioning adrenal incidentaloma. J Nucl Med. 2003; 44: 1057-64.
4. **Imperiale A**, Olianti C, Sestini S, Materassi M, Seracini D, Ienuso R, La Cava G. ^{123}I-hippuran renal scintigraphy with evaluation of single-kidney clearance for predicting renal scarring after acute urinary tract infection: comparison with ^{99m}Tc-DMSA scanning. J Nucl Med. 2003; 44: 1755-60.
5. Olianti C, **Imperiale A**, Materassi M, Seracini D, Ienuso R, Tommasi M, Pupi A, La Cava G. Urinary Endothelin-1 Excretion According to the Morpho-Functional Damage Lateralisation in Reflux Nephropathy. Nephrol Dial Transplant. 2004; 19: 1774-8.
6. Sciagrà R, **Imperiale A**, Antoniucci D, Migliorini A, Parodi G, Comis G, Pupi A. Relationship of infarct size and severity versus left ventricular ejection fraction and volumes obtained from ^{99m}Tc-sestamibi gated single-photon emission computed tomography in patients treated with primary percutaneous coronary intervention. Eur J Nucl Med Mol Imaging. 2004;7: 969-74.
7. Imperiale C, **Imperiale A**. Some fast calculations simulating measurements from single-photon emission computed tomography (SPECT) imaging. Measurement. 2005; 37:218-40
8. **Imperiale A**, Olianti C, Mannelli M, Pupi A, La Cava G. Tomographic Evaluation of ^{131}I-6β-Iodomethyl-norcholesterol Standardized Uptake Trend in Clinically Silent Adrenocortical Monolateral and Bilateral incidentalomas. Q J Nucl Med Mol Imaging. 2005; 49:287-96.
9. **Imperiale A**, Olianti C, Comis G, La Cava G. Evaluation of 123I-Orthoiodohippurate Single Kidney Clearance Rate by Renal Sequential Scintigraphy in a Large Cohort of Likely Normal Subjects aged between nought and eighteen years. Eur J Nucl Med Mol Imaging. 2006; 33: 1483-90.
10. **Imperiale A**, Blondet C, Choquet P, Constantinesco A.In-111 DTPA-D-Phe1-Octreotide SPECT in a Rare Case of Anorectal Small-Cell Undifferentiated Neuroendocrine Carcinoma. Clin Nucl Med. 2006; 31: 652-4.
11. **Imperiale A**, Cimarelli S, Ben Sellem D, Blondet C, Constantinesco A. Focal F-18 FDG Uptake Mimicking Malignant Gastric Localizations Disappearing After Water Ingestion on PET/CT Images. Clin Nucl Med. 2006; 31: 835-7.

12. **Imperiale A**, Blondet C, Fohrer C, Cimarelli S, Herbrecht R, Constantinesco A. 18F-Fluoro-2-deoxy-D-glucose Positron Emission Tomography/Computed Tomography for Early Evaluation of Treatment Efficacy in Advanced Non-Hodgkin Lymphoma of Uterine Corpus: A Case Report. Clin Lymph Myel. 2007;7:421-4.
13. **Imperiale A**, Heymann S, Claria M, Cimarelli S, Ben Sellem D, Goetz C, Onea A, Blondet C, Constantinesco A. F-18 FDG PET-CT in a Rare Case of Bartholin's Gland Undifferentiated Carcinoma Managed With Chemoradiation and Interstitial Brachytherapy. Clin Nucl Med. 2007;32: 498-500.
14. Imperiale C, **Imperiale A**. Space-domain non-iterative approach for SPECT/CT systems considering attenuation and space-variant detector response. Comput Med Imaging Graph. 2007; 31:492-501.
15. Cimarelli S, **Imperiale A**, Ben Sellem D, Rischner J, Detour J, Morel O, Ohlmann P, Constantinesco A. Nuclear medicine imaging of Takotsubo cardiomyopathy: typical form and mid-ventricular ballooning syndrome. J Nucl Cardiol. 2008; 15: 137-41.
16. Braun JJ, Kessler R, Constantinesco A, **Imperiale A**. 18F-FDG PET/CT in sarcoidosis management: review and report of 20 cases. Eur J Nucl Med Mol Imaging. 2008; 35:1537-43.
17. Federici L, Blondet C, **Imperiale A**, Sibilia J, Pasquali JL, Pflumio F, Goichot B, Blaison G, Weber JC, Christmann D, Constantinesco A, Andrès E. Value of (18)F-FDG-PET/CT in patients with fever of unknown origin and unexplained prolonged inflammatory syndrome: a single centre analysis experience. Int J Clin Pract. 2010; 64:55-60 (Epub 2008).
18. **Imperiale A**, Blondet C, Ben-Sellem D, Forestier E, Mohseni M, Piemont Y, Ojeda M, Christmann D, Constantinesco A, Hansmann Y. Unusual abdominal localization of cat scratch disease mimicking malignancy on ^{18}F-FDG PET/CT examination. Clin Nucl Med. 2008; 33: 621-3.
19. Braun JJ, **Imperiale A**, Schultz P, Molard A, Charpiot A, Gentine A. Pharyngolaryngeal sarcoidosis: Report of 12 cases. Otolaryngol Head Neck Surg. 2008;139:463-5.
20. Morel O, Sauer F, **Imperiale A**, Cimarelli S, Blondet C, Jesel L, Trinh A, De Poli F, Ohlmann P, Constantinesco A, Bareiss P. Importance of inflammation and inflammatory status in Tako-tsubo cardiomyopathy. J Card Fail. 2009; 15: 206-13 (Epub 2008).
21. **Imperiale A**, Moser T, Ben-Sellem D, Mertz L, Gangi A, Constantinesco A. Osteoblastoma and osteoid osteoma: morphofunctional characterization by MRI and dynamic F-18 FDG PET/CT before and after radiofrequency ablation. Clin Nucl Med. 2009; 34: 184-8.
22. Piotto M, Moussallieh FM, Dillmann B, **Imperiale A**, Neuville A, Brigand C, Bellocq JP, Elbayed K, Namer IJ. Metabolic characterization of primary human colorectal cancers using high resolution magic angle spinning 1H magnetic resonance spectroscopy. Metabolomics. 2009;5: 293-301.
23. Cimarelli S, Sauer F, Morel O, Ohlmann P, Constantinesco A, **Imperiale A**. Transient left ventricular dysfunction syndrome: patho-physiological bases through nuclear medicine imaging. Int J Cardiol 2010; 144: 212-8.

24. Ben-Sellem D, Kun-Lun L, Cimarelli S, Constantinesco A, **Imperiale A**. Desmoplastic small round cell tumor: impact of 18F-FDG PET induced treatment strategy in a patient with long-term outcome. Rare Tumors. 2009; 1:e19.
25. Andres E, Federici L, **Imperiale A**. Value of 18 FDG-PET/CT in clinical practice in patients with fever of unknown origin and inflammatory syndrome. Eur J Radiol 2010; 75:122.
26. Morel O, Jesel L, Cimarelli S, Trinh A, Ohlmann P, **Imperiale A**. Recurrent form of neurogenic stunned myocardium: is myocardial adrenergic receptor distribution a dynamic process? Int J Cardiol 2010; 145: 237-9.
27. Radulescu B, **Imperiale A**, Germain P, Ohlmann P. Severe ventricular arrhythmias in a patient with cardiac sarcoidosis: insights from MRI and PET imaging and importance of early corticosteroid therapy. Eur Heart J 2010; 31:400 (Epub 2009).
28. Morel O, Jesel L, Morel N, Nguyen A, Trinh A, Ohlmann P, **Imperiale A**. Transient left ventricular dysfunction syndrome during anaphylactic shock: vasospasm, Kounis syndrome or epinephrine-induced stunned myocardium? Int J Cardiol 2010; 145:501-3.
29. Braun JJ, **Imperiale A**, Riehm S, Veillon F. Imaging in sinonasal sarcoidosis: CT, MRI, (67)Gallium scintigraphy and (18)F-FDG PET/CT features. J Neuroradiol 2010; 37:172-81.
30. **Imperiale A**, Federici L, Lefebvre N, Braun JJ, Pflumio F, Kessler R, Hansmann Y, Andres E, Constantinesco A. 18F-FDG PET/CT as a valuable imaging tool for assessing treatment efficacy in inflammatory and infectious diseases. Clin Nucl Med. 2010; 35:86-90.
31. **Imperiale A**, Greget M, Chabrier G, Keomany J, Rust E, Detour J, Pessaux P, Goichot B. Solitary hepatic metastasis from medullary thyroid carcinoma mimicking atypical hemangioma: insight from multimodality diagnostic approach by MRI, F-18 FDG and F-18 FDOPA PET/CT. Clin Nucl Med. 2010; 35:434-7.
32. **Imperiale A**, Elbayed K, Moussallieh FM, Neuville A, Piotto M, Bellocq JP, Lutz P, Namer IJ. Metabolomic pattern of childhood neuroblastoma obtained by 1H-High-resolution magic angle spinning (HRMAS) NMR spectroscopy. Pediatr Blood Cancer 2011; 56:24-34.
33. **Imperiale A**, Riehm S, Veillon F, Namer IJ, Braun JJ. FDG PET coregistered to MRI for diagnosis and monitoring of therapeutic response in aggressive phenotype of sarcoidosis. Eur J Nucl Med Mol Imaging 2011; 38:983-4.
34. **Imperiale A**, Cimarelli S, Brigand C, Faure G, Karcher G, Rohr S, Atlani D, Olivier P. Does the association of 18F-FDG uptake intensity and lesion topography reveal histological phenotype and tumor differentiation in esophageal cancer? Hell J Nucl Med 2011; 14:239-42.
35. **Imperiale A**, Olianti C, Bernini G, Tamburini A, Tommasi MS, La Cava G. Urinary endothelin-1-like immunoreactivity excretion in Wilms' tumor survivors. Pediatr Nephrol 2012; 27:1351-9.
36. Hubele F, Bilger K, Kremer S, **Imperiale A**, Lioure B, Namer IJ. Sequential FDG PET and MRI findings in a case of human herpes virus 6 limbic encephalitis. Clin Nucl Med 2012; 37:716-7.
37. Rust E, Hubele F, Marzano E, Goichot B, Pessaux P, Kurtz JE, **Imperiale A**. Nuclear medicine imaging of gastro-entero-pancreatic neuroendocrine tumors. The key role of

cellular differentiation and tumor grade: from theory to clinical practice. Cancer Imaging 2012; 12:173-84.

38. **Imperiale A**, Rust E, Boulanger C, Roedlich MN, Ollier JC, Schneegans O. Terminal ileum neuroendocrine incidentaloma in a patient with sporadic medullary thyroid carcinoma: findings from 18F-FDOPA PET/CT investigation. Clin Nucl Med 2012; 37:e206-8.
39. **Imperiale A**, Taquet MC, Rust E, Hubele F, Veillon F, Taieb D, Goichot B. Head-to-head comparison between SRS, (18)F-FDG and (18)F-FDOPA PET/CT in a patient with recurrent SDHC-related jugular paraganglioma. Eur J Nucl Med Mol Imaging 2012;39:1662-3.
40. Hubele F, **Imperiale A**, Kremer S, Namer IJ. Asymptomatic giant arachnoid cyst. Clin Nucl Med 2012; 37:982-3.
41. Mikail N, Hess S, Jesel L, El Ghannudi S, El Husseini Z, Trinh A, Olhmann P, Morel O, **Imperiale** A. Takotsubo and Takotsubo-like syndrome: a common neurogenic myocardial stunning pathway? Int J Cardiol 2013; 166:248-50.
42. Rust E, Gomes Ferreira C, Sebastia Sancho C, Becmeur F, **Imperiale A**. When bone scan reveals appendicitis. J Ped Surg Case Reports 2013 (in press).
43. **Imperiale A**, Cabral JF, Rust E, Flores-Turk G, Renard C, Hubele F, Detour J, Lang H, Gangi A, Namer IJ. 18F-fluorocholine uptake in a case of adrenal incidentaloma: possible diagnostic pitfall or potential tool for adrenocortical tumors characterization? Clin Nucl Med 2013; 38:e83-4.
44. **Imperiale A**, Riehm S, Braun JJ. Interest of [18F]FDG PET/CT for treatment efficacy assessment in aggressive phenotype of sarcoidosis with special emphasis on sinonasal involvement. Q J Nucl Med Mol Imaging 2013;57:177-86
45. **Imperiale A**, Elbayed K, Moussallieh FM, Reix N, Piotto M, Bellocq JP, Goichot B, Bachellier P, Namer IJ. Metabolomic profile of the adrenal gland: from physiology to pathological conditions. Endocr Relat Cancer 2013;20: 705-16.
46. **Imperiale A**, Addeo P, Averous G, Namer IJ, Bachellier P. Solid pseudopapillary pancreatic tumor mimicking a neuroendocrine neoplasm on 18F-FDOPA PET/CT. J Clin Endocrinol Metab 2013; 98: 2643-4.
47. Morel O, Mikail N, Jesel L, Hess S, Ohlmann P, **Imperiale A**. Reply to the letter by Ando et al. Int J Cardiol 2013; 168: 5112.
48. **Imperiale A**, Bergerat JP, Saussine C, Abu Eid M, Kehrli P, Namer IJ. Isolated cerebellar metastasis from prostate adenocarcinoma diagnosed by (18)F-fluorocholine PET/CT: a rare but not impossible complication. Eur J Nucl Med Mol Imaging. 2014; 41:397-8.
49. **Imperiale A**, Rust, Gabriel S, Detour J, Goichot B, Duclos B, Kurtz JE, Bachellier P, Namer IJ, Taïeb D. ^{18}F-fluorodihydroxyphenylalanine PET/CT in patients with neuroendocrine tumors of unknown origin: relation to tumor origin and differentiation. J Nucl Med. 2014; 55:367-72.
50. **Imperiale A,** Moussallieh FM, Sebag F, Brunaud L, Barlier A, Elbayed K, Bachellier P, Goichot B, Pacak K, Namer IJ, Taïeb D. A new specific succinate-glutamate metabolomic hallmark in SDHx-related paragangliomas. PLoS One. 2013; 8:e80539.

51. **Imperiale A**, Chenard MP, Rohr S, Barlier A, Goichot B. In Vivo and In Vitro Evidence of Somatostatin Receptors Expression in a Dedifferentiated Retroperitoneal Liposarcoma. Clin Nucl Med. 2014; 39:892-3.
52. Heymann S, **Imperiale A**, Schlund-Schoettel E, Sauer B, Dourthe LM. [A rare case of bone metastasis from gastro-intestinal stromal tumour: place of radiotherapy]. Cancer Radiother. 2014; 18:55-8.
53. **Imperiale A**, Averous G, Chilinseva-Natorov N, Hubelé F, Triki E, Bellocq JP, Namer IJ, Brigand C. Unknown Multifocal Ileal Carcinoid Revealed by (18)F-FDOPA PET/CT. J Clin Endocrinol Metab. 2014; 99:1510-1.
54. **Imperiale A**, Sebag F, Vix M, Castinetti F, Kessler L, Moreau F, Bachellier P, Guillet B, Namer IJ, Mundler O, Taïeb D. $_{18}$F-FDOPA PET/CT imaging of insulinoma revisited. Eur J Nucl Med Mol Imaging. 2015; 42:409-18.
55. Dietemann S, Noblet V, **Imperiale A**, Blondet C, Namer IJ. FDG PET Findings of the Brain in Sudden Blindness Caused by Bilateral Central Retinal Artery Occlusion Revealing Giant Cell Arteritis. Clin Nucl Med. 2014 Sep 30. [Epub ahead of print]
56. Montaut S, Mallaret M, Laguna AE, Lagha-Boukbiza O, Entz Werle N, Marcellin L, Bachellier P, **Imperiale A**, Namer IJ, Thomas L, Anheim M, Tranchant C. Anti-Hu-associated brainstem encephalitis with ganglioneuroblastoma in a young adult. J Neurol. 2014;261:1822-4.
57. Leyendecker P, **Imperiale A**, Matern JF, Noël G, Namer IJ. Intense 18F-Choline Uptake After Minor Head Injury: Misleading PET/CT Result in a Patient With Biochemical Relapse of Prostate Adenocarcinoma. Clin Nucl Med. 2014;39:1012-3.
58. Namer IJ, Valenti-Hirsch MP, Scholly J, Lannes B, **Imperiale A**, Hirsch E. Hypermetabolism During Resting-State FDG-PET Suggesting Intrinsic Epileptogenicity in Focal Cortical Dysplasia. Clin Nucl Med. 2014; 39:993-5.
59. Burgy M, Brossat H, Barthelemy P, **Imperiale A**, Trinh A, Hazam CA, Bergerat JP, Mathelin C. First report of trastuzumab treatment after postoperative Takotsubo cardiomyopathy. Anticancer Res. 2014; 34:3579-82.
60. **Imperiale A**, Bahougne T, Goichot B, Bachellier P, Taïeb D, Namer IJ. Dynamic 18F-FDOPA PET Findings After Carbidopa Premedication in 2 Adult Patients With Insulinoma-Related Hyperinsulinemic Hypoglycemia. Clin Nucl Med. 2014; 29. [Epub ahead of print]
61. **Imperiale A**, Garnon J, Bachellier P, Gangi A, Namer IJ. Simultaneous 18F-FDOPA PET/CT-Guided Biopsy and Radiofrequency Ablation of Recurrent Neuroendocrine Hepatic Metastasis: Further Step Toward a Theranostic Approach. Clin Nucl Med. 2015; 40:e334-5.
62. Vilgrain V, Abdel-Rehim M, Sibert A, Ronot M, Lebtahi R, Castéra L, Chatellier G; SARAH Trial Group. Radioembolisation with yttrium–90 microspheres versus sorafenib for treatment of advanced hepatocellular carcinoma (SARAH): study protocol for a randomised controlled trial. Trials. 2014; 15:474.
63. **Imperiale A**, Moussallieh FM, Roche P, Battini S, Cicek AE, Sebag F, Brunaud L, Barlier A, Elbayed K, Loundou A, Bachellier P, Goichot B, Stratakis CA, Pacak K, Namer IJ, Taïeb D.

Metabolome profiling by HRMAS NMR spectroscopy of pheochromocytomas and paragangliomas detects SDH deficiency: clinical and pathophysiological implications. Neoplasia. 2015; 17:55-65.

64. Szarek E, Ball ER, **Imperiale A**, Tsokos M, Faucz FR, Giubellino A, Moussallieh FM, Namer IJ, Abu-Asab MS, Pacak K, Taïeb D, Carney JA, Stratakis CA. Carney triad, SDH-deficient tumors, and Sdhb+/- mice share abnormal mitochondria. Endocr Relat Cancer. 2015; 22:345-52.
65. Guffroy A, Helali M, Merle B, **Imperiale A**, Chatelus E. Chloroma: An uncommon cause of arthritis. Arthritis Rheumatol. 2015; 67:2239.
66. Dietemann S, Debry C, Onea A, Namer IJ, **Imperiale A**. Epiglottic Squamous Cell Carcinoma Showing Unexpected 18F-FDOPA Uptake on PET/CT Investigation. Clin Nucl Med. 2015; 40:e370-1.
67. Messas N, Blondet C, Jesel L, Hess S, Girardey M, **Imperiale A**, Khouri T, Ohlmann P, Morel O. Diagnostic relevance of optical coherence tomography imaging in aborted acute myocardial infarction with a "Takotsubo component". Int J Cardiol. 2015; 195:123-5.
68. Leyendecker P, de Cambourg G, Mahé A, **Imperiale A**, Blondet C. 18F-FDG PET/CT Findings in a Patient With a Proliferating Trichilemmal Cyst. Clin Nucl Med. 2015; 40:598-9.
69. **Imperiale A**, Battini S, Averous G, Mutter D, Goichot B, Bachellier P, Pacak K, Taïeb D, Namer IJ. *In vivo* Detection of Catecholamines by Magnetic Resonance Spectroscopy: A potential specific biomarker for pheochromocytoma diagnosis. Surgery. 2016; 159:1231-3.
70. Varoquaux A, Le Fur Y, **Imperiale A**, Reyre A, Montava M, Fakhry N, Namer IJ, Moulin G, Pacak K, Guye M, Taieb D. Magnetic resonance spectroscopy of paragangliomas: new insights into in vivo metabolomics. Endocr Relat Cancer. 2015; 22:M1-8.
71. Matuszak J, Blondet C, Durckel J, Lipsker D, Sibilia J, **Imperiale A**. Is sarcoid dactylitis worse than we "exPEcT" ?. Arthritis Rheumatol. 2016 Feb; 68:417.
72. Simon L, De Martino S, Garnon J, **Imperiale A**, Argemi X, Raoult D, Hansmann Y. Positron emission tomography to diagnose chronic Q fever. Med Mal Infect. 2015; 45:420-2.
73. Messas N, Blondet C, Jesel L, Hess S, Girardey M, **Imperiale A**, Khouri T, Ohlmann P, Morel O. Reply to "Post-ischemic myocardial stunning was the starting point of takotsubo syndrome: Restitution is justified after falling down on". Int J Cardiol. 2015;201:30-1.
74. Archier A, Heimburger C, Guerin C, Morange I, Palazzo FF, Henry JF, Schneegans O, Mundler O, Abdullah AE, Sebag F, **Imperiale A**, Taïeb D. 18F-DOPA PET/CT in the diagnosis and localization of persistent medullary thyroid carcinoma. Eur J Nucl Med Mol Imaging. 2015;24 (sous-presse).

75. Abdullah AE, Guerin C, **Imperiale A**, Barlier A, Battini S, Pertuit M, Roche P, Essamet W, Vaisse B, Pacak K, Sebag F, Taïeb D. Paraganglioma of the organ of Zuckerkandl associated with somatic HIF2A mutation. Oncol Lett. 2016 (sous-presse).
76. El Ghannudi S, **Imperiale A**, Dégot T, Germain P, Trinh A, Petean R, Le Van Quyen P, Chenard MP, Letscher-Bru V, Kessler R, Herbrecht R. Multimodality Diagnosis Approach of Cardiac Aspergillosis. Echocardiography. 2016;20 (sous-presse).
77. Taieb D, **Imperiale A**, Pacak K. 18F-DOPA: the versatile radiopharmaceutical. Eur J Nucl Med Mol Imaging. 2016 (sous-presse).
78. Cazzato RL, Garnon J, Ramamurthy N, Tsoumakidou G, **Imperiale A**, Namer IJ, et al. 18F-FDOPA PET/CT-guided radiofrequency ablation of liver metastases from neuroendocrine tumors: technical note on a preliminary experience. Cardiovasc Intervent Radiol. 2016;5 (sous-presse).
79. Battini S, **Imperiale A**, Taïeb D, Elbayed K, Cicek E, Sebag F, Brunaud L, Namer IJ. High-Resolution Magic Angle Spinning ^{1}H Nuclear Magnetic Resonance Spectroscopy Metabolomics of hyperfunctioning parathyroid glands. Surgery. 2016 (sous-presse).
80. Heimburger C, Averous G, Charlin E, Lang H, Kurtz JE, **Imperiale A**. Adrenal metastasis of a poorly differentiated adenocarcinoma mimicking a pheochromocytoma on ^{18}F-FDOPA PET/CT. Clin Nucl Med. 2016 (sous-presse).

b. Publications nationales dans des revues à comité de lecture

81. Cimarelli S, **Imperiale A**, Sauer F, Morel O, Ben Sellem D, Goetz C, Blondet C, Ohlmann P, Constantinesco A. Explorations cardiologiques nucléaires dans la cardiomyopathie de Takotsubo. Médecine Nucléaire. 2008; 32:57-65.
82. Federici L, Andrès E, Blondet C, **Imperiale A**, Constantinesco A. Place de la TEP-FDG dans l'exploration des fièvres et syndromes inflammatoires prolongeès. Médecine Nucléaire. 2008:32; 311–2.
83. Federici L, **Imperiale A**, Blaison G, Constantinesco A, Andrès E. Intérêt de la tomographie par émission de positon au 18F-fluorodesoxyglucose (18F-FDG-TEP) pour le diagnostic des fièvres et syndromes inflammatoires prolonges d'origine indéterminée. M Thérapeutique. 2009; 14:306-13.
84. Keomany J, **Imperiale A**, Thiriat S, Braun JJ, Constantinesco A. Résultats atypiques et faux-negatifs de la scintigraphie au 67Ga et de la TEP-TDM au 18F-FDG dans une patiente avec sarcoïdose et cancer du sein bilateral. Médecine Nucléaire. 2009; 33:758–63.
85. Braun JJ, Riehm S, **Imperiale A**, Schultz-Carpentier AS, Gentine A, de Blay F. Sarcoïdose des voies aérodigestives supérieures. Rev Mal Respir 2011; 28:164-73.
86. Roux-Keomany J, **Imperiale A**, Schneegans O, Detour J, Chabrier J, Goichot B, Constantinesco A. La TEP-TDM à la 18F-DOPA aurait-elle un rôle dans le suivi post opératoire des patients atteints de carcinome médullaire de la thyroïde ? Résultats

préliminaires de l'expérience strasbourgeoise et revue de la littérature. Médecine Nucléaire. 2011; 35:167-79.

87. Rust E, Goichot B, Kurtz JE, Pessaux P, **Imperiale A**. Performances de la TEP-TDM à la 6-Fluoro-[18F]-L-Dihydroxyphénylalanine (FDOPA) et de l'imagerie radiologique conventionnelle dans la prise en charge des patients avec maladie tumorale endocrine dont le primitif est inconnu. Médecine Nucléaire. 2012; 36:278–90.
88. Heimburger C, Andres E, Rust E, Ghiura C, Dakayi Nono C, Hassler S, Hubele F, Riehm S, Namer IJ, **Imperiale A**. Imagerie morphologique et fonctionnelle des tumeurs brunes. À propos d'un cas de localisation maxillo-mandibulaire. Rev Med Interne. 2013; 34:377-81.
89. Lussey-Lepoutre C, Hindié E, Montravers F, Detour J, Ribeiro MJS, Taïeb D, **Imperiale A**. The current role of 18F-FDOPA PET for neuroendocrine tumor imaging. Médecine Nucléaire. 2016; 40:20-30.

CONGRES

a. Congrès internationaux : communications orales et affichées

1. **Imperiale A**, Ladu C, Gheri RG, Mannelli M, Olianti C, La Cava G. Adrenal incidentalomas: SPECT semiquantitative analysis of adrenocortical NP-59 uptake. Annual Congress of the European Association of Nuclear Medicine (Vienna, 2002). *Eur J Nucl Med Mol Imag*. 2002;29 (suppl):S171.
2. Olianti C, **Imperiale A**, Seracini D, Materassi M, Danti AD, La Cava G. Functional recovery in children's hydronephrotic kidneys after pyeloplasty. Annual Congress of the European Association of Nuclear Medicine (Amsterdam, 2003). *Eur J Nucl Med Mol Imag*. 2003;30(suppl):S239.
3. Olianti C, **Imperiale A**, Seracini D, Tommasi M, Materassi M, La Cava G. Urinary Endothelin excretion in reflux nephropathy. Annual Congress of the European Association of Nuclear Medicine (Amsterdam, 2003). *Eur J Nucl Med Mol Imag*. 2003;30(suppl):S634.
4. Olianti C, **Imperiale A**, Sotgia B, Comis G, La Cava G. Reference values of ^{123}I-OIH single kidney clearance in normal subjects from 0 to 18 years old. International Scientific Committee of Radionuclides in Nephro-urology (ISCORN), 12th International Symposium (La Baule, 2004).
5. Olianti C, **Imperiale A**, Caruso S, La Cava G. ^{123}I-OIH and ^{99m}Tc-DTPA renography in evaluation of renal hemodynamic behaviour in acute ACE-inibition. Annual Congress of the European Association of Nuclear Medicine (Helsinki, 2004). *Eur J Nucl Med Mol Imag*. 2004;31(suppl):S227.
6. Briganti V, **Imperiale A**, Ferri P, Vaggelli L, Gheri RJ, Pieroni C. Qualitative and quantitative octreoscan evaluation in medullary thyroid carcinoma: diagnostic and therapeutic implications. 17th IRIST Meeting (Ghent, 2004).
7. Inglese E, Marcassa C, Medolago G, **Imperiale A**, De Rimini ML, Bertagna F, Leva L, Cappagli M, Campini R, Sullo P, Lupo M, Ferro A, Brambilla M. LV function evaluated by Gated-SPECT myocardial perfusion imaging at rest and after exercise : observational data of a multicenter study after enrolment of 464 patients. Annual Congress of the Italian Association of Nuclear Medicine (Palermo, 2004). *Q J Nucl Med Mol Imaging*. 2004;48(suppl):16.
8. Briganti V, **Imperiale A**, Ferri P, Vaggelli L, Pieroni C. Semiquantitative SPECT evaluation of Octreoscan uptake in patients with bronchial carcinoid and pulmonary neuroendocrine carcinoma: diagnostic and prognostic value. Annual Congress of the Italian Association of Nuclear Medicine (Palermo, 2004). *Q J Nucl Med Mol Imaging.* 2004;48(suppl):31.
9. Briganti V, **Imperiale A**, Ferri P, Vaggelli L, Pedercini S, Bemporad D, Gheri RJ, Pieroni C. Planar acquisition versus SPECT evaluation of Octreoscan uptake in patients with residual

or metastatic medullary thyroid carcinoma: diagnostic value of the proposed semiquantitative index and therapeutic implications. Annual Congress of the Italian Association of Nuclear Medicine (Palermo, 2004). *Q J Nucl Med Mol Imaging.* 2004;48(supp1):32.

10. Briganti V, Ribecco AS, **Imperiale A**, Ferri P, Vaggelli L, D'Agata A, Fioretto L, Pieroni C. Positron emission tomography (FDG PET) in the detection of recurrences of colorectal cancer: a clinical experience in Florence. Annual Congress of the Italian Association of Nuclear Medicine (Palermo, 2004). *Q J Nucl Med Mol Imaging.* 2004;48(suppl):88.
11. Briganti V, **Imperiale A**, Ferri P, Vaggelli L, Pieroni C. Utility of Somatostatin receptor scintigraphy in the management of patients with proven or suspect pituitary morpho-functional dysfunction. Annual Congress of the Italian Association of Nuclear Medicine (Palermo, 2004). *Q J Nucl Med Mol Imaging.* 2004;48(suppl):118.
12. Inglese E, Marcassa C, Medolago G, Imperiale A, De Rimini ML, Bertagna F, Sullo P, Lupo M, Ferro A, Cappagli M. Incidence of post exercise stunning evaluated by Gated-SPET myocardial perfusion imaging. A multicenter study. 7th International Conference of Nuclear Cardiology (Lisbon, 2005). *J Nucl Cardiol.* 2005;12(suppl1):S48.
13. Blondet C, Herb G, **Imperiale A**, Elbayed K, Piotto M, Herbrecht R, Neuville A, Namer IJ. Metabolomics and 18F-FDG imaging in Hodgkin's disease. Annual Congress of the European Association of Nuclear Medicine (Copenhagen, 2007). *Eur J Nucl Med Mol Imaging*. 2007.
14. Moser T, **Imperiale A**, Buy X, Goyault G, Dietemann J, Gangi A. Osteoblastic bone metastases: how to crack a tough nut? Annual Congress of the Radiological Society of North America (Chicago, 2007).
15. Dillmann B, Moussallieh FM, Elbayed K, Piotto M, Neuville A, **Imperiale A**, Erb G, Ben Sellem D, Bellocq JP, Namer IJ. HRMAS-NMR metabolomics in a medical environment: applications in cancerology. Frontiers of Magnetic Resonance: from tumor cell to cancer patient – International Society for Magnetic Resonance in Medicine, Workshop series 2008 (Nice, 2008).
16. Piotto M, Erb G, Elbayed K, Raya J, Neuville A, Mohr M, Maitrot D, Kehrli P, **Imperiale A,** Herbrecht R, Garillon A, Moussallieh FM, Martínez-Bisbal M, Monleon D, Assemat O, Celda B, Namer I. Metabolic analysis of human brain biopsies in a medical environment using HRMAS NMR. Metabomeeting (Lion, 2008).
17. Piotto M, Moussallieh FM, Dillmann B, **Imperiale A**, Neuville A, Brigand C, Bellocq JP, Elbayed K, Namer IJ. Metabolic characterization of primary human colorectal cancers using high resolution magic angle spinning 1H magnetic resonance spectroscopy. International Society for Magnetic Resonance in Medicine, Workshop series 2009 (Onolulu, 2009).
18. Clavier JB, Letscher-Bru V, Dupont L, Waller J, **Imperiale A**, Fornecker L, Fohrer C, Herbrecht R. Primary Aspergillus Fumigatus liver Abscess. 4th Advances against aspergillosis (Rome, 2010).

19. Battini S, **Imperiale A**, Taieb D, Elbayed K, Sebag F, Brunaud L, Namer IJ. Metabolome profiling by HRMAS NMR spectroscopy of hyperfunctioning parathyroid glands. International Society for Magnetic Resonance in Medicine, Workshop series 2015 (Toronto, 2015; ISMRM merit awards 2015 "magna cum laude).
20. **Imperiale A**, Battini S, Roche P, Moussallieh FM, Cicek EA, Sebag F, Brunaud L, Barlier A, Elbayed K, Loundou A, Bachellier P, Goichot B, Stratakis CA, Pacak K, Taieb D, Namer IJ. Metabolomic assessment of succinate dehydrogenase dysfunction in pheochromocytomas and paragangliomas by 1H-HRMAS NMR spectroscopy: clinical and pathophysiological implications. International Society for Magnetic Resonance in Medicine, Workshop series 2015 (Toronto, 2015; ISMRM merit awards 2015 "magna cum laude).
21. Battini S, **Imperiale A**, Taieb D, Elbayed K, Sebag F, Brunaud L, Namer IJ. Metabolomic profiling by HRMAS NMR spectroscopy in hyperparathyroidism. EuCC 22nd annual meeting (Freiburg, 2015).
22. Battini S, Faitot F, **Imperiale A**, Elbayed K, Cicek AE, Averous G, Bachellier P, Namer IJ. Metabolomics distinguishes long-term survival in patients with pancreatic adenocarcinoma. Pancreas 2016 (Glasgow, 2016).

b. Congrès nationaux : communications orales et affichées

1. Grunenberger F, Millot S, **Imperiale A**, Chenard MP, Abdi L, Bui E, Zores F, Schlienger JL. Carcinome surrenalien à expression corticale et neuroendocrine. Congres Annuel de la Société Française d'Endocrinologie (Montpellier, 2006). Ann Endocrinol. 2006;67:441.
2. Ben Sellem D, **Imperiale A**, Serra S, Goetz C, Cimarelli S, Schaeffer F, Constantinesco A. Interet de la TEP-TDM au 18F-FDG dans le cancer de l'ovaire. Congres Annuel de la Société Française de Biophysique et de Médicine Nucléaire (Bordeaux, 2007). Médecine Nucléaire. 2007;31(9).
3. Blondet C, Herb G, **Imperiale A**, Elbayed K, Piotto M, Herbrecht R, Neuville A, Namer IJ. Maladie de Hodgkin : étude métabolique croisée en HRMAS-NMR et TEP-TDM au 18F-FDG. Congres Annuel de la Société Française de Biophysique et de Médicine Nucléaire (Bordeaux, 2007). Médecine Nucléaire. 2007;31(9).
4. Ben Sellem D, **Imperiale A**, Goetz C, Cimarelli S, Constantinesco A. Apport de la médicine nucléaire dans la sarcoïdose musculo-cutanée : 18F-FDG et 67Ga. Congres Annuel de la Société Française de Biophysique et de Médicine Nucléaire (Bordeaux, 2007). Médecine Nucléaire. 2007;31(9).
5. **Imperiale A**, Ben Sellem D, Cimarelli S, Constantinesco A. Cancer de l'œsophage: intérêt de la mesure de la SUV max lors de l'examen TEP-TDM au 18F-FDG pre-thérapeutique. Congres Annuel de la Société Française de Biophysique et de Médicine Nucléaire (Bordeaux, 2007). Médecine Nucléaire. 2007;31(9).
6. Cimarelli S, **Imperiale A**, Goetz C, Ben Sellem D, Sauer F, Morel O, Blondet C, Constantinesco A. Exploration cardiologique nucléaire de la cardiomyopathie de

Takotsubo. Congres Annuel de la Société Française de Biophysique et de Médicine Nucléaire (Bordeaux, 2007). Médecine Nucléaire. 2007;31(9).

7. Ben Sellem D, Heymann S, **Imperiale A**, Kremer S, Noel G, Namer IJ. Spectroscopie RMN et 18F-FDG-TEP dans le suivi des glioblastomes. Journée de Recherche en Imagerie (Dijon, 2007).
8. Federici L, Blondet C, **Imperiale A**, Blaison G, Pasquali C, Weber C, Christmann E, Goichot B, Pflumio F, Sibilia J, Blicklé JF, Andres E. Diagnostic des fièvres et syndromes inflammatoires prolongés inexpliqués: analyse retrospective de l'intérêt du 18F-FDG PETscan. Congres Annuel de la Société Française de Médecine Interne (Versailles, 2007).
9. Ben Sellem D, Braun JJ, Kessler R, **Imperiale A**, Constantinesco A. Existe-t-il encor un rôle pour la scintigraphie au 67Ga dans le suivi de la sarcoïdose à l'ère du 18F-FDG TEP/TDM? Congres Annuel de la Société Française de Biophysique et de Médicine Nucléaire (Hammamet, 2008). Médecine Nucléaire. 2008;32(4).
10. Ben Sellem D, **Imperiale A**, Moser T, Gangi A, Constantinesco A. 18F-FDG TEP/TDM dans les ostéomes ostéoïdes et les osteoblastomes: à propos de 3 cas. Congres Annuel de la Société Française de Biophysique et de Médicine Nucléaire (Hammamet, 2008). Médecine Nucléaire. 2008;32(4).
11. Ben Sellem D, Braun JJ, Kessler R, **Imperiale A**, Constantinesco A. Apport de la 18F-FDG TEP/TDM dans le suivi thérapeutique de la sarcoïdose. Congres Annuel de la Société Française de Biophysique et de Médicine Nucléaire (Hammamet, 2008). Médecine Nucléaire. 2008;32(4).
12. Ben Sellem D, Cojean N, Lutz P, **Imperiale A**, Constantinesco A. Neuroblastome: TEP-TDM au 18F-FDG et scintigraphy à la 123I-mIBG. Congres Annuel de la Société Française de Biophysique et de Médicine Nucléaire (Hammamet, 2008). Médecine Nucléaire. 2008;32(4).
13. Ben Sellem D, Serra S, Schaeffer F, Hubele F, Barats JC, Goetz C, **Imperiale A**, Constantinesco A. Intérêt de la TEP au 18F-FDG dans la suspicion de récidive du cancer de l'ovaire. Congres Annuel de la Société Française de Biophysique et de Médicine Nucléaire (Hammamet, 2008). Médecine Nucléaire. 2008;32(4).
14. Ben Sellem D, Heymann S, **Imperiale A**, Kremer S, Noel G, Namer IJ. Intéret de l'imagerie métabolique dans le suivi des glioblastomes. Congres Annuel de la Société Française de Biophysique et de Médicine Nucléaire (Hammamet, 2008). Médecine Nucléaire. 2008;32(4).
15. Federici L, Argemi X, **Imperiale A**, Blaison G, Coumaros D, Andres E. Quand maladie céliaque et lymphome T ne font plus qu'un. Congres Annuel de la Société Française de Médecine Interne (Bordeaux, 2008).
16. **Imperiale A**, Neuville A, Elbayed K, Piotto M, Bellocq JP, Lutz P, Namer IJ. Métabolomique des tumours neuroblastiques de l'enfant. 2me Forum du Cancéropôle du Grand-Est (Vittel, 2008).

17. **Imperiale A**, Neuville A, Elbayed K, Piotto M, Blondet C, Bellocq JP, Herbrecht R, Namer IJ. Maladie de Hodgkin: analyse comparative des données métabolomiques en HRMAS-RMN et du PET-FDG. 2me Forum du Cancéropôle du Grand-Est (Vittel, 2008).
18. Dilmann B, **Imperiale A**, Moussallieh FM, Neuville A, Elbayed K, Piotto M, Brigand C, Bellocq JP, Namer IJ. Métabolomique des adénocarcinomes du colon. 2me Forum du Cancéropôle du Grand-Est (Vittel, 2008).
19. Braun JJ, Riehm S, **Imperiale A**. Sarcoïdose ORL et imagerie: TDM, IRM, scintigraphie au 67Ga et 18F-FDG TEP/TDM. Congres Annuel de la Société ORL de l'Est de la France (Strasbourg, 2008).
20. Dillmann B, Moussallieh FM, Elbayed K, Piotto M, Neuville A, **Imperiale A**, Erb G, Ben Sellem D, Bellocq JP, Namer IJ. HRMAS-NMR metabolomics in a medical environment: applications in cancerologie. 1re Colloque inter-regional Grand-Est de recherche translationnelle en oncologie (Nancy, 2009). Oncologie. 2009;11(3).
21. Ben Sellem D, **Imperiale A**, Braun JJ, Constantinesco A. Apport de la TEP/TDM au 18F-FDG dans les sarcoidoses pharyngo-laryngéens. Congres Annuel de la Société Française de Biophysique et de Médicine Nucléaire (Brest, 2009). Médecine Nucléaire. 2009;33(5).
22. Ben Sellem D, Hubele F, Keomany J, Goetz C, **Imperiale A**, Constantinesco A. Apport de la lymphoscintigraphie dans le diagnostic étiologique d'un oedème chronique: à propos d'un cas. Congres Annuel de la Société Française de Biophysique et de Médicine Nucléaire (Brest, 2009). Médecine Nucléaire. 2009;33(5).
23. Ben Sellem D, Lefebvre N, Hubele F, Hansmann Y, **Imperiale A**, Constantinesco A. Intérêt de la TEP-TDM au 18F-FDG dans la prise en charge d'une tuberculose. Congres Annuel de la Société Française de Biophysique et de Médicine Nucléaire (Brest, 2009). Médecine Nucléaire. 2009;33(5).
24. **Imperiale A**, Detour J, Chabrier G, Ben Sellem D, Keomany J, Beretz L, Goichot B, Constantinesco A. Carcinome médullaire de la thyroïde et suivi thérapeutique à l'aide de la TEP-TDM à la 18F-DOPA: à propos de quatre cas. Congres Annuel de la Société Française de Biophysique et de Médicine Nucléaire (Brest, 2009). Médecine Nucléaire. 2009;33(5).
25. Ben Sellem D, Hubele F, Hassler S, Goetz C, **Imperiale A**, Constantinesco A. Lymphoscintigraphie et chilothorax. Interet de l'acquisition tomographique et du couplage anatomo-fonctionnel: à propos d'un cas. Congres Annuel de la Société Française de Biophysique et de Médicine Nucléaire (Brest, 2009). Médecine Nucléaire. 2009;33(5).
26. Moreau F, **Imperiale A**, Pinget M, Jeandidier N, Schneegans O, Kessler L. Suspicion de microadénomatose pancréatique: à propos d'un cas. Congres Annuel de la Société Française d'Endocrinologie (Nice, 2009). Ann Endocrinol. 2009;70.
27. Grunenberger F, Hodonou I, Epailly E, Thiranos JC, Bachellier P, **Imperiale A**, Schlienger JL. Insuffisance cardiaque aiguë et NEM1: quelle relation? Congres Annuel de la Société Française d'Endocrinologie (Nice, 2009). Ann Endocrinol. 2009;70:400.

28. Detour J, **Imperiale A**, Hammer C, Lucas A, Constantinesco A, Beretz L. Fixation physiologique pancréatique de la 18F-DOPA: effet dose dépendant de la carbidopa. 4èmes Rencontres Convergences Santé Hôpital (Reims, 2009).
29. Rust E, Keomany J, Goichot B, Constantinesco A, **Imperiale A**. Caractérisation fonctionnelle in vivo du degree de differenciation cellulaire dans la pathologie tumorale endocrine. Congres Annuel de la Société Française de Biophysique et de Médicine Nucléaire (Nice, 2010). Médecine Nucléaire. 2010;34(5).
30. Detour J, **Imperiale A**, Hammer C, Lucas A, Beretz L, Constantinesco A. Carbidopa et biodistibution physiologique de la 18F-DOPA. Congres Annuel de la Société Française de Biophysique et de Médicine Nucléaire (Nice, 2010). Médecine Nucléaire. 2010;34(5).
31. Rust E, Taquet M, Riehm S, Vinzio S, Goichot B, Constantinesco A, **Imperiale A**. Apport de l'imagerie fonctionnelle multimodalité dans la pathologie tumorale endocrine digestive. Congres Annuel de la Société Française de Biophysique et de Médicine Nucléaire (Nice, 2010). Médecine Nucléaire. 2010;34(5).
32. **Imperiale A**, Greget M, Chabrier G, Keomany J, Rust E, Detour J, Pessaux P, Goichot B, Constantinesco A. Métastase hépatique pseudoangiomateuse d'un carcinome médulaire de la thyroïde: approche diagnostique multimodalité. Congres Annuel de la Société Française de Biophysique et de Médicine Nucléaire (Nice, 2010). Médecine Nucléaire. 2010;34(5).
33. Keomany J, Detour J, Chabrier G, Rust E, Schneegans O, Goichot B, Constantinesco A, **Imperiale A**. Carcinome médullaire de la thyroïde et TEP-TDM à la 18F-DOPA dans le suivi post-chirurgical : résultats préliminaires. Congres Annuel de la Société Française de Biophysique et de Médicine Nucléaire (Nice, 2010). Médecine Nucléaire. 2010;34(5).
34. Schlienger JL, Glasser L, Chatelus E, **Imperiale A**. Hypercalcémie severe à PTH basse dans une sarcoidose chronique. Congres Annuel de la Société Française d'Endocrinologie (Clermont-Ferrand, 2011). Ann Endocrinol. 2011.
35. Nndiaye N, Luca F, **Imperiale A**, Brigand C, Chenard MP, Goichot B. Une tumeur gastrointestinale : cause rare de faux positif à la scintigraphie à la MIBG. Congres Annuel de la Société Française d'Endocrinologie (Clermont-Ferrand, 2011). Ann Endocrinol. 2011.
36. Ben Sellem D, Hubele F, **Imperiale A**, Hassler S, Goetz C, Herbrecht R, Constantinesco A. Interet de la TEP-TDM au 18F-FDG dans la prise en charge d'une aspergillose systémique. Congres Annuel de la Société Française de Biophysique et de Médicine Nucléaire (Luxemburg, 2011). Médecine Nucléaire. 2011;35(5).
37. Hubele F, Bilger C, Kremer S, **Imperiale A**, Lioure B, Namer IJ. Apport de la TEP-TDM au 18F-FDG dans l'orientation et la réponse au traitement antiviral : à propos d'un cas d'encephalite limbique à HHV6. Congres Annuel de la Société Française de Biophysique et de Médicine Nucléaire (Luxemburg, 2011). Médecine Nucléaire. 2011;35(5).
38. Rust E, Andrianatoandro N, Constantinesco A, **Imperiale A**. Les fixations mammaires focales en médecine nucléaire nécessitent des investigations complémentaires

systématiques. Congres Annuel de la Société Française de Biophysique et de Médicine Nucléaire (Luxemburg, 2011). Médecine Nucléaire. 2011;35(5).

39. Hassler S, Goetz C, Hubele F, **Imperiale A**, Constantinesco A. Diagnostic de certitude de la splénose intra-abdominale par la TEMP/TDM : à propos de 3 cas suspects de carcinose péritonéale. Congres Annuel de la Société Française de Biophysique et de Médicine Nucléaire (Luxemburg, 2011). Médecine Nucléaire. 2011;35(5).
40. Rust E, Schneegans O, Roedlich MN, Boulanger C, Ollier JC, Constantinesco A, **Imperiale A**. TEP-TDM à la 18F-FDOPA : un incidentalome heureux. Congres Annuel de la Société Française de Biophysique et de Médicine Nucléaire (Luxemburg, 2011). Médecine Nucléaire. 2011;35(5).
41. Hubele F, **Imperiale A**, Ben Sellem D, Hassler S, Schultz A, Constantinesco A Goetz C. Fixations atypiques extra-osseuses en scintigraphie osseuse au 99Tc-HMDP : l'apport de la TEMP/TDM en complément diagnostique. Congres Annuel de la Société Française de Biophysique et de Médicine Nucléaire (Luxemburg, 2011). Médecine Nucléaire. 2011;35(5).
42. Rust E, Flores G, Dumas J, Schlienger JL, Schneegans O, Constantinesco A, **Imperiale A**. Différents degrés de différentiation tumorale chez un même patient porteur d'un carcinome médullaire de la thyroïde : intérêt d'une exploration combinée par TEP/TDM à la 18F-FDOPA et au FDG. Congres Annuel de la Société Française de Biophysique et de Médicine Nucléaire (Luxemburg, 2011). Médecine Nucléaire. 2011;35(5).
43. Kachur AA, Kosenok VK, **Imperiale A**, Bellocq JP, Falcoz PE, Massard G. Mediastinal lymph node staging in patients with non-small-cell lung cancer: accuracy of integrated positron emission tomography. Journées d'Automne de la Societé Francaise de Chirurgie Thoracique et cardio-vasculaire (Paris, 2011).
44. Hubelé F, Rust E, **Imperiale** A, Namer IJ. Semi-quantification du FP-CIT en TEMP chez des sujets sans atteinte du système dopaminergique : relation avec l'age. Congres Annuel de la Société Française de Biophysique et de Médicine Nucléaire (Montpellier, 2011). Médecine Nucléaire. 2012;36(4).
45. Hubelé F, Morland D, Rust E, **Imperiale** A, Namer IJ. Syndrome de Bertolotti : un diagnostic accessible en scintigraphie osseuse hybride TEMP/TDM. Congres Annuel de la Société Française de Biophysique et de Médicine Nucléaire (Montpellier, 2011). Médecine Nucléaire. 2012;36(4).
46. Hammer-Lefevre C, **Imperiale A**, Namer IJ, Gourieux B, Detour J. Comparaison des trois methods de controle du radiomarquage de l'Octreoscan. 7èmes Rencontres Convergences Santé Hôpital (Ajaccio, 2012).
47. Grunenberger F, Gassmann AS, Bergerat JP, **Imperiale A**, Bachellier P, Goichot B. Un pheochromocytoma malin. Congres Annuel de la Société Française d'Endocrinologie (Toulouse, 2012). Ann Endocrinol. 2012;73.
48. Braun JJ, Riehm S, **Imperiale A,** Schultz P. Imagerie multimodale de la sarcoïdose nasosinusienne. Congres Annuel de la Société ORL de l'Est de la France (Strasbourg, 2013).

49. Rust E, Brigand C, Hubelé F, Namer IJ, **Imperiale** A. Intérêt de la TEP/TDM au FDG dans le diagnostic initial des cancers coliques présumes non métastatiques : étude prospective. Congres Annuel de la Société Française de Biophysique et de Médicine Nucléaire (Rouen, 2013). Médecine Nucléaire. 2013;37(5).
50. Hubelé F, Rust E, **Imperiale** A, Namer IJ. TEP/TDM au 18F-FDG dans le cadre d'un syndrome paraneoplasique d'une fascite palmaire. Congres Annuel de la Société Française de Biophysique et de Médicine Nucléaire (Rouen, 2013). Médecine Nucléaire. 2013;37(5).
51. Hubelé F, Rust E, Namer IJ, **Imperiale** A. TEP/TDM au 18F-FDG et sarcoidose hépatorénale. Congres Annuel de la Société Française de Biophysique et de Médicine Nucléaire (Rouen, 2013). Médecine Nucléaire. 2013;37(5).
52. Hubelé F, Rust E, **Imperiale** A, Namer IJ. TEP/TDM au 18F-FDG et granulomatose lymphomatoïde : bilan initial et évaluation sous traitement. Congres Annuel de la Société Française de Biophysique et de Médicine Nucléaire (Rouen, 2013). Médecine Nucléaire. 2013;37(5).
53. Rust E, Gomes Ferreira C, Sebastia Sancho C, Becmeur F, **Imperiale A**, Namer IJ. Quand la scintigraphie osseuse révèle une appendicite. Congres Annuel de la Société Française de Biophysique et de Médicine Nucléaire (Rouen, 2013). Médecine Nucléaire. 2013;37(5).
54. Braun JJ, **Imperiale A,** Veillon F, Riehm S. Imagerie multimodale de la sarcoïdose nasosinusienne. Journées Françaises de Radiologie (Paris, 2013).
55. Battini S, **Imperiale A**, Taïeb D, Elbayed K, Sebag F, Brunaud L, Namer IJ. Étude métabolomique par spectroscopie RMN-HRMAS dans les différents types d'hyperparathyroïdie. 8ème Forum du Cancéropôle du Grand-Est (Strasbourg, 2014).
56. **Imperiale A**, Sebag F, Vix M, Castinetti F, Kessler L, Bachellier P, Guillet B, Namer IJ, Mundler O, Taieb D. TEP/TDM à la 18F-FDOPA pour le diagnostic d'insulinome chez l'adulte. Intérêt de la prémédication par carbidopa et des acquisitions pancréatiques précoces. Journées Francophones de Médicine Nucléaire (La Rochelle, 2015). Médecine Nucléaire. 2015;39(3).
57. Muller N, Blondet C, Heinburger C, Kessler R, Caillard S, Epailly E, Hubele F, Namer IJ, **Imperiale A**. Complcations tumorales tumorales ou infectieuses dans le suivi des patients avec grefe d'organe : role de la TEP-TDM au 18F-FDG. Journées Francophones de Médicine Nucléaire (La Rochelle, 2015). Médecine Nucléaire. 2015;39(3).
58. Hubelé F, Rust E, Heinburger C, Blondet C, Becmeur F, **Imperiale** A, Namer IJ. Exploration isotopique digestive chez les patients IMC. Journées Francophones de Médicine Nucléaire (La Rochelle, 2015). Médecine Nucléaire. 2015;39(3).
59. Hubelé F, Rust E, Heinburger C, Blondet C, Goldfarb L, **Imperiale** A, Fornecker L, Namer IJ. Periostite sous voriconazole en scintigraphie osseuse. Journées Francophones de Médicine Nucléaire (La Rochelle, 2015). Médecine Nucléaire. 2015;39(3).
60. Heimburger C, El Adraa E, Hubelé F, Blondet C, Namer IJ, **Imperiale** A. Apport de la TEP/TDM au 18F-FDG pour l'évaluation d'une masse cardiaque : illustration à propos

d'un cas. Journées Francophones de Médicine Nucléaire (La Rochelle, 2015). Médecine Nucléaire. 2015;39(3).

61. Blondet C, Crimizade U, Heinburger C, Hubelé F, **Imperiale A**, Morel O, Namer IJ. Syndrome de Takotsubo biventriculaire suivi par étude isotopique au 18F-FDG et à la 123I-mIBG. Journées Francophones de Médicine Nucléaire (La Rochelle, 2015). Médecine Nucléaire. 2015;39(3).
62. Leyendecker P, Schohn C, De Cambourg , Mahé C, Namer IJ, **Imperiale A,** Blondet C. Tumeur trichilemmale proliférante et TEP-TDM au 18F-FDG : une tumeur rare de malignité incertaine peut en cacher une autre. Journées Francophones de Médicine Nucléaire (La Rochelle, 2015). Médecine Nucléaire. 2015;39(3).
63. Matuszak J, Meyer A, Hubelé F, Heinburger C, **Imperiale** A, Namer IJ, Blondet C. Myopathies inflammatoires : intérêt de la TEP/TDM au 18F-FDG pour le diagnostic de néoplasie occulte. Journées Francophones de Médicine Nucléaire (La Rochelle, 2015). Médecine Nucléaire. 2015;39(3).
64. Heimburger C, Veillon F, Charpiot A, Riehm S, Hubelé F, Goichot B, Blondet C, Namer IJ, **Imperiale** A. La TEP/TDM à la 18F-FDOPA et l'imagerie radiologique en coupes dans l'évaluation post-thérapeutique des paragangliomes de la tête et du cou. Journées Francophones de Médicine Nucléaire (La Rochelle, 2015). Médecine Nucléaire. 2015;39(3).
65. Battini S, **Imperiale A**, Taïeb D, Elbayed K, Sebag F, Brunaud L, Namer IJ. Metabolome profiiling by HRMAS NMR spectroscopy in hyperparathyroïdism. 1er Congrès de *Physiologie & de Biologie Intégrative* (Strasbourg, 2015).
66. Battini S, **Imperiale A**, Taïeb D, Cicek EA, Elbayed K, Sebag F, Brunaud L, Namer IJ. Metabolome profiling by HRMAS NMR spectroscopy in parathyroid disorders. ONCOTRANS 2015 (Dijon, 2015).
67. **Imperiale A**, Battini S, Roche P, Moussallieh FM, Cicek EA, Sebag F, Brunaud L, Barlier A, Elbayed K, Loundou A, Bachellier P, Goichot B, Stratakis CA, Pacak K, Taieb D, Namer IJ. HRMAS NMR metabolomics in pheochromocytoma and paraganglioma. ONCOTRANS 2015 (Dijon, 2015).
68. Battini S, **Imperiale A**, Elbayed K, Averous G, Bachellier P, Namer IJ. Metabolome profiling by HRMAS NMR spectroscopy in pancreatic adenocarcinoma. ONCOTRANS 2015 (Dijon, 2015).
69. Battini S, **Imperiale A**, Elbayed K, Averous G, Bachellier P, Namer IJ. Study of the pancreatic adenocarcinoma's metabolomic profile by HRMAS NMR spectroscopy. 9ème forum du Cancéropôle du Grand-Est (Strasbourg 2015).
70. Helali M, Addeo P, Detour J, Heimburger C, Goichot B, Bachellier P, Taieb D; Namer IJ, **Imperiale A**. Comparaison entre TEP/TDM à la 18F-FDOPA avec Carbidopa et scintigraphie aux récepteurs de la somatostatine pour examen des TNE pancréatiques non fonctionnelles Journées Francophones de Médicine Nucléaire (Grenoble, 2016). Médecine Nucléaire. 2016.
71. Heimburger C, Veillon F, Riehm S, Charpiot A, Goichot B, Namer IJ, **Imperiale A**. Etude de

la cinétique de fixation de la 18F-FDOPA dans les paragangliomes de la tête et du cou avant traitement et après chirurgie ou radiothérapie. Journées Francophones de Médicine Nucléaire (Grenoble, 2016). Médecine Nucléaire. 2016.

72. Heimburger C, Averous G, Charlin E, Blondet C, Kurtz JE, **Imperiale A**. Une suspicion de phéochromocytome : tout ce qui brille n'est pas de l'or ! Journées Francophones de Médicine Nucléaire (Grenoble, 2016). Médecine Nucléaire. 2016.
73. Heimburger C, Veillon F, Charpiot A, Pidello F, Onea M, Hubelé F, **Imperiale A**. Profile métabolique d'un nodule méso-tympanique : adénome de l'oreille moyenne. Journées Francophones de Médicine Nucléaire (Grenoble, 2016). Médecine Nucléaire. 2016.
74. Bund C, **Imperiale A**, Chenard MP, Lefebvre F, Kremer S, Proust F, Namer IJ. Place de la 18F-FDOPA dans la caractérisation des lésions expansives ne prenant pas le contraste en IRM. Journées Francophones de Médicine Nucléaire (Grenoble, 2016). Médecine Nucléaire. 2016.

CONFERENCES INVITÉES

1. Médecine Nucléaire: applications en oncologie. Séminaire de la Société Médicale des Hôpitaux Universitaires de Strasbourg, Strasbourg, 2006.
2. Place de l'imagerie TEP-TDM au 18F-FDG dans les cancers digestifs. Journée de Gastroentérologie, Strasbourg, 2006.
3. Progrès en imagerie: le PETSCAN. 3émes Rencontres de Cancérologie du Centre Alsace – Médecine Générale et Cancer, Wettolsheim, 2008.
4. Mise au point sur le TEP-TDM au 18F-FDG dans la maladie de Hodgkin de l'enfant. Ateliers de Radiothérapie Pédiatrique, Maladie de Hodgkin – Protocole EURONET, Strasbourg, 2008.
5. Particularités de la prise en charge des métastases hépatiques des tumeurs endocrines: imagerie fonctionnelle. Congres Français de Chirurgie, Paris, 2009.
6. Imagerie métabolique dans les tumeurs endocrines: laquelle, quand, pourquoi? Actualités thérapeutiques dans les tumeurs endocrines, RENATEN, Strasbourg, 2010.
7. Tumeurs Endocrines digestives: Quel bilan en 2011 en biologie et imagerie fonctionnelle? Congres National de la Société Française de Chirurgie Endocrine, Nancy, 2011.
8. Le nodule pulmonaire. TEP-TDM au ^{18}F-FDG : actualité et nouvelles perspectives**.** Réunion d'automne de l'Association pour la Promotion de la Pneumologie Libérale de l'Est, Strasbourg, 2012.
9. Imagerie fonctionnelle. Cours annuel du Groupe d'étude des Tumeurs Neuroendocrines (GTE) Diagnostic de tumeurs endocrines et prises en charge de formes localisées. Strasbourg, 2012.
10. Les tumeurs neuroendocrines de primitif inconnu: apport de l'imagerie fonctionnelle, RENATEN, Strasbourg, 2014.
11. Métabolomique par spectroscopie RMN à Haute Résolution en Rotation à l'Angle Magique (HRMAS) appliquée à la pathologie tumorale surrénalienne, RENATEN, Nancy, 2015.
12. Imagerie endocrinienne. Quoi de neuf en endocrinologie ? Nancy, 2015.
13. Functional Imaging of Gastro-Entero-Pancreatic Neuro-Endocrine Tumors. Shining New Lights: Cutting Edge Imaging in Endocrinology. ENDOCRINE, San Diego, California, 2015.
14. Quelle imagerie isotopique pour quelle TNE ? 3éme édition des Journées Digestives Régionales Nord-Est, Paris 2015.
15. Imagerie fonctionnelle des tumeurs neuroendocrines. Journée de la Fédération Française de Cancérologie Digestive. Strasbourg, 2015.
16. Facteurs pronostiques de récidive et de survie : apports de l'imagerie et des marqueurs moléculaires. Point de vu du médecin Nucléaire. Congrès national annuel du GTE. Paris, 2015.
17. Quel bilan d'imagerie réaliser devant une suspicion de tumeur endocrine d'origine digestive : l'imagerie fonctionnelle. 1ère Journée de Pathologies Digestives et 2eme

Journée de Chirurgie HPB. Strasbourg, 2015.

18. Métabolomique par spectroscopie RMN appliquée à la pathologie tumorale surrénalienne: de l'ex-vivo è l'in-vivo. Séminaire, Laboratoire DC2N (Différenciation et Communication Neuronale et Neuroendocrine), Inserm U982. Rouen, 2015.

OUVRAGES

1. La Cava G, **Imperiale A**, Olianti C, Gheri RG, Ladu C, Mannelli M, Pupi A. SPECT semiquantitative analysis of adrenocortical ^{131}I-6-beta iodomethyl-norcholesterol uptake to discriminate subclinical and preclinical functioning adrenal incidentaloma. 2003 *YEAR BOOK of NUCLEAR MEDICINE*, Mosby, Elsevier Health Sciences Company.
2. **Imperiale A**. Tecniques d'imagerie naso-sinusienne : TEP au 18F-FDG et scintigraphie au 67Ga (pg. 1-8). In : Imagerie naso-sinusienne. Braun JJ & Riehm S. 2012, Lavoisiere, Paris.
3. Piotto M, Moussallieh FM, **Imperiale A**, Benahmed MA, Detour J, Bellocq JP, Namer IJ, Elbayed K. Reproducible sample preparation and spectrum acquisition techniques for metabolic profiling of human tissues by proton high-resolution magic angle spinning nuclear magnetic resonance. Lutz NW editor. Cambridge: Cambridge University Press. 2013; 496-524.
4. **Imperiale A**. Radionuclide Imaging of Gastrointestinal Neuroendocrine Tumors. In Radionuclide Imaging and Therapy for Endocrine Tumors. Springer. 2017.

REFERENTIELS

1. Tumeurs neuroendocrines du grêle. Référentiel Interrégional de bonnes pratiques en cancérologie digestive (Alsace, Franche-Comté, Lorraine) – OncoLogiK 2016 – Tumeurs Neuroendocrines du grêle et du pancréas.
2. Tumeurs neuroendocrines du pancréas. Interrégionaux de bonnes pratiques en cancérologie digestive (Alsace, Franche-Comté, Lorraine) – OncoLogiK 2016 – Tumeurs Neuroendocrines du grêle et du pancréas.